PHOTOCONDUCTIVITY IN AMORPHOUS SILICON

A thesis presented by

CHARLES BULLOCH

(Sponsoring establishment
Dundee College of Technology)
to the CNAA
in partial fulfilment of the
requirements for the degree of
Doctor of Philosophy
December 1986

Declaration

I declare that while registered as a candidate for the degree for which this thesis is presented I have not been a candidate for any other award. I further declare that except where stated the work contained in this thesis is original and was performed by the author. The author is grateful to Dr. M.J. Powell of Philips Research Laboratories who supplied some of the samples.

Signed 

Advanced Studies

In addition to the original research reported in this thesis, the author attended the Chelsea Meeting on Amorphous Semiconductors in 1982 and 1983, and the International Conference on Amorphous and Liquid Semiconductors, Rome, 1985.

Acknowledgments

The author is greatly indebted to and wishes to thank the following without whose help this work would not have been possible.

Dr. Charles Main and Dr. Joseph Marshall for their supervision and encouragement throughout this investigation.

Tony Hepburn, John Berkin and Mark Monroe for many enlightening and critical discussions during this project.

Dr. R.R. Gardner for extending to the author the use of the facilities of the Physics Department at Dundee College of Technology.

Mr. J. Anderson and the technical staff of the Department of Physics for their help and advice during the course of this study.

Dundee College of Technology for providing the financial assistance which made this work possible.

ABSTRACT

PHOTOCONDUCTIVITY IN AMORPHOUS SILICON

CHARLES BULLOCH

The photoconductive properties of undoped hydrogenated amorphous silicon have been extensively studied. Measurements of optical absorption, dark d.c. conductivity, steady state photoconductivity, step response transient rise photoconductivity and impulse response flash decay photoconductivity have been made. In addition, computer simulation has been used to give an insight into the physical processes involved in the photoconductivity experiments.

Two materials were used in the study, to provide a comparison. All the above measurements, except the transient measurements were made on sputtered material prepared by the author. a-Si:H prepared elsewhere by the glow discharge decomposition of silane was measured by all the above experiments, except optical absorption.

The results obtained from the glow discharge material were interpreted as due to recombination in distributed states, which are restricted in energy, extending from the dark Fermi level upwards to 0.6eV below E_c. The capture cross section of these states was of a value expected for the neutral dangling bond, so they have been denoted as D^o states. States outside this energy were seen to be ineffective as recombination centres. The model thus has features intermediate between a simple 2-trap system and a distributed density of states. Chapter 5 presents a detailed analysis of steady state photoconductivity for the case of a single correlated defect level, and demonstrates its near equivalence to a simple 2-defect one electron system. This partly justifies the subsequent use of one electron states in computer modelling. Computer simulation successfully predicts the form of the experimental step response. The flash decay required the existence of an extra discrete state at 0.4eV, but gave a better quantitative fit.

The sputtered material appeared to have the recombination in the steady state controlled by discrete states 0.6eV below E_c, but inconsistencies remain between the interpretations of different measurements on this material.

Table of Contents

List of Figures

Chapter 1

Introduction

1.1 General

The use of amorphous materials as a tool is very old. Glasses present the so called chonchoidal fracture surface, which is a curved surface with striations at right angles to the edge of the fracture. This edge can be very sharp, and broken glasses have been used as cutting tools for a very long time.

The man-made manufacture of glass is also very old, and is believed to be the invention of the ancient Egyptians.

Crystals can be broken into regular shapes such as cubes and prisms. In 1912, when von Laue directed the then new X-rays onto single crystals, a regular internal structure was deduced. But when amorphous materials were examined by X-ray diffraction it was shown that glasses did not possess such a regular internal structure, i.e. glasses do not have long range order.

Up to about 1970, the scientific study of amorphous materials was, despite major advances, of less importance than today. However, since the demonstration of the ability of amorphous silicon to be doped and its use as a solar energy material, a great deal of interest has been shown in the subject, which is now the basis of a multi-million dollar industry.

1.1.0.1 Types of Amorphous Solids

Non-crystalline solids can be arbitrarily subdivided into two

groups : glasses, which are formed by supercooling the molten material; and other amorphous solids, in particular those which are formed from the vapour phase by methods such as r.f. sputtering or glow discharge decomposition of a gas.

Amorphous silicon(a-Si) is the archetypal example of those substances which cannot be cooled from the melt sufficiently quickly to avoid crystallisation. This is because the preparation techniques available at present are too slow to allow the melts of such materials to be supercooled. It should be recognised, however, that the two groups are not independent; amorphous arsenic selenide ($a\text{-}As_2Se_3$)prepared by r.f.sputtering, and then annealed, possesses similar properties to that prepared from the melt.

1.2 Electronic properties of amorphous materials

Because amorphous materials have no periodic structure and thus no long range order(L.R.O.), there is no periodic lattice to interfere with the extended state wave-function and a band structure should not be expected.

But consider a crystalline substance as it melts and its L.R.O. vanishes. One would expect a fundamental change in properties on melting, but major properties such as resistivity or indeed colour are not always observed to change appreciably. It can therefore be implied that the basic band structure depends more upon short range order(S.R.O.). This should come as no surprise to chemists, who examine solids with a different approach; full or empty atomic or molecular orbitals lead to full or empty bands in

the solid.

The transparency of ordinary window glass to ordinary daylight, and its onset of absorption in the u.v. region is a typical consequence of the existence of a band structure.

1.2.0.1 The Wave Function in Amorphous Solids

In classical Band Theory an electron in a Bloch wave function ψ, exists in a delocalised extended state which has the periodicity of the lattice, and crystal momentum, k. Eventually, after an average time, τ, the electron wave function will be scattered, i.e. in simple terms, the wave-vector, k_1, will change by Δk to k_2. As the electrons have average velocity v_{th} one can define a mean free path, L, as

$$L=v_{th}\tau \tag{1.1}$$

This scattering limits mobility as

$$\mu=e\tau/m^* \tag{1.2}$$

where m^* is the effective mass. In crystalline solids

$$L>>a \tag{1.3}$$

where a is the lattice spacing.

1.2.0.2 The Continuous Random Network

Amorphous solids do not have a regular lattice spacing; however they can be described by the concept of a Continuous Random Network(C.R.N.).

Starting from the crystalline bond angles and bond lengths, models can be built by changing those angles and lengths by a few percent at random. The strain caused by this is made to be a minimum, but it should always be remembered that an amorphous

material will always have an higher internal energy than the corresponding crystal, which is thermodynamically stable. Large networks can be built in this way, and some properties calculable from large models have been shown to have similar properties to real materials, particularly X-ray diffraction patterns[1].

A major effect of disorder in amorphous materials is that the disorder in the lattice will increase the number of scattering events, and the lifetime in a particular state will decrease, and the mean free path will also decrease. In the limiting case of

$$L \simeq a \tag{1.4}$$

all L.R.O. is lost, and k is no longer a useful description of the electron wave function.

If we write Heisenberg's Uncertainty Principle as

$$\Delta x \Delta k \gtrsim 1 \tag{1.5}$$

where Δx is the uncertainty in position of the electron, then as one approaches the limiting position

$$\Delta x \simeq L \tag{1.6}$$

and therefore,

$$\Delta k \simeq 1/L \tag{1.7}$$

Now, from Bloch theory,

$$k \simeq 1/a \tag{1.8}$$

and dividing equation (1.7) by (1.8), we have

$$\Delta k/k \simeq a/L \tag{1.9}$$

So when $L \simeq a$, $\Delta k \simeq k$ and k is no longer a good quantum number.

1.2.0.3 Anderson Localisation

The following ideas on the Quantum Mechanical properties of

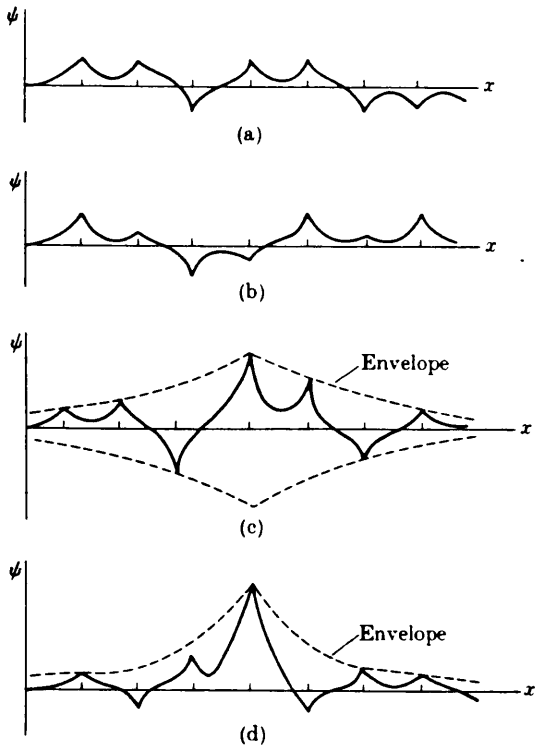

Form of the wavefunction in the Anderson model: (a) when $L \sim a$; (b) when states are just non-localized ($E \geq E_C$); (c) when states are just localized ($E \leq E_C$); (d) strong localization.

Figure 1-1: The wave function of an amorphous solid has a random phase.

non-crystalline solids are due to Anderson [2] and Mott and Davis [1]. The function k appears in the phase factor of the Bloch wave function

$$\psi = U(r).e^{-ik.r} \qquad (1.10)$$

and the wave function thus has a random phase, fig.1-1.

The periodic part of the Bloch function, U(r), needs to reflect the disorder now introduced to the solid. This is done by introducing the disorder potential, V_o.

If V_o is large enough, in the narrow band considered by Anderson, i.e.

$$V_o/B \simeq 2 \qquad (1.11)$$

where B is the band width of the narrow band, then all of the electronic states in that band will be localised, or

$$\langle\sigma\rangle = 0 \text{ at } T=0 \qquad (1.12)$$

where $\langle\sigma\rangle$ is the ensemble of the conductivity, which includes all the electronic contributions to it.

Although equation (1.12) holds for all semiconductors, note that when localisation occurs, it also holds for amorphous metals.

1.2.0.4 The Origin of the Mobility Gap

The idea of the Anderson transition has been extended to that of a Tight Binding wide band. Here the concept of B no longer applies, and the quantum mechanical transfer integral, I, is used instead. The new criterion for localisation is now the value of

$$(V_o/I)_{crit} \qquad (1.13)$$

But I is dependent on energy, as

$$I \propto e^{-\alpha R} \qquad (1.14)$$

where α is a constant and R is the separation of the overlapping orbitals which is shown to be a function of energy in the following manner.

At the band edges, the density of states, g(E) is small. (g(E)dE is the number of states per cubic cm. in the energy range E to E+dE.)

If g(E) is small, then the states will be, on average, far apart in space, and R(E) will be large. Consequently I is smallest in the band edges and the critical value for Anderson localisation,

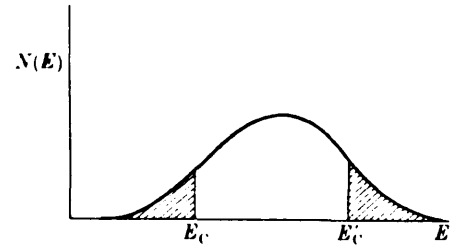

Density of states in the Anderson model when states are non-localized in the centre of the band. Localized states are shown shaded. E_C, E'_C separate the ranges of energy where states are localized and non-localized.

Figure 1-2: The wave functions firstly become localised in the tail states.

eq (1.13) will firstly be reached in the tail states,fig.1-2.

1.2.0.5 Band Structure of an Arbitrary Amorphous Material

The major features of the band structure of amorphous materials can now be considered. As usual one considers the upper filled band, the valence band; and the lowest empty band, the conduction band. A representation of the top and bottom of those bands is shown in fig. 1-3. Mott and Davis [1] show that at a given energy, localised and extended states cannot coexist. This has the consequence, implied in fig.1-3, that a region of localised states in the tails of their respective bands separate two regions of extended states. Clearly the mobility of an electron in the region of localised states will be considerably lower than the mobility in the region of extended states (fig.1-3).

The energy which separates localised and extended states is therefore called the mobility edge, and the range of energy which

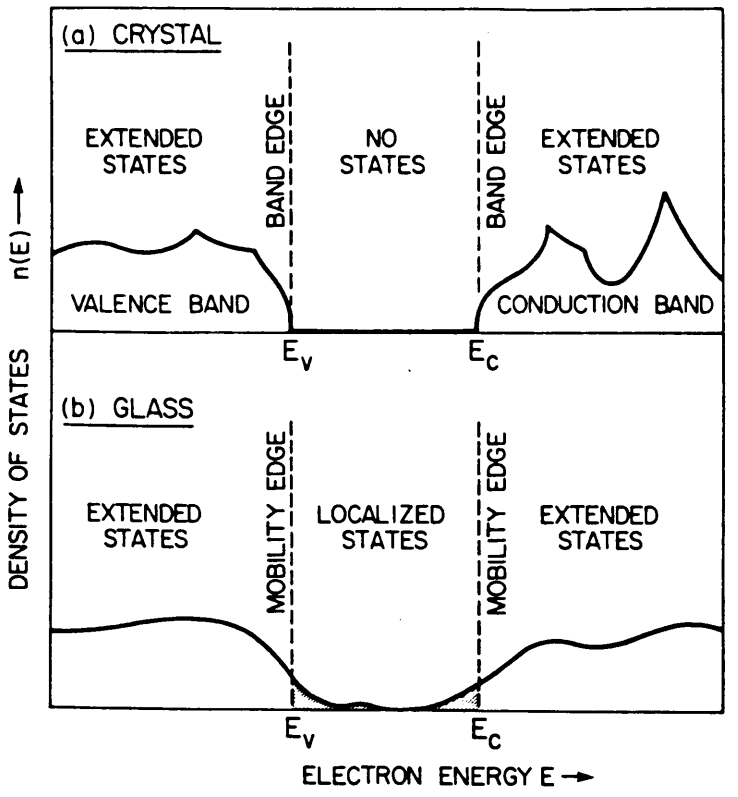

Schematic density-of-states diagram for a crystalline and an amorphous semiconductor, in the vicinity of the highest occupied and lowest empty states. $n(E)dE$ is the number of electron states, per unit volume, with energies in the interval from E to $E + dE$. With respect to many electrical properties, the mobility edges in the amorphous solid play a role analogous to that played by the band edges in the crystal.

Figure 1-3: A pseudo-gap of localised states exists in amorphous solids.

encompasses the localised states is called the mobility gap. Analogously to the crystalline case, the conduction band mobility edge is given the symbol, E_c; and at the valence band, E_v.

In the case of crystalline materials, the carriers are excited from the valence band into the conduction band across the forbidden gap, which is a region of zero density of states. However in amorphous materials the carriers are excited across the mobility gap, which can be considered as a region of negligible mobility, although at low temperatures hopping conduction in the mobility gap is important.

1.2.0.6 Occupation Statistics

The concept of the Fermi Energy (E_f) remains in amorphous material theory, and the electron occupation of states is still described by the Fermi-Dirac distribution function

$$f(E)=1/(\exp[(E-E_f)/kT]+1) \qquad (1.15)$$

where the symbols have their usual meanings.

1.2.0.7 Extended State Dark Conductivity

Thus the carrier density near E_c is written as

$$n=N_c\exp[-(E_c-E_f)/kT] \qquad (1.16)$$

where N_c is the effective density of states in the conduction band.

At high temperature, when the conductivity ensemble is mainly dominated by carriers in extended states, we can write[3]

$$\sigma=\sigma_o\exp[-(E_c-E_f)/kT] \qquad (1.17)$$

where σ_o is a constant of proportionality. σ_o has physical significance in that its magnitude can indicate the conduction mechanism, a relatively high value of about 100 cm^{-1} indicates extended state conduction.

1.2.0.8 Low Temperature Hopping Conductivity

At lower temperatures the major contribution to the conductivity will be from localised states, when the higher occupation of those states begins to outweigh their lower mobility.

In localised states, transport is due to phonon-assisted hopping, as shown by Mott and Davis[1] from work by Miller and Abrahams. Two types of hopping can be described.

Firstly hopping between nearest neighbours in the tail

states, when

$$\sigma = \sigma_1 \exp[-(E_H - E_f + W)/kT] \qquad (1.18)$$

E_H is the energy through which most of the hopping occurs, and W is a hopping energy of 0.1 to 0.03eV. Note that σ_1 is not the same as σ_0, indeed σ_1 is the lower, which is an indicator for the presence of hopping conduction. The temperature shift of the Fermi Level is ignored for simplicity.

Secondly, hopping can occur between nearest neighbours at the Fermi Level, when temperatures are lower than in the previous case. Then

$$\sigma = \sigma_2 \exp[-2\alpha R_o . -W/kT] \qquad (1.19)$$

where α is a constant and R_o represents the average distance between nearest neighbours.

1.2.0.9 Variable Range Hopping

At the lowest temperatures, Mott predicts[4] variable range hopping behaviour, where an electron will jump much further than the distance to the nearest neighbour if the energy difference between initial and final site is small. In this case

$$\sigma = \sigma_3 \exp[-(T_o/T)^{1/4}] \qquad (1.20)$$

1.3 Density of States

A knowledge of the density of states in the mobility gap is necessary in order to calculate the magnitude of such phenomena as photoconductivity. Photogeneration of carriers proceeds at a constant rate, dependent on measureable quantities such as illumination intensity, optical absorbtion coefficient, α, and quantum efficiency. Recombination, however, depends on the density

of recombination centres, which can not be measured directly.

Unfortunately it has not yet been possible to establish a fully accepted density of states for any amorphous material, but the past and current models are reviewed in this section.

1.3.1 The C.F.O. model

The C.F.O. model was an early attempt to show how the Fermi level in an amorphous semiconductor could be pinned [5]. It was originally postulated for multi-component chalcogenide glasses although the scope of the model has since been extended to other materials.

This model considered the tail states in the amorphous material to be so broadened by disorder that they overlapped in the middle of the gap fig.1-4. The states tailing off from the valence band are neutral when occupied, and are therefore positively charged when empty. So the part of the valence band curve above the Fermi energy will consist of positively charged tail states, as states above E_f are substantially empty. Likewise the conduction band tail states, neutral when empty, will be negatively charged below E_f, where those states are substantially full. The position of the Fermi level, which is determined by the necessity for overall charge neutrality, is pinned near mid gap by the charged tail states.

This model survives to the present day, somewhat modified, in the Spear-LeComber model, and the Exponential Tail model.

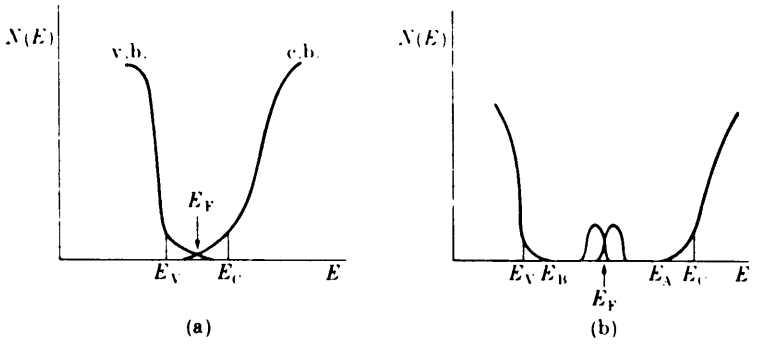

Density of states in amorphous non-crystalline semiconductor: (a) model ofCohen *et al.* (1969) (CFO model); (b) with states in the gap due to dangling bonds acting as deep donors below acceptors.

Figure 1-4: Two Models of the Density of States

1.3.2 The Davis-Mott model

Because it was not thought that the band tails would spread out enough to overlap, especially in the more rigid a-Si lattice, the model of Davis and Mott was proposed[1] fig.1-4. There is some tailing of the band edges into the gap, but E_f is pinned by the presence of defect states near mid gap. These states are caused by unsatisfied, or dangling bonds in the C.R.N.

1.3.3 The Spear-LeComber model

This model was postulated by the Dundee group from field effect measurements taken from different samples doped to move the Fermi energy throughout the mobility gap[6, 7]. The density of states was shown as having a finite value throughout the mobility gap, fig.1-5 containing two major features:

(1) Peaks in the density of states curve at E_x and E_y. These peaks are associated with traps detected in drift mobility studies[8]

and in photoconductivity studies[9, 10]. Goodman and Fritzsche[11] using field effect have confirmed the peak at E_y, but not that at E_x.

(2) A low density of states in the centre of the gap in amorphous silicon prepared by glow discharge decomposition, of about $10^{17} cm^{-3} eV^{-1}$. This suggested that amorphous silicon could be doped, which was verified experimentally[12]. It has been suggested[13] that the reduction in the density of states using this method of preparation is caused by the presence of hydrogen in the plasma, which reduces the number of mid gap defects by chemically combining with the silicon dangling bonds, and analysis of a-Si films of good electrical properties shows that they contain from 5% of hydrogen atoms. The material has thus been referred to as a-Si:H to indicate the importance of the hydrogen to its properties.

An interesting feature of the model is that the gap features E_x and E_y tail off towards the centre of the gap and form overlapping charged states in the manner of the C.F.O. model. This concept has been used to explain the photoconductive properties of doped a-Si[14].

1.3.4 Models using Exponential Tails

These models can be considered to be extensions of the C.F.O. model. The featureless logI vs. logt plots obtained by transient photoconductivity measurements on some materials in the dispersive transport regime [15, 16] have lead some authors to deduce that the states with which the free carriers interact during the time scale

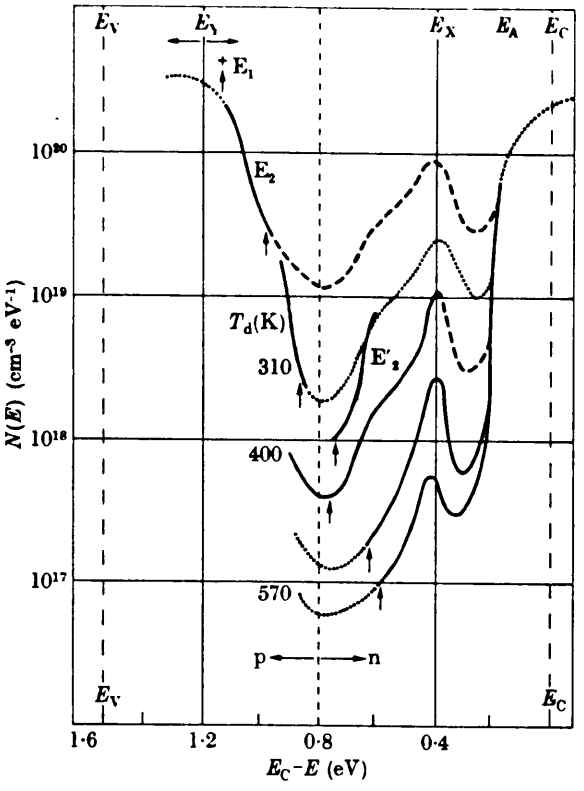

Figure 1-5: The Spear-LeComber model of the density of states.

of the experiment are distributed exponentially with energy, i.e.

$$g(E) = g_o \exp(-E/kT_c) \qquad (1.21)$$

where E is measured from the appropriate band and T_c is called the characteristic temperature of the band tail, which is a measure of its steepness.

This model assumes that electrons trapped in shallow states come into quasi-equilibrium with the extended states first, and deeper states progressively come into equilibrium during the time scale of the experiment. A demarcation energy separating equilibrium and non-equilibrium states is given by

$$E_D = kT \ln \omega t \qquad (1.22)$$

where ω is an attempt to escape frequency, about 10^{12}Hz.

If a transient is featureless from time t_1 to t_2, then an exponential tail is deduced in the range E_1 to E_2.

Rose[17] has predicted that the intensity dependence of the steady state photoconductivity for a material with an exponential tail and a discrete level of recombination centres will be of the form

$$I \propto G^{\gamma} \qquad (1.23)$$

where G is the incident photon intensity, and

$$\gamma = T_c/(T+T_c) \qquad (1.24)$$

where T_c is the characteristic temperature.

Kastner and Monroe[18] report this in a-As_2Se_3, and Hack[19] for a-Si.

1.3.5 Models using the Concept of Correlation

Chalcogenide glasses do not exhibit an e.s.r. signal and variable range hopping is not observed: these suggest that chalcogenides have a low density of states at E_f. A.C. hopping is observed, and chalcogenides are very difficult to dope: these suggest that chalcogenides have a high density of states at E_f.

These apparently opposing statements have been reconciled by the application of the concept of negative correlation energy to amorphous chalcogenide materials. Although a-Si is not thought to exhibit negative effective correlation, the phenomenon has

importance in photoconductivity studies.

Correlation was firstly applied to amorphous materials by Anderson[20] who first suggested that states in the gap in amorphous chalcogenides might have negative effective correlation energy. This idea was further developed by Mott, Davis and Street [21, 22], and from a slightly different point of view by Kastner, Adler and Fritzsche [23, 24, 25].

1.3.5.1 Coordination and Charge State in a-Se

Consider chains of amorphous selenium. The Se atoms at the ends of the chains are only bonded to one other atom, and as Se is divalent, there is therefore an unpaired electron (called a dangling bond) on the end of each chain. Each of these defects contains one electron, and is electrically neutral, so it is designated a D^o state. If an electron is transferred from one end of the chain to the other, a positively charged D^+ state and a negatively charged D^- state will be formed. The basis of the theory is that the reaction

$$2D^o \rightarrow D^+ + D^- \qquad (1.25)$$

is exothermic. Clearly the first electron in the D^o state will repel the second by Coulombic repulsion, and D^- will be higher in energy than D^o by the positive correlation energy U_c. But the D^+ state can interact and form a chemical bond with a lone pair on another selenium atom. The energy liberated by this step is required to be greater than U_c to give a net negative effective correlation energy, U_{eff} for reaction fig.(1.25) to be exothermic. The D^+ state is therefore three fold coordinate fig.1-6, and the lattice distortion associated with its formation is held to cause

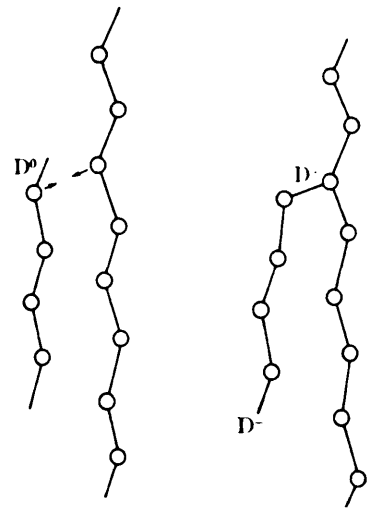

Figure 1-6: The defects have various coordination numbers.

(1.25) to be exothermic in amorphous chalcogenides. Mott et. al. suppose that distortion of the lattice increases from a little in the D^- state to an intermediate value in the D^o state and to a high level in the D^+ state. Note that the Se atoms in the D^- and D^+ states possess a stable octet of valence electrons, and all the electrons are in pairs. Therefore no e.s.r. signal will be observed in amorphous chalcogenides if the concept of negative effective correlation energy is applicable, and variable range hopping is unlikely, as electrons will have to hop in pairs. A.C. conductivity will be possible, as the electrons only have to hop

back and forward in pairs.

1.3.5.2 Extension of the Theory to Arbitrary Materials

D^+, D^o and D^- can be considered as different charge states (none, one or two electrons) of the same defect, allowing the discussion to be extended generally to amorphous materials by ignoring the real nature and coordination of each defect.

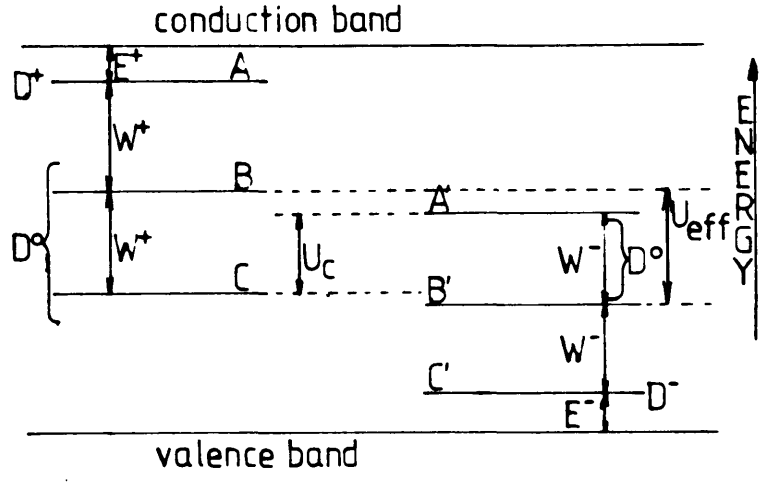

Figure 1-7: The energy level diagram to take correlation into account.

1.3.5.3 Energy Level Diagram for the Correlated System

A rather complicated energy level diagram can be drawn for this system fig.1-7, which is explained by reference to the configuration-coordinate diagram in fig.1-8. First consider the possible transitions between the valence band and the D^+ state fig.1-8; E_A is the optical exitation energy and E_C the optical relaxation energy; they differ because of lattice relaxation, and are drawn vertically in the diagram because of the Franck-Condon principle. E_B represents the total difference in energy between ground and excited states, the energy of thermal excitation. W^+,

the lattice relaxation energy is assumed to be unchanged for both states. In fig.1-7 E_A is represented by level A; E_B by level B; E_C by level C. Note that the lines on fig.1-7 do not represent one-electron energy levels, but transitions on fig.1-8.

Now consider the possible transitions between the conduction band and the D^- state. To optically excite an electron from the D^- state into the conduction band to create a D^o state absorbs energy E_C^1 in fig.1-8, and is represented by level C^1 in fig.1-7. Optical relaxation emits energy E_A^1, represented by level A^1, and thermal relaxation or excitation involves energy E_B^1 and level B^1.

Level A represents the D^+ state, as energy E_A is required to create a D^o state optically. Levels B and C represent the D^o state as they represent thermal and optical relaxations respectively, creating the D^+ state from D^o. Likewise level C^1 represents the D^- state and levels B^1 and C^1 represent D^o states.

Now consider the transition $D^+ \rightarrow D^o \rightarrow D^-$ with lattice relaxation. The first step requires energy equivalent to level B in fig.1-7, but the second step requires energy equivalent to level B^1, which is drawn lower than B. Addition of a second electron to the same defect has required less energy than the first. This is what is meant when one says that defects can have negative effective correlation energy, U_{eff} represented by $B-B^1$.

Now consider reaction (1.25) without lattice relaxation. Consider excitation of the D^o state to give a D^+ state and an

Figure 1-8: The configuration-coordinate diagram for systems with lattice relaxation

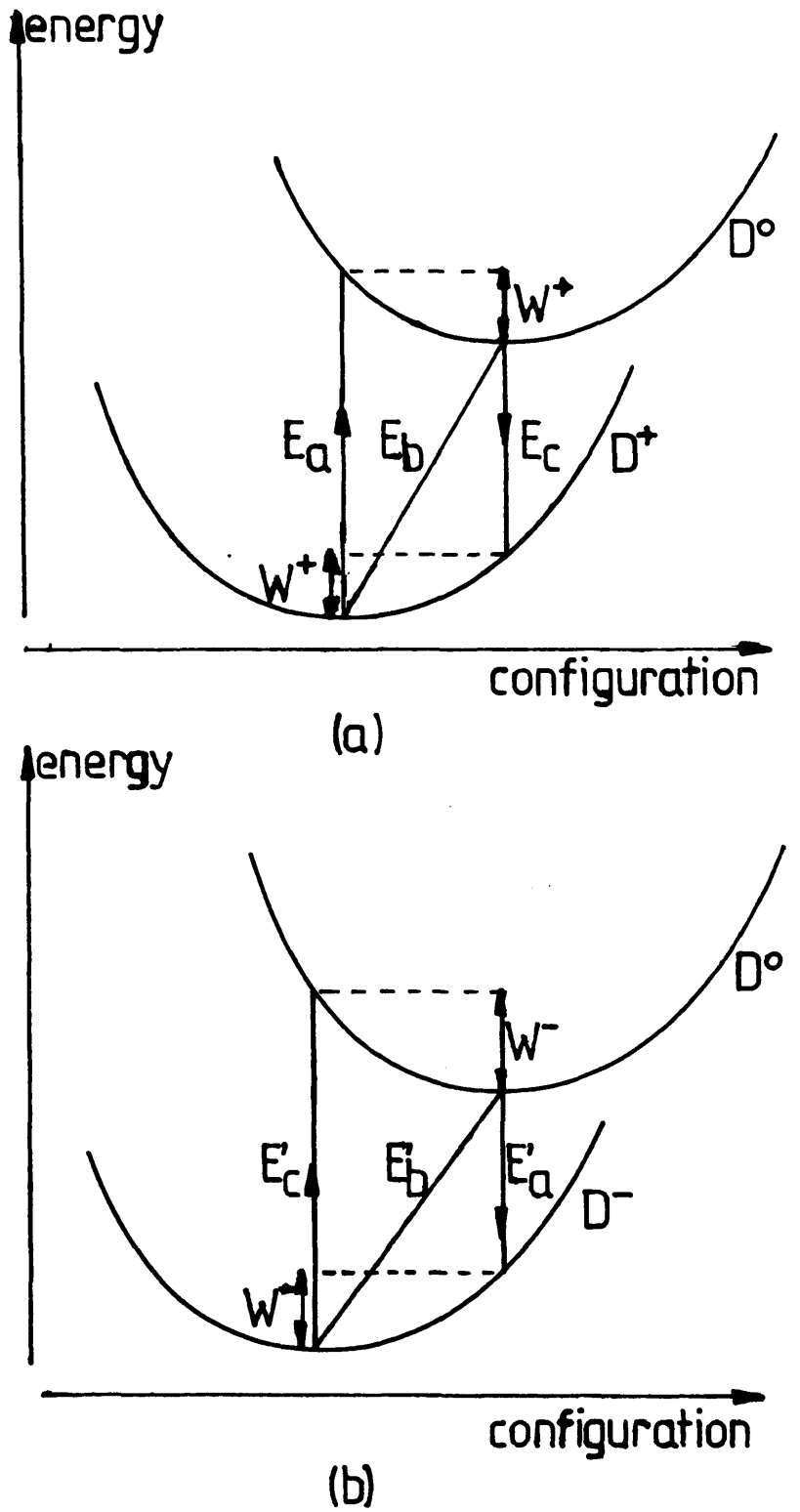

electron in the conduction band; this requires energy E_g-C. But to create a D^- state from a transition of an electron from the conduction band into a D^o state emits energy A^1. So the difference in energy between A^1 and C represents the energy required to overcome Coulombic repulsion as the second electron is added to the system, and the real positive correlation energy is given by

$$U_c=A^1-C \tag{1.26}$$

An important result of this theory is that for negative U_{eff}, the Fermi energy is pinned. To take one electron from the D^- state and place it in the conduction band, we need to add energy equivalent to E_g-B^1: but to take the second electron from the same defect, now a D^o state, we need energy equivalent to level B. The energy per electron is thus

$$(E_g-B^1+B)/2 \tag{1.27}$$

which is , of course equivalent to E_c-E_f, and E_f is therefore midway between B^1 and B,[26].

A consequence of this is that chalcogenides are difficult to dope, as extra electrons from the donors will convert D^+ states to D^- states as the electrons are absorbed in pairs, equivalent to stating that extra charge carriers are compensated by the establishment of a change in the number of D^+ or D^- states from their equilibrium densities[27]. Only impurities which destroy or neutralise defect states of one sign and that can cause virtually all of the defect states of that sign to disappear will unpin E_f and allow doping of chalcogenides to occur.

Chapter 2

Introduction to Photoconductivity

2.1 Introduction

Various models of the density of localised states in a-Si have been given in the last chapter. As the density of states profile is a controversial subject, a reliable technique to measure it is required. Photoconductivity is such a technique. Steady state photoconductivity measurements, as shown later, can give information on the trapping parameters and localised state distribution over a large range of energy about E_f, which is only restricted by the experimentally achievable illumination intensity and minimum temperatures available. Transient measurements can probe the band tails, if the measuring apparatus has a sufficiently short response time. Furthermore, if a suitable wavelength of light is used, the measured photocurrent is a bulk property, unlike other experiments such as field effect.

2.2 Interaction of Semiconductors with Light

2.2.1 Introduction

It is a consequence of the band structure of a semiconductor that it can absorb light. If a photon of energy $h\nu$, greater than the energy gap, E_g, is incident on a semiconductor, it may be absorbed and its energy may excite an electron from the valence band to the conduction band. The photo-excited electron and hole pair is available to carry an electric current as do the thermally excited carriers. Because of the excess current observed in an illuminated

material of this type, it is said to be photoconductive, and the excess conductivity over that in the dark is called the photoconductivity.

2.2.2 Optical Absorption

Optical absorption is a quantum mechanical process. As with other quantum events, one has to deal with probabilities of electron transitions, quantum mechanical selection rules and densities of states before transition rates can be calculated. However, as the wave functions of amorphous materials are not known exactly, an empirical approach is often used.

As the rate of absorption of the photons is proportional to the intensity, then Beer's Law applies,

$$I(x)=I_0\exp(-\alpha x) \qquad (2.1)$$

where $I(x)$ is the intensity at x, in photons/cm^2, I_0 is the incident intensity, and α is the optical absorption coefficient with units of reciprocal length.

α is frequency dependent for the following reason. In a pure crystalline semiconductor, if the energy of the photon is less than E_g, then it cannot be absorbed, and $\alpha=0$. If $h\nu$ is slightly greater than E_g, then the joint density of states will be small, as $g(E)$ is small at the band edges. The transition probability will increase as $h\nu$ increases above E_g when the total numbers of initial and final states are very much greater. α increases with photon energy(when $h\nu \simeq E_g$), and the threshold of absorption can be used to give E_g.

Amorphous semiconductors have substantial densities of

localised states within the mobility gap, and transitions involving localised and extended states as initial and final states can occur, fig2-1.

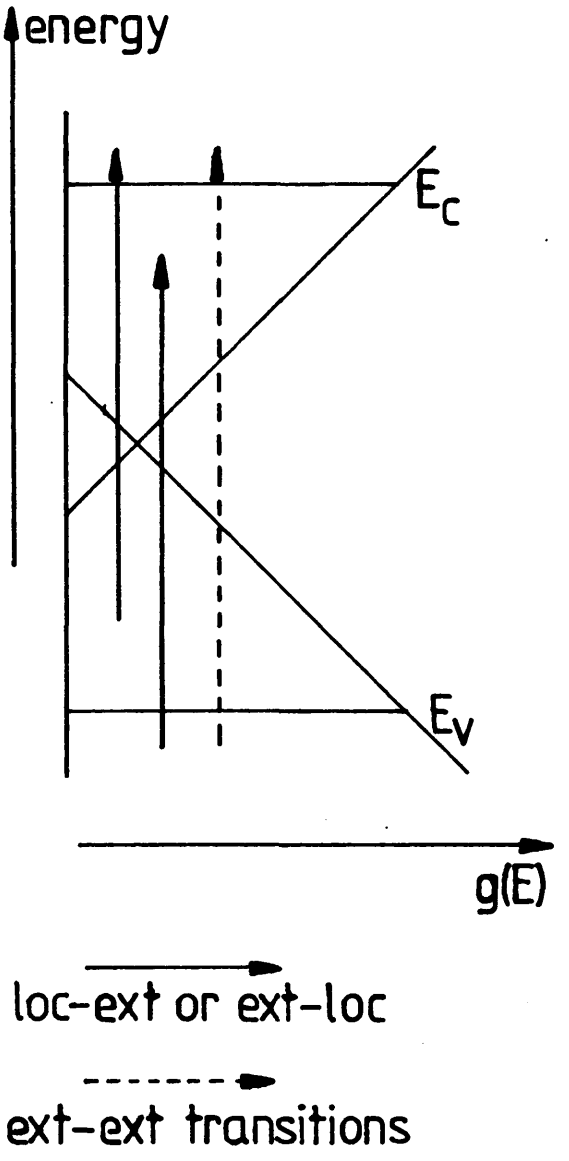

Figure 2-1: Optical Absorption in Amorphous Materials

These are photon absorbing transitions and also cause photoconductivity, so the threshold of optical absorption is not sharp in amorphous semiconductors, and it is not so easy to find the mobility gap in this way as the band gap above. Note that in this

case only one of the photo-excited carriers is in an extended state, and the other is in a localised gap state. In fact, as reviewed in Brodsky[28], amorphous semiconductors with exponential tails have been observed to have the so-called Urbach edge of absorption below the onset of extended state absorption, i.e.

$$\alpha(\omega) = \text{const.} \exp[-\beta(E - h\omega)] \qquad (2.2)$$

where β is a constant.

Also the same reference shows that if parabolic band edges are assumed,

$$\alpha = (h\omega - E_o)^2 \qquad (2.3)$$

where E_o is the value of the mobility gap. A plot of $(\alpha h\omega)^{1/2}$ vs. $h\omega$, fig.2-2 can give a value of E_o from the straight line portion of the graph.

2.2.2.1 Inhomogenous Absorption

The effects of inhomogenous absorption may complicate the interpretation of photoconductivity measurements, e.g. resulting in different pathways for dark currents and photocurrents. In addition, lifetimes may be excitation dependent, and therefore position dependent.

I(x) decreases exponentially, and this causes the photoconductivity to vary with depth. This effect will not be observed if the wavelength of the light is chosen such that it has an absorption depth of at least the sample thickness. Also, if the diffusion coefficients of the carriers are such that their diffusion lengths are greater than the sample thickness, lateral excess density variations will be reduced. Another cause of thickness

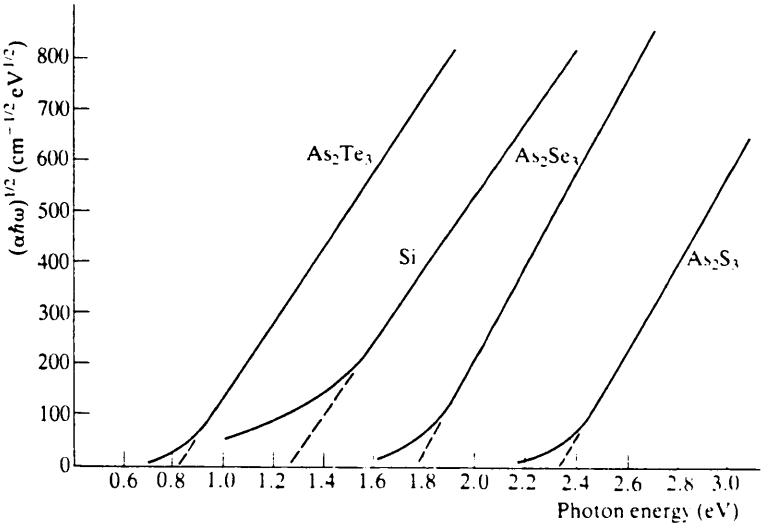

Figure 2-2: Graphical Determination of the Mobility Gap

dependent photoconductivity is the possible presence of band bending at the surface. The analytical treatments used below assume homogeneity, but possible effects of non-uniform excitation and diffusion will be examined in Chapter 8.

2.3 Steady-State Photoconductivity

2.3.1 General

For background reading on this broad subject, two definitive references are Ryvkin[29] and Rose[17].

When the optical absorption described in the previous section produces free carriers, the electrical conductivity of the material

is increased. Assuming for the moment, a negligible hole contribution, the thermal equilibrium conductivity is

$$\sigma_o = n_o e \mu_o \tag{2.4}$$

Then under illumination

$$\sigma = ne\mu \tag{2.5}$$

where $\sigma = \sigma_o + \Delta\sigma$ and $n = n_o + \Delta n$ and $\mu = \mu_o + \Delta\mu$.

Subtracting the previous two equations gives an expression for the photoconductivity

$$\Delta\sigma = \sigma - \sigma_o = \Delta n e \mu_o + n e \Delta\mu \tag{2.6}$$

It is usually assumed that the mobility of the carriers is not changed by the photo-excitation process. If an electron is excited into the conduction band at an energy considerably higher than the band edge, the excess energy over E_c is lost by emission of phonons until an energy of order kT in excess of the band edge is attained. This excess energy is lost in about 10^{-10}s, or less. At longer times the excess and equilibrium carriers have the same energy distribution near the band edges, and all the other electronic properties are therefore expected to be the same.

The above account can be used analogously to describe equilibrium and photo-generated holes. In most accounts of photoconductivity, only one carrier is assumed to be mobile, i.e. unipolar conduction. Nonetheless, large densities of the minority carrier are produced, and they play an important rôle in recombination. In this account the photoconductivity is considered to be dominated by electrons.

2.3.2 Lifetime

If the excess electron generation rate is uniformly G $cm^{-3}s^{-1}$ throughout the sample, the excess carrier density n is given by

$$\Delta n = G\tau_n \tag{2.7}$$

where τ_n is called the lifetime of the photo-generated carriers.

A change in n can occur either by a change in τ_n or G. If τ_n is independent of G, i.e.

$$\Delta n \propto G \tag{2.8}$$

then the photoconductivity is said to be monomolecular, or linear. However if the previous equation does not hold, and the lifetime is not constant with G, then we have superlinear or sublinear photoconductivity. Substituting (2.7) into (2.6) gives

$$\Delta\sigma = Ge\tau_n/\mu_o \tag{2.9}$$

if constant mobility is assumed, and the photoconductivity is proportional to the lifetime-mobility product.

Furthermore, in materials that contain shallow traps the possibility of two definitions of mobility must be taken into account.

Firstly the free carrier mobility, the drift velocity of the free carrier per unit field, needs to be associated with the free lifetime, the average time that a carrier spends in the conduction band before recombination.

Secondly the effects of trapping can be taken into account. If shallow traps are present, then for most amorphous materials, at any one instant the majority of excess carriers will be in traps.

So if n free carriers are in the band, and n_t are in traps, then the trap limited mobility μ_D is defined as

$$\mu_D=\mu_o(n/(n+n_t)) \qquad (2.10)$$

If the carriers spend a considerable time in traps, and only free carriers recombine, the effective ensemble lifetime will be greater than the free carrier value. The appropriate mobility-lifetime products are equal. The time that the carriers spend in traps has consequences for the speed of response of the semiconductor to a change of light level, as the traps have to empty or fill in response to any disturbance in illumination.

2.3.2.1 Quantum Efficiency

Not every absorbed photon gives rise to a free electron-hole pair, as a localised-extended state carrier pair may be created, only one of which is free, or geminate recombination may occur. The quantum efficiency, η, is the fraction of absorbed photons which create a photoconductive electron-hole pair. So equation (2.6) can be written

$$\Delta\sigma = F\eta\tau_n\mu_o e \qquad (2.11)$$

where F is the total number of incident photons per second per unit volume.

2.3.3 Shockley-Read Statistics

Fermi-Dirac statistics no longer apply to a semiconductor under illumination. The occupation statistics under non-equilibrium conditions were first set out for a mono-energetic set of localised states by Shockley and Read[30]. This has been put forward very clearly by Simmons and Taylor[31], and extended to the case of an

arbitrary distribution of traps.

The photoconductive processes described here involve the so called Shockley-Read-Hall type of recombination, which assumes that each electron trap is in contact by trapping and release with both band edges. Although the rate of electron capture and release is more rapid with the nearest band, recombination is a two step process. If an electron is trapped at a defect state, then subsequent hole capture constitutes a recombination event. Note there is no difference between viewing the event as described above or as a two stage electron transition. Therefore all transitions on an energy level diagram can be drawn as electron transitions.

Fig.2-3 shows the processes that determine trap occupancy in a trap at arbitrary energy E_t. Band to band recombination is ignored. Process a is the capture of a free electron in the conduction band by the trap. If one considers ballistic capture and the trap has a capture cross-section σ_n for electrons moving with thermal velocity v_{th}, a volume of

$$C_n = \sigma_n v_{th} \tag{2.12}$$

is probed by the trap per second. C_n is called the capture coefficient for electrons, which will be different from that for holes, as the charge state of the trap will strongly influence the capture cross-section. The rate of process a is given by

$$r_a = C_n n N_t (1-f(E_t)) \tag{2.13}$$

where n is the density of free electrons in the conduction band, N_t is the density of traps per unit volume, and $(1-f(E_t))$ represents the fraction of empty traps, which must be included as only an empty

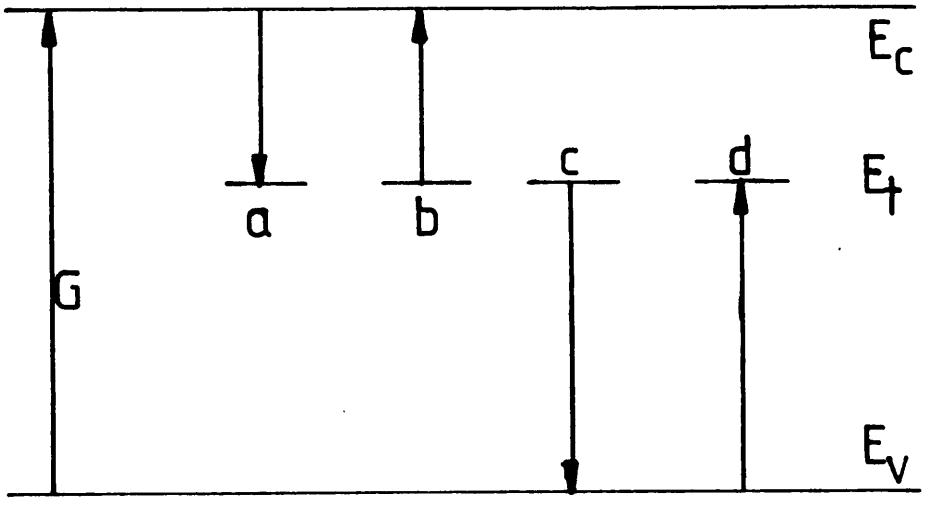

Figure 2-3: The Transitions Occurring for an Arbitrary Trap

trap can capture an electron, i.e. we consider one electron states.

Process b is the emission of electrons from the trap to the conduction band, which proceeds at the rate

$$r_b = e_n N_t f(E_t) \tag{2.14}$$

where e_n represents the emission probability of electrons from the trap.

Similarly the capture of holes from the valence band, rate c is given by

$$r_c = C_p p N_t f(E_t) \tag{2.15}$$

Where C_p is the capture coefficient for holes, and the rate of emission of holes to the valence band, rate d is

$$r_d = e_p N_t (1-f(E_t)) \tag{2.16}$$

In thermal equilibrium the concept of detailed balance applies,

$$r_a=r_b \text{ and } r_c=r_d \tag{2.17}$$

Using the left hand equality gives

$$e_n=C_nN_c\exp(-(E_c-E_t)/kT) \tag{2.18}$$

It is convenient to use

$$n_1=N_c\exp(-(E_c-E_t)/kT) \tag{2.19}$$

so

$$e_n=C_nn_1 \tag{2.20}$$

Similarly,

$$e_p = C_pN_v\exp(-(E_t-E_v)/kT) \tag{2.21}$$

and

$$p_1=N_v\exp(-(E_t-E_v)/kT) \tag{2.22}$$

so

$$e_p=C_pp_1 \tag{2.23}$$

The emission of electrons can also be regarded as follows

$$r_b=n_t\nu\exp(-(E_c-E_t)/kT) \tag{2.24}$$

where n_t is the density of occupied traps and ν is the so called attempt to escape frequency which is expected to have an upper limit of a phonon frequency, about 10^{12}Hz. If eq.(2.19) is substituted into (2.14), then one finds

$$C_nN_c=\nu \tag{2.25}$$

That is to say the attempt to escape frequency is proportional to the capture coefficient.

2.3.3.1 The Occupancy Statistic

In steady state conditions under illumination the occupancy of any trap will be constant, so the four electron transitions which fill and empty the trap will be in balance and

$$r_a - r_b - r_c + r_d = 0 \qquad (2.26)$$

or

$$C_n n N_t (1-f) - C_n n_1 N_t (1-f) - C_p p N_t f + C_p p_1 N_t (1-f) = 0 \qquad (2.27)$$

f is used instead of f(E) to indicate that the system is no longer in thermal equilibrium, and eq.(2.27) can be solved to give

$$f = (C_n n + C_p p_1)/(C_n n_1 + C_n n + C_p p + C_p p_1) \qquad (2.28)$$

Note that this expression can be applied to arbitrary trap distributions, and is not limited to the original Shockley-Read case of a single level.

2.3.3.2 Trap Species

A particularly surprising consequence of eq.(2.28) is that f may be multivalued. If three traps with three different capture cross sections exist at the same energy, then f will have three different values. Also a distribution of traps could have different capture cross sections for holes and electrons throughout the distribution, and they would need different distribution functions. However, if the ratio of the cross sections for electrons and holes is constant

$$R = \sigma_n(E)/\sigma_p(E) \qquad (2.29)$$

then eq(2.28) shows that this system is described by a single distribution function f. A particular value of R defines a <u>species</u> of trap. $\sigma_p(E)$ and $\sigma_n(E)$ may be constant with E, or may vary with E in such a manner that R is constant with energy to define a species.

2.3.3.3 Statistics for a Single Trap Species

Fig.2-4 shows a plot of eq.(2.28) as a function of energy for a single species of trap, before and after illumination. In the

dark, the occupation is determined by Fermi-Dirac statistics. Under illumination the electron occupation above the dark Fermi level E_{fo} has increased substantially, and the occupation below E_{fo} has decreased substantially.

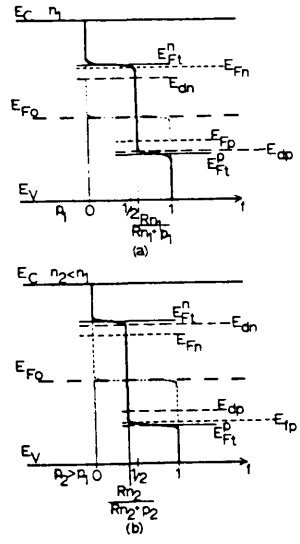

Two typical occupational functions for an arbitrary distribution of traps.

Figure 2-4: Occupation Functions for an Arbitrary Distribution of Traps

Above E_{fo} the occupation of the traps under illumination is shown to be

$$f = \frac{C_n n}{(C_n n + C_p p)} \left\{ \frac{1}{1 + \exp\left[(E_t - E_{ft}^n)/kT\right]} \right\} \tag{2.30}$$

where E_{ft}^n is defined by

$$C_n N_c \exp[(E_c - E_{ft}^n)] = C_n n + C_p p \tag{2.31}$$

The trap occupation is therefore a Fermi-Dirac function about E_{ft}^n with a modulating factor $C_n n/(C_n n + C_p p)$, which is a constant for any one light intensity. The energy E_{ft}^n is defined as the quasi-Fermi

level for trapped electrons, or the trap quasi-Fermi level, and traps higher in energy are occupied according to a Boltzmann function

$$f = Rn(Rn+p)^{-1}\exp[(E_t-E_{ft}^n)/kT] \tag{2.32}$$

and are in quasi thermal equilibrium with the conduction band.

Below E_{ft}^p the traps are occupied to a constant level given by

$$f = Rn/(Rn+p) \tag{2.33}$$

The quasi Fermi level for free electrons is defined by

$$n=N_c\exp[-(E_c-E_{fn})/kT] \tag{2.34}$$

so by inspection

$$E_{ft}^n > E_{fn} \tag{2.35}$$

at all times under steady state illumination. The two quasi-Fermi levels are the same in thermal equilibrium.

For energies below E_{fo} it is more appropriate to use the fraction of empty traps, 1-f, and the hole occupation can be calculated analogously to the case for electrons, giving the following results.

$$1-f = C_p p/(C_n+C_p).\left\{\frac{1}{1+\exp\left[(E_t-E_{ft}^p)/kT\right]}\right\} \tag{2.36}$$

Below the hole trap quasi-Fermi level, the traps are filled with holes according to a Boltzmann function

$$1-f = p/(Rn+p)\exp[(E_{ft}^p-E_t)/kT] \tag{2.37}$$

and above the trap quasi-Fermi level for holes, they are filled with

holes to a constant level given by

$$1-f = p/(Rn+p) \qquad (2.38)$$

Analogously to the case for electrons a free hole quasi Fermi energy can be defined as

$$p=N_v\exp(-(E_{fp}-E_v)/kT) \qquad (2.39)$$

For the holes, the trap quasi-Fermi level is always less than the quasi Fermi level for free holes and the two levels are equal under the case of no illumination.

Examination of fig2-4 shows that the area above E_{fo} that has increased its occupation under illumination is equal in size to the area below E_{fo} that has decreased its occupation under illumination. This is a consequence of charge neutrality.

2.3.3.4 Occupation with Distributed States

Interestingly, if the density of states varies exponentially at the band edges, then an excess concentration of electrons occurs substantially around one energy value, and likewise for holes. This is because although f is constant between the two trap quasi-Fermi levels, the density of states is decreasing exponentially on the lower side and the occupancy falls exponentially on the upper side.

For constant T, if the intensity of illumination increases, then the quasi-Fermi levels become closer to the band edges. If they reach the band edges, then there is a constant occupancy throughout the gap, for a given species. Decreasing the temperature has the same effect, for constant illumination. At absolute zero, the occupation again becomes a constant throughout the gap.

Remember that each species has its own values of trap quasi-Fermi levels, etc. and must be examined separately. However in the literature pertaining to real materials, it is often assumed that only one species is present.

In Chapter 8 of this work, it is shown that a single species model is inadequate to describe the photoresponse in undoped a-Si.

2.4 Analysis of a Two Level System

2.4.1 Introduction

This analysis is one of the simplest that can predict qualitatively the photoresponse of an amorphous semiconductor. As such it provides a relatively simple introduction to Shockley-Read-Hall recombination. A second reason for its inclusion here, is that in the high light intensity regime, this model successfully predicts the photoresponse of undoped a-Si. The general features of the photoconductive behaviour of an amorphous semiconductor are described first.

2.4.1.1 General Photoconductive Response

In fig.2-5 can be seen the general features of the graph of photoconductivity plotted against intensity. At low intensities, region I, the gradient of the double logarithmic plot is unity, and recombination is described as monomolecular. For higher intensities, region II, the gradient is less than unity, and recombination is said to be bimolecular if there is a gradient of exactly 0.5 This commences when the excess photoconductivity approaches the equilibrium dark conductivity. Finally, region III

is often observed where the the photoresponse is linear with intensity.

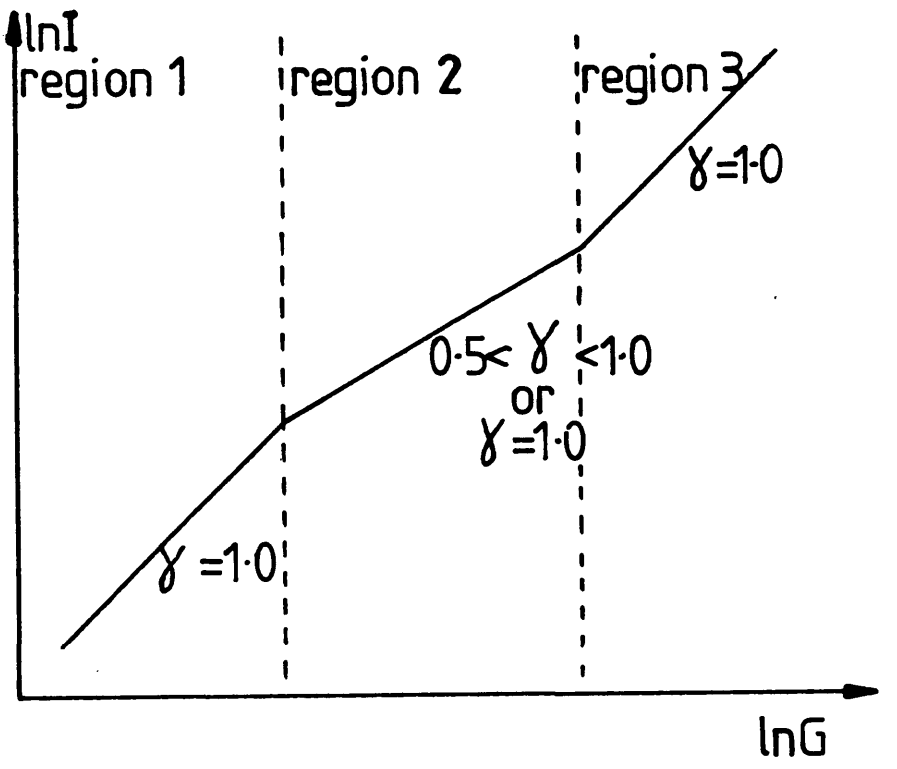

Figure 2-5: The General Shape of the Intensity Dependance of the Steady State Photoconductivity

The figure2-6 shows the usual Arrhenius plot of the photoconductivity. Regions I, II, and III correspond to those described above. At high temperatures there is a positive slope which corresponds to region I of the intensity dependence. This region has a well defined activation energy, although it cannot often be measured as the photocurrent is much less than the dark current.

In region II, the slope is negative and the activation energy may, or may not, be well defined. At the lowest temperatures, in

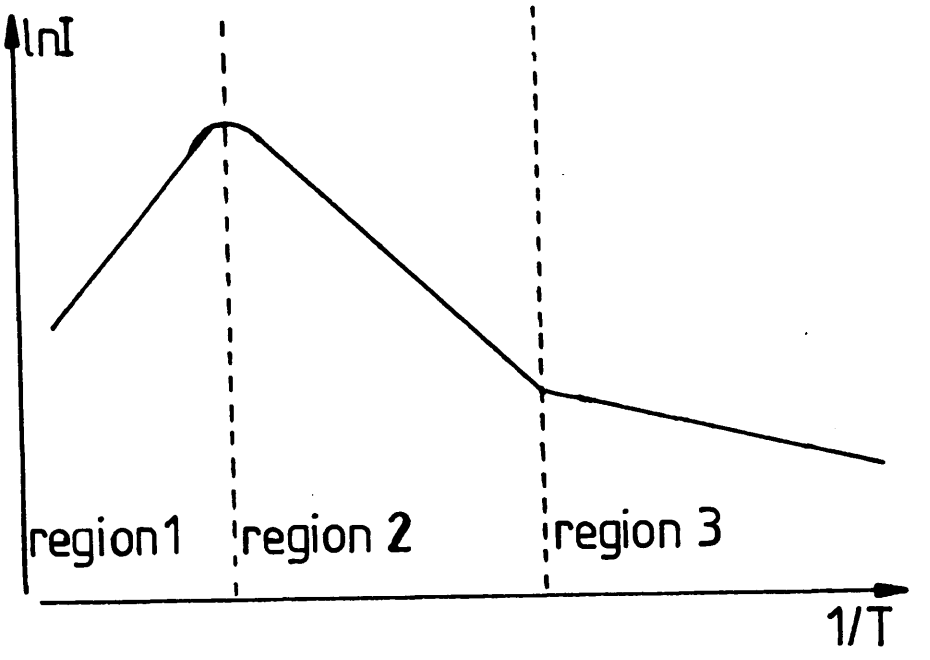

Figure 2-6: General Temperature Dependence of Steady State Photoconductivity

region III, the activation energy becomes very low, or zero.

2.4.2 The Two Level System

In this section the preceeding ideas of Shockley-Read-Hall recombination are presented[32] in the simple case of two localised defect levels, as depicted in fig.2-7. This is a simple model system which exhibits the photoconductive behaviour as just described. Chapter 5 presents the analysis of a single discrete defect, including the effects of electronic correlation, and it is shown that the expressions obtained from both analyses are very similar. This similarity will then be carried over into the more complex case of distributed states where the one electron approach is more tractable analytically and numerically. The distributed

states model still retains many of the features predicted by the simpler two level Shockley-Read-Hall model and single defect correlated state model. Furthermore, the basic assumptions and simplifications of the Shockley-Read-Hall system are also used in the analysis of the correlated state model, so it is apposite to describe them for the simpler case stated here.

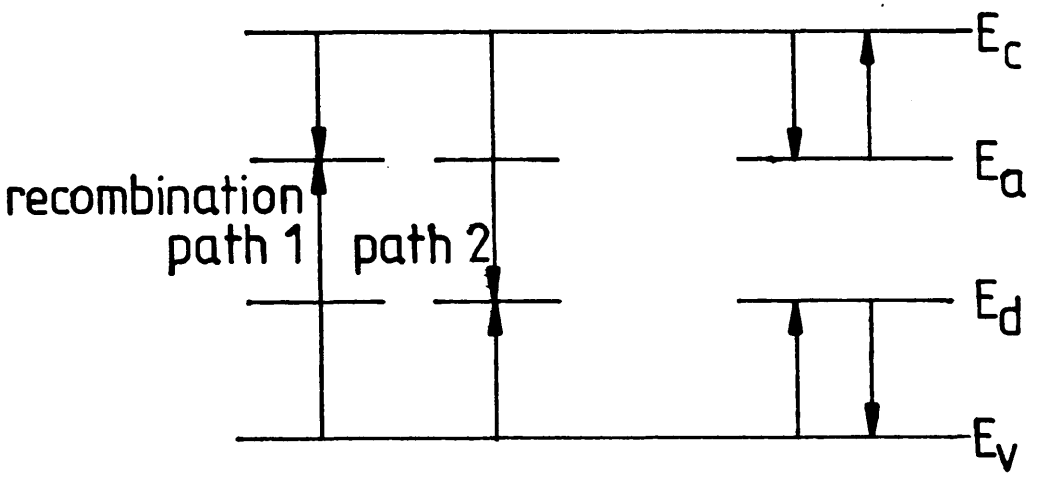

Figure 2-7: The Two Level System

2.4.2.1 Shockley-Read-Hall Recombination

The above ideas can be developed to give the basic equations governing recombination in the simple two level system under discussion here. The sequence of operations is as follows.

1. The full Shockley-Read statistic for each trap is set out.

2. The occupation function is simplified by removing small emission and capture probability terms.

3. The charge neutrality equation for the system is written

down, i.e. the sum of free and trapped negative charges is equal to the sum of free and trapped positive charges.

4. A full expression is formulated for the recombination rate via each level. This is simply the difference between electron capture and release rates for each level. The total recombination rate is the sum of all such terms.

5. A combination of steps 2 and 3 can be used to eliminate one of the variables, e.g. hole density, p.

6. Total densities are split into equilibrium and excess values, and the solutions are made for the excess densities. Recombination "paths" via particular sets of states can be defined. The path which gives the highest recombination rate will be dominant, and the slowest step within that path will control the recombination rate.

These ideas are now illustrated for the two level system.

2.4.2.2 1, Occupation

Equation (2.28) is rewritten by dividing throughout by C_p, so

$$f=Rn+p_1/[R(n+n_1)+p+p_1] \qquad (2.40)$$

The upper localised state in fig.2-7 is considered to be acceptor-like, and as acceptors are negatively charged when occupied and neutral when empty, then R_a will be less than unity. The lower localised state is considered to be donor-like, and as donors are neutral when full and positively charged when empty, R_d will be

greater than unity.

2.4.2.3 2, Simplification of the Occupation Function

The case for low and medium intensities is considered first. These regimes of the photoconductive response require that the quasi Fermi levels are nearer the centre of the gap than the defect energy levels, $E_{fn}<E_a$. Inspection of equations (2.34) and (2.19) reveals that $n_{1a}>>n>>p>>p_{1a}$. The occupancy of acceptor states is,

$$f_a=\frac{R_a n+p_{1a}}{R_a(n+n_{1a})+p+p_{1a}} \tag{2.41}$$

which can now be simplified to

$$f_a=n/n_{1a} \tag{2.42}$$

For the donor-like level it is more appropriate to use 1-f, the hole occupation function. Using arguments analogous to those above,

$$1-f_d=p/p_{1d} \tag{2.43}$$

2.4.2.4 3, Charge Neutrality

The charge neutrality equation can be written,

$$n+N_a f_a-N_d(1-f_d)-p=0. \tag{2.44}$$

2.4.2.5 4, Recombination Rate

The recombination rate for electrons at any one defect level must be equal to the trapping rate less the rate of re-emission back to the conduction band. So the rate of recombination at one defect level, rr, is given by

$$rr=[C_n n(1-f)-C_n n_1 f]N_t \tag{2.45}$$

If eq.(2.40) is used for f, as no simplifications can yet be made, and as, from inspection,

$$n_1 p_1=n_o p_o \tag{2.46}$$

then

$$rr=C_nN_t\left[\frac{(np-n_op_o)}{(R(n+n_1)+p+p_1)}\right]$$

which is the standard Shockley-Read-Hall result. Figure2-7 shows the two possible reconbination paths: path 1, where an electron hole recombination occurs via E_a; path 2 where recombination occurs via E_d. The total recombination rate is given by

$$R=C_{na}N_a\left[\frac{np-n_op_o}{R_a(n+n_{1a})+p+p_{1a}}\right] \quad \text{(path 1)} \qquad (2.48)$$

$$+C_{nd}N_d\left[\frac{np-n_op_o}{R_d(n+n_{1d})+p+p_{1d}}\right] \quad \text{(path 2)}$$

2.4.2.6 5, Elimination of the Appropriate Variable

If the reasonable assumption is made that most of the charge is in traps so n and p can be ignored, $N_a=N_d$, which gives

$$f_a=1-f_d \qquad (2.49)$$

so

$$n/n_{1a}=p/p_{1d} \qquad (2.50)$$

Also, for the thermal equilibrium electron and hole densities, n_o and p_o,

$$n_o/n_{1a}=p_o/p_{1a} \qquad (2.51)$$

These results are used in step 6 to eliminate the unwanted variable, in this case, p.

2.4.2.7 6, Path Selection

In the low intensity regime, $n<n_o$ and $p<p_o$. If it is assumed that path 1 predominates,

$$R=C_{na}N_a\left[\frac{(n_o+\Delta n)(p_o+\Delta p)-n_op_o}{R_a(n_o+\Delta n+n_{1a})+p_o+\Delta p+p_{1a}}\right] \qquad (2.52)$$

if one uses $n=\Delta n+n_o$. If it is assumed that $n_{1a}>n_o,p_o,p_{1a}$, then the simplified equation is

$$R=C_{na}N_a\left[\frac{\Delta np_o+\Delta pn_o}{R_a n_{1a}}\right]$$

Using equation(2.51) and

$$p/n=\Delta p/\Delta n \tag{2.53}$$

then

$$\Delta np_o=\Delta nn_o p_{1d}/n_{1a}=\Delta pn_o \tag{2.54}$$

This gives

$$R=C_{na}2\ nn_o p_{1d}/R_a n_{1a}^2 \tag{2.55}$$

and as in steady state, R=G,

$$\Delta n=\frac{GR_a n_{1a}^2}{2C_{na}p_{1d}n_o} \tag{2.56}$$

In this case, the photoconductivity is monomolecular in G. Using the appropriate Boltzmann functions, (2.19),(2.22), the temperature dependence is

$$\Delta n\propto\exp[(2(E_a-E_{fi})-(E_f-E_d))/kT] \tag{2.57}$$

where E_{fi} is the intrinsic Fermi level, the centre of the band gap. The activation energy will be positive unless there is large asymmetry of the defect levels and Fermi levels with respect to the mobility gap. Note that this corresponds to region 1 in figures 2-5 and 2-6.

For the case of path 2, using similar assumptions, one obtains

$$n=Gn_{1a}/2C_{nd}N_d n_o \tag{2.58}$$

which is also monomolecular in G. If the same substitutions are made as in the case of path 1, then the temperature dependence of the

photoconductivity is

$$\Delta n \propto \exp[(E_a-E_f)/kT] \tag{2.59}$$

which again describes a positive activation energy, and has the same magnitude as in path 1 if $E_c-E_a=E_d-E_v$.

Unfortunately the similarity of the magnitudes of the activation energies of the two paths means that the precise recombination mechanism cannot be established from an Arrhenius plot. However both the temperature dependence and intensity dependence of the photoconductivity of a semiconductor are qualitatively explained.

2.4.2.8 Lifetime

The analysis above assumes that the rate of one path will greatly exceed the other, allowing them to be separated, which makes it easy to understand the processes involved. If one writes

$$R=G=R_1+R_2 \tag{2.60}$$

and solves for n, then

$$n=G\left[\frac{C_{na}N_a 2p_{1d}n_o}{R_a n_{1a}^2} + \frac{C_{nd}N_d 2n_o}{n_{1a}}\right]^{-1} \tag{2.61}$$

The first term represents the lifetime for path 1, the second, path 2. The path with the largest recombination rate will predominate. If one term is divided by the other, then

$$\tau_1/\tau_2=C_{na}p_{1d}/C_{nd}n_{1a} \tag{2.62}$$

as in this simple analysis $N_a=N_d$. Assymetry in capture cross sections or defect energies will cause one recombination path to be dominant.

2.4.2.9 Medium Light Intensities

In this regime, $\Delta n > n_o$, $\Delta p > p_o$, but the quasi Fermi levels are between the defect levels, so n_1 and p_1 are not negligible. The recombination rate for any one defect level is given by eq.(2.47)

2.4.2.10 Path 1

n, p, and p_1 will be negligible compared to n_1, so if the proper simplifications are made to eq.(2.47) and using

$$\Delta p/\Delta n = p_{1d}/n_{1a} \tag{2.63}$$

one obtains

$$\Delta n = \left[\frac{GR_a n_{1a}^2}{C_{na} N_a p_{1a}}\right]^{1/2} \tag{2.64}$$

and separating the strongly temperature dependent terms, n_{1a} and p_{1d}, gives

$$\Delta n \propto \exp[-2((E_c - E_a) + (E_d - E_v))/2kT] \tag{2.65}$$

which yields a negative activation energy unless $E_d - E_v$ is greater than $2(E_c - E_a)$. Note that this region of the photoresponse is represented by region II in figures2-5 and 2-6.

2.4.2.11 Path 2

By similar arguments, for this recombination path

$$\Delta n = [G n_{1a}/C_{na} N_d]^{1/2} \tag{2.66}$$

which, again, is bimolecular. The only temperature dependent term is n_{1a}, so

$$\Delta n \propto \exp[-(E_c - E_a)/2kT] \tag{2.67}$$

Again, as with the low intensity case, it is difficult to use activation energies to distinguish between the two recombination paths.

2.4.2.12 High Light Intensities

Light intensities are defined as high when the quasi Fermi levels are between the band edges and the defect levels. In this case n_1 and p_1 are negligible as compared to n and p, and n_o and p_o are negligible.

2.4.2.13 Occupation

In this case eq.(2.40) can be simplified to

$$f_a=R_an/(R_an+p) \tag{2.68}$$

and using $R_a<<1$

$$f_a=R_an/p \tag{2.69}$$

likewise, using $R_d>>1$

$$1-f_d=p/R_dn \tag{2.70}$$

2.4.2.14 Charge Neutrality

As it is assumed in this simple analysis that most of the charge is trapped and $N_d=N_a$, it is still the case that $f_a=1-f_d$, so

$$R_nn/p=p/R_dn \tag{2.71}$$

hence

$$p=(R_aR_d)^{1/2}n \tag{2.72}$$

and if for simplicity one assumes $R_aR_d=1$, then p=n.

2.4.2.15 Path 1

Again eq.(2.47) gives the recombination rate for each individual path. The n_op_o term is ignored, as are n_1 and p_1. $R_a<<1$ so $R_an<<p$. Δn is substituted for p and Δn^2 for $\Delta n\Delta p$, which gives

$$\Delta n=G/C_{na}N_a \tag{2.73}$$

which is monomolecular. The electron density has no temperature dependence, and this result represents region III of the photoconductivity response.

2.4.2.16 Path 2

Using the same substitutions and approximations as in the last section, but letting $R_d >> 1$ gives

$$\Delta n = GR_d / C_{nd} N_d \qquad (2.74)$$

This expression gives the same intensity and temperature dependence as path 1.

2.4.2.17 Conclusion

The two-defect system can explain the major features of the photoconductive response, as observed in many amorphous semiconductors.

2.5 Photoconductivity with a Slowly Varying Density of States

2.5.0.1 The Model of Rose

In some materials the photoconductivity is neither monomolecular nor bimolecular, that is to say

$$I_p \propto F^{\gamma} \quad (0.5 \leq \gamma \leq 1) \qquad (2.75)$$

Rose [17] did not consider the mechanism to be that of a mixture of the two recombination systems because this would only allow a short transitional region between regimes rather than the several decades of light intensity over which this behaviour is observed in some materials.

He proposed a model with the following features. Firstly, a discrete level of recombination centres of density N_r, of which p_r are occupied by holes and n_r by electrons. At zero light intensity, the p_r states are absent or negligible, which means that E_f is above those states, fig2-8.

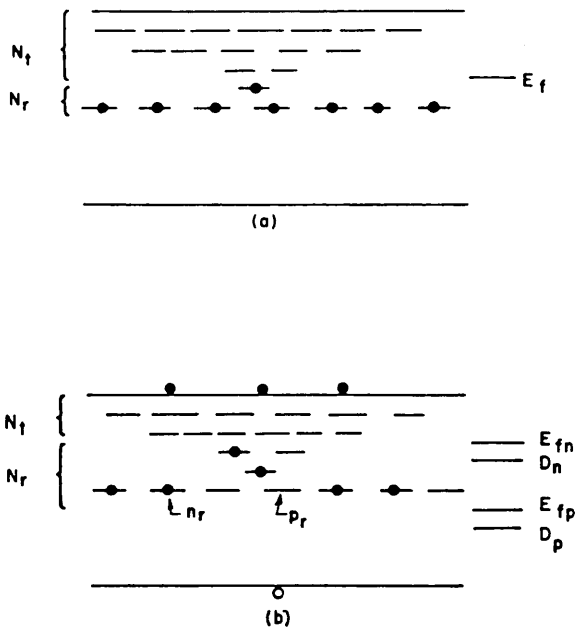

Model for exponents of current-light curve lying between 0.5 and 1.0. (a) Unilluminated. (b) Illuminated.

Figure 2-8: Rose's Exponential Tail Model

Secondly there is an exponential distribution of traps, density N_t such that

$$N_t(E) = A\exp(-(E_c-E_t)/kT_c) \qquad (2.76)$$

and electrons are considered to be the predominant carrier. T_c is called the characteristic temperature.

$T_c > T$(a slowly varying density of states) otherwise the density of states varies faster than the Fermi function, and the unoccupied recombination centres (p_r) are all between E_c and E_{fn}.

The total number of states at N_r is assumed to be greater

than the sum of those over the range of N_t.

$$N_r > \int N_t(E)dE \qquad (2.77)$$

For simplicity the capture cross sections of N_t and N_r are taken to be the same, although this does not alter the argument. To ensure that n>p, we need $\sigma_n < \sigma_p$.

Consider the effect of a moderate level of illumination, fig2-8. E_{fn} and E_{fp} are as defined in the previous section. Rose states that the occupation of the states is homogenous and constant between the two demarcation levels. This is not in exact agreement with the discussion of Simmons and Taylor, who use the trap Fermi levels for this, but it does not alter the end result. Because of the difference in capture cross sections of electrons and holes, the demarcation energies are lower than their respective quasi-Fermi levels.

As the light intensity is increased, E_{fn} rises, and more N_t states are changed into recombination states. This increases the number of recombination states for electrons, p_r, because the occupation between the demarcation energies is homogenous and constant. Therefore the lifetime of the free electrons decreases and is thus less than unity.

P_r is given approximately by the number of N_t states that are between the original E_f and the steady state E_{fn}. We have

$$P_r = \int N_t(E)dE \qquad (2.78)$$
$$= A\exp(-(E_c-E_t)/kT_c)$$
$$\simeq kT_c N_t(E_{fn})$$

Now

$$\Delta n = f\tau_n = f/p_r v_{th} \sigma_n \qquad (2.79)$$

substituting the above equation for p_r is shown to lead to

$$n = \text{const.}\ T_c/(T+T_c) \qquad (2.80)$$

and since $T_c > T$, the exponent $T_c/(T+T_c)$ is between 0.5 and unity.

The argument does not need an exponential tail of states throughout the whole band gap: only the region through which E_{fn} moves need be exponential, as the greatest contribution to p_r occurs from states between E_{fn} and E_f. As the absolute temperature of the sample falls towards zero, the exponent approaches unity. Also a very slowly varying density of states corresponds to a very high value of T_c, so this also gives an exponent between 0.5 and unity. So such an exponent can be said to imply a distributed density of states.

2.5.0.2 The Model of Taylor and Simmons

The theories of Taylor and Simmons[33] are applicable to an arbitrary density of states and can be considered as more complete. Occupation is described by Shockley-Read statistics, eq.(2.28), with the trap quasi-Fermi levels as defined by eq.(2.31).

As most of the electrons and holes are trapped under illumination, the charge neutrality equation can be written,

$$\int_{E_{fo}}^{E_{fc}} g(E)(C_n n/C_n n+C_p p)dE = \int_{E_{ft}^p}^{E_{fo}} g(E)(C_p p/C_p p+C_n n)dE \qquad (2.81)$$

As only the levels between the trap quasi-Fermi levels contribute effectively to the recombination process (re-emission to the appropriate band is at a faster rate from the other levels), then the net rate of recombination is easily shown to be

$$R=G=C_n n C_p p(C_n n+C_p p)^{-1} \int_{E_{ft}^p}^{E_{fc}^n} g(E)dE \qquad (2.82)$$

where $C_n n C_p p (C_n n + C_p p)^{-1}$ is known as the recombination efficacy which is assumed to be constant for all states, which is why it is placed outside the integral. If this equation is combined with the equation for charge neutrality, then

$$G = \Delta n C_n \int_{E_{fo}}^{E_{ft}^n} g(E)dE \qquad (2.83)$$

and

$$G = \Delta p C_p \int_{E_{ft}^p}^{E_{fo}} g(E)dE \qquad (2.84)$$

Note that the occupation fractions of the states have cancelled out in the analysis and the total number of states between the trap quasi-Fermi levels are all that need to be known. Equations (2.83) and (2.84) allow the photocurrent to be calculated for any density of states. Also, if the density of states is not known, calculations using a model density can be used to confirm or reject it. This approach is used in the discussion section of this thesis.

2.5.0.3 Application to an Exponential Tail Model

Simmons and Taylor[34] have applied this theory to an exponential tail model. Using appropriate parameters for generation etc., they calculated the expected form of the photoconductive response, which was similar to that in fig.2-6 with the following feature; a well defined activation energy is not obtained with distributed localised states. Also the very low temperature region of the curve does not become constant, indeed the photoconductivity continues to drop slowly with temperature, unlike the case for discrete states described above.

The intensity dependence was also considered, and the response was monomolecular when Δn was less than n, sublinear as in

eq.(1.23) for high intensities. Because the density of states was distributed throughout the mobility gap, a constant density of recombination centres would not be obtained until the quasi-Fermi levels reached the band edges, so in this case, the monomolecular region III will not be observed.

2.6 Summary

The temperature and intensity dependencies of the photoconductivity of a semiconductor can be used to find if the material has discrete or distributed states. If there is not a well defined activation energy for the temperature dependence of the photoconductivity, γ values are given by eq.(1.23), and the low temperature temperature dependence does not become constant, then one is dealing with a material with distributed states. If there is a well defined activation energy, intensity dependence is linear or square root, and the temperature dependence disappears at very low temperatures, then one is studying a material with discrete states.

Later in this thesis, the photoconductive response in undoped a-Si:H is interpreted as a mixture of the two responses. At low intensities and high temperatures, the behaviour of the system is that of a distributed state system as the electron trap quasi-Fermi level is moved through a set of distributed localised states, which act as recombination centres. At high intensities and low temperatures, the Fermi levels are moved outside this region, the density of recombination centres has become constant, and in this regime the system appears to act like the discrete state type of

model. This is why both cases have been examined in this chapter.

Chapter 3

A Review of Previous work on Transient Photoconductivity

3.1 Transient Photodecay

3.1.1 Introduction

This experiment has been variously referred to in the literature as transient photodecay, transient photoconductivity, flash response, and delta response; a description of the experiment is given in the chapter on experimental methods. Excess free carriers are created at the band edges in a coplanar gap-cell structure by a short flash of light. Subsequently the excess carriers are redistributed into the localised states below the band edge, and they eventually recombine. The geometry of the experiment and the use of "ohmic" contacts minimise transit time effects and extraction at the electrodes, and allow the redistribution mechanisms themselves to be studied by measurement of the decay of the photocurrent.

Amorphous materials often display so called anomalously dispersive transport. This term originally was applied to time of flight drift mobility studies and it describes the phenomenon where there is a large spread of arrival times at the back electrode of a "sandwich" specimen. The initial part of the drift mobility curve before carrier extraction at the back electrode represents trapping and release of the carriers, and can be compared with the transient photoconductivity response, if contact effects can be neglected in the latter.

The form of the drift mobility current vs. time curve before carrier extraction, (or the transient photoconductivity current) was interpreted by Scher and Montroll[35] to be due to a spread of release time constants, $\psi(t)$ caused by a range of hopping probabilities among the localised states. However it is now generally accepted that multiple trapping (MT) can well explain this phenomenon.

3.1.1.1 Multiple Trapping

In multiple trapping, the excess free electrons in extended states with relatively high mobility are trapped by the localised states below the mobility edge at a rate

$$R_t = n(1-f)C_n \qquad (3.1)$$

where the n is the free electron density, 1-f is the fraction of empty traps, and C_n is the capture coefficient for electrons at the particular state involved. Once a carrier is trapped it may be released and then recaptured. Shallow traps are more likely to release trapped carriers than deep traps because the probability of release depends on exp[E/kT]. There is therefore a range of release time constants, $\psi(t)$ implicit in MT if the traps sre energetically distributed in significant numbers over a few kT. So shallow traps are in thermal contact with the band edge, and will have their occupancy determined by capture and release; the deep traps are defined as those which have not had an average of one release event during the time scale of the experiment, and the occupancy of these centres is determined by trapping parameters only. Fig. 3-1 shows that the density of occupied deep traps is proportional to the localised state density, whereas the shallow traps have their

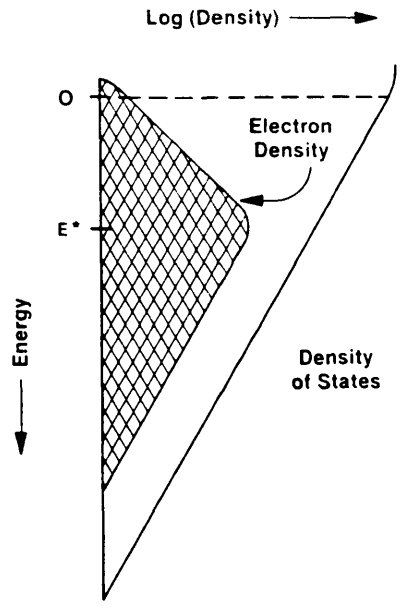

Figure 3-1: Electron Densities during Thermalisation

occupancy decreasing as a Boltzmann function times the trap density.

Note that the energy position of the traps is not the only factor here. A trap with a very low capture cross section will take longer to establish quasi-thermal equilibrium with the carriers at the band edge than a trap with a large capture cross-section because capture occurs at a slower rate. If the distributed states are all assumed to have the same capture cross sections, an energy E_d will separate shallow and deep traps if E_d lies in a region where there is a broad spread of states, where

$$E_d = kT.\ln(\omega t) \qquad (3.2)$$

This demarcation energy evolves into deeper states with time, and states above E_d are said to have thermalised. The trapping of the free carriers in conjunction with the release of trapped carriers

determines the rate at which the density of free carriers decays.

3.1.2 TROK analysis

Some amorphous semiconductors display an approximately featureless transient decay curve. This has led to a deceptively simple model independently proposed by Tiedje and Rose[36] and Orenstein and Kastner[37] to explain transient photoconductivity data. This approach is described below and its major failings are pointed out.

The relatively featureless decay curve of the transient photocurrent implies a distributed density of states below the band edge, because dispersive transport is not predicted to occur if there is a quasi-discrete set of trapping states at a narrow range of energy. Note that it is assumed that we are dealing with the time regime of the experiment before the onset of recombination for simplicity. Then

$$n=N_o[g(E_c)/g(E_d)].\gamma\exp[-(E_c-E_d)/kT] \qquad (3.3)$$

N_o is the total injected carrier density, and γ is the fraction of trapped carriers in shallow traps, which is constant. Making the appropriate substitutions gives

$$I(t)\propto \Delta n/N_o \qquad (3.4)$$
$$\simeq g(E_c)\gamma(\omega t)^{-1}/g(E_c-kT\ln\omega t)$$

If an exponential variation of trap density is assumed

$$g(E)=g_o\exp[-(E_c-E)/kT_c] \qquad (3.5)$$

where g_o is the extrapolation of the density of states up to E_c and T_c is the characteristic temperature of the distribution, then

$$I(t)=c.N_c(\omega t)^{-1+\alpha} \qquad (3.6)$$

where c is a constant, α is T/T_c, T_c is greater than T, and N_c is

the effective density of states.

The big advantage of this analysis is that it enables the density of states to be found by simple calculation of the slope of a double logarithmic plot of carrier density against time because

$$\Delta n \propto t^{-(1-\alpha)} \qquad (3.7)$$

if the localised state distribution is exponential. Experimentally, as relatively featureless plots were obtained, an exponential density of states was inferred over the energies represented by the time scale of the experiment by eq.(3.2), and these states have been identified with the disorder broadened band edge tail states expected in amorphous materials.

Alternatively, if there is structure in the decay curve the density of states can still be obtained as equation (3.3) implies that

$$g(E)=\text{const.}/(I(t).t) \qquad (3.8)$$

The limitations of the validity of this expression are discussed later.

3.1.3 Some Problems with the TROK Model

The TROK analysis has been seen by many workers as an oversimplification of the situation in real materials. In particular the analysis needs the capture cross-section to be constant throughout the gap, and the density of states profile needs to be slowly varying. The presence of well defined structure in the localised state density can be shown to cause errors in the analysis[38], particularly as most of the charge is assumed to be

concentrated at E_d. A large feature in the localised state density below E_d would concentrate charge at the feature, causing errors in the calculated density at E_d.

Work by Marshall et. al. has also raised objections to an uncritical acceptance of the TROK analysis. A major success of TROK is the ability to calculate the localised state distribution from the transient decay curve, but Marshall and Main[39] performed computer modelling to calculate the expected decay curve for a particular density of states, then the TROK analysis was used to get a density of states. For a situation with three discrete levels, the TROK analysis gave complete inversion of g(E), probably due to the invalidity of the concept of demarcation energy for discrete states.

Marshall, Michiel and Adriaenssens[40] used Monte Carlo simulations for the drift mobility experiment on various localised state distributions to test the TROK model. The α values at either side of the "knee" were not equal (as found experimentally), except for exponential band tails.

Michiel and co-workers have determined the release time parameter by numerical solution of a Volterra equation[41]. From this agreement could always be found between the original density of states model and the deconvoluted density of states from the analysis. Unfortunately, the analysis is mathematically difficult.

Marshall et. al.[42] measured the transient photocurrent in

crystalline As_2Se_3 slightly disordered by electron bombardment. The data were analysed by both the Volterra technique and TROK. As the decay curve exhibited a substantial degree of structure, so did the calculated density of states. The two techniques produced inverse results, that is where peaks were seen on the Volterra analysis, troughs were seen in the TROK analysis and vice versa. This is because for a slowly varying density of states

$$g(E)=\text{const.}/(I(t).t) \qquad (3.9)$$

and for highly structured densities

$$g(E)=\text{const.}I(t).t \qquad (3.10)$$

The release time distribution function $\psi(t)$ is very similar in shape to I(t) for highly structured density of states distributions. However for relatively featureless distributions the concept of E_d is valid and TROK gives qualitatively correct results. Thus TROK can only be used if

(i) The density of states and transient photoconductivity decay curves do not show significant structure.

(ii) The capture coefficients are approximately constant with energy.

Arkhipov and Rudenko[43, 44] analysed the expected response for the drift mobility experiment, and showed that the error produced by assuming a sharp transition in the nature of the occupation at E_d will be small if $T_c > T$. They also used a correction function for E_d when significant structure occurs in g(E). Unfortunately the analysis is very much more complicated mathematically than TROK and

is a less attractive approximation.

An objection to many measurements of the transient photodecay has been made by Street[45], who has suggested that some measurements are dominated by surface band bending for a time of up to one second.

3.2 Step Response Transient Measurements

3.2.1 Introduction

The transient rise, or step response, is where a sample in thermal equilibrium has at t=0 a constant intensity of light incident on it which continues until a steady state value of the photocurrent is observed. The aim is to obtain details of density of states and trap parameters from the precise form that the step response takes. This was used for practical reasons in the first instance since the L.E.D. light source extensively used in this work did not produce a sufficient intensity for the flash response measurement. Standard control theory shows that the step response is the convolution of the impulse response. i.e. the flash decay.

3.2.2 Step Response with Discrete States

At the beginning of the transient rise the semiconductor is in thermal equilibrium, with the occupancy of all states determined by the Fermi-Dirac distribution function, and the free carrier density is only dependent on the Fermi level position. At the end of the experiment, the sample is photoconductive at a steady level, and as shown in the previous chapter, the occupancy of the localised states are determined by Shockley-Read statistics, and the presence

of localised states strongly influences the free carrier density. One can imagine the quasi-Fermi levels slowly moving from the dark positions to the illuminated positions, but the Fermi level is a concept of thermodynamic equilibrium, and is of no use here. However an expected curve for the transient rise for a system with shallow, discrete traps is illustrated in fig.3-2. The trapping processes are shown in fig.3-3

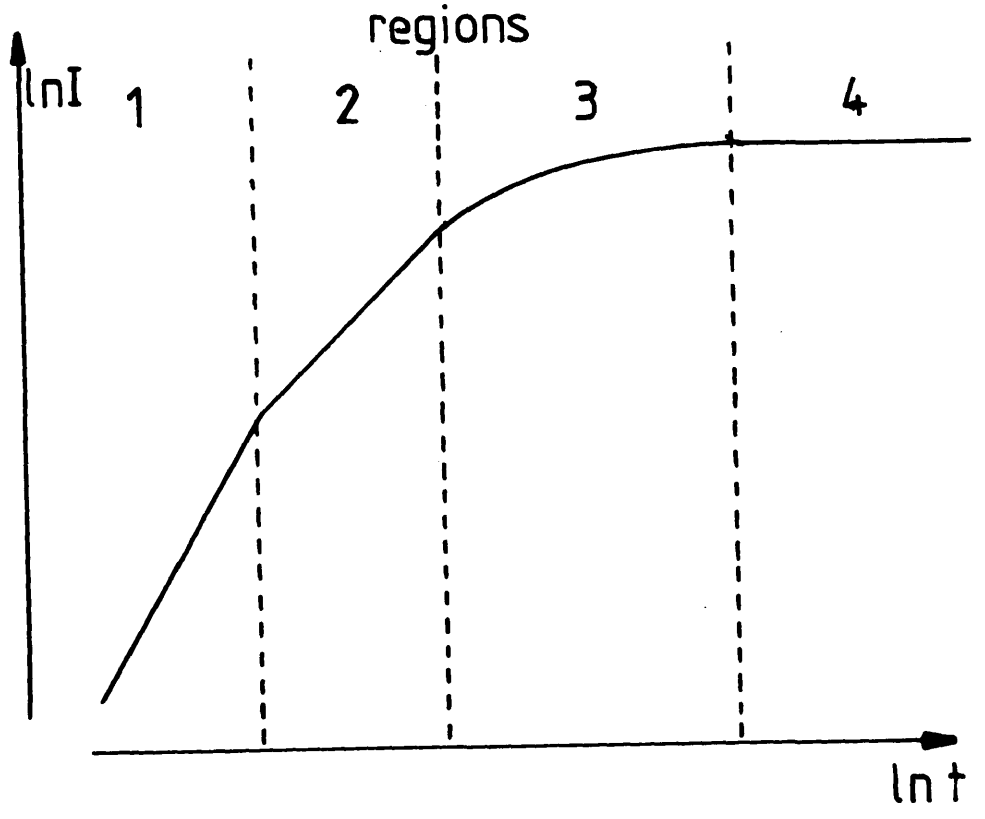

Figure 3-2: The Expected Response for the Transient Rise

Region 1 is the early part of the response where trapping is assumed to be the only significant process to occur rapidly. Ryvkin[29] shows that

$$\Delta n = \gamma G t^{\alpha} \qquad (3.11)$$

If the transient photocurrent is measured, then the free carrier mobility can be obtained from the slope of region 1, as

$$\Delta I = \gamma G t e \mu_o E A \qquad (3.12)$$

where e is the electronic charge, E is the electric intensity and A is the cross sectional area of the sample. In the presence of traps Region one will be very short, so region 2 may be the earliest observable region. Here we may postulate that quasi-thermal equilibrium has been established between a shallow set of traps at, say, E_{t1} and the band edge, so

$$\Delta n/\Delta n_{t1} = N_c/N_{t1} \cdot \exp[-(E_c - E_{t1})/kT] \qquad (3.13)$$

where n_{t1} is the excess density of electrons at energy E_{t1} below E_c. The drift mobility, or trap limited mobility is defined as

$$\mu_{d1} \simeq \mu_o n/n_{t1} \simeq \mu_o \Delta n/\Delta n_{t1} \qquad (3.14)$$

Here the trap limited mobility for the trap at E_{t1}, μ_{d1}, can be obtained from the rate of rise of the transient photocurrent, as a constant slope is expected since

$$\Delta n + \Delta n_{n1} = \gamma G t \qquad (3.15)$$

Substituting for Δn_{t1} from the above gives

$$\Delta I = \gamma G t e \mu_{d1} E A \qquad (3.16)$$

If there is more than one set of discrete traps (fig.3-3) there may be more than one straight line portion in region 2.

In region 3 the effects of recombination are seen to reduce the rate of rise of the transient more quickly as the recombination rate increases. In the first three regions generation of carriers continues at rate G, but recombination occurs at a steadily increasing rate as steady state is approached, region 4.

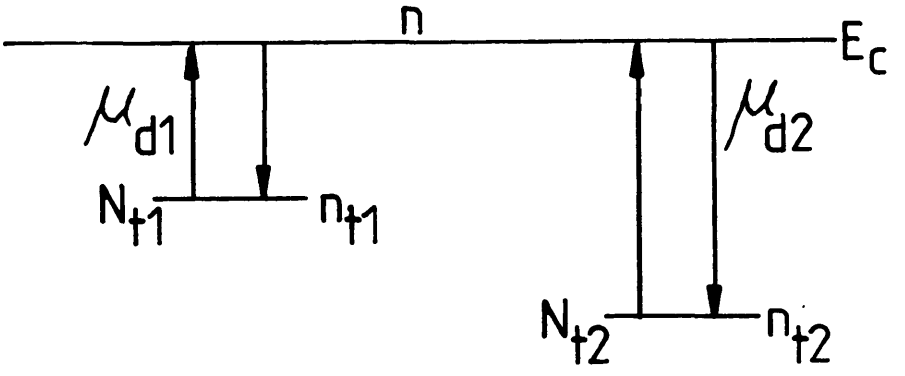

Figure 3-3: Trapping and Release during Transient Rise

Semiconductors in which anomalously dispersive transit pulses are measured clearly do not satisfy the conditions for which region 2 will be well defined, i.e. these materials have distributed traps with release times which vary with energy.

3.2.3 Step Responses with Distributed States

Arkhipov et. al. [46] have calculated the expected form of the transient rise experiment for a semiconductor using the multiple trapping model for an exponential density of states. They found that the photocurrent would pass through a maximum before reaching steady state. Furthermore, the slope of the photocurrent curve would be a power law before and after the maximum. The exponent of the power law is α, the dispersion parameter. Also the curves would show universality with the appropriate scaling of the axes of the double logarithmic plots.

The mathematics involved in Arkhipov's analysis do not appear

to allow easy modification for other localised state distributions, however Kastner and Monroe [18] have used the TROK approximation to calculate the transient rise with results similar to those of the Moscow group. Under conditions for a density of localised states not exactly exponential, but when TROK is still valid, a deviation from an exact power law could indicate the presence of a feature in the density of states at an energy given by eq.(3.2). As control theory shows that the step response is a mathematical convolution of the impulse (i.e. the flash decay) similar information could be obtained from both experiments.

If discrete states are present, it was shown previously that the drift mobility can be obtained from the gradient of the straight line portion of the ΔI vs. t plot. When distributed states are present, the transport is dispersive and no straight line portion is observable, however the time dependent mobility can still be obtained from the instantaneous gradient at time t.

Chapter 4

A Review of Previous work on the Steady State Photoconductivity in Amorphous Silicon

4.1 Steady-state Photoconductivity

4.1.1 Introduction

An important facet of the study of the steady state photoconductivity in a-Si:H has been to explain a feature which has been observed since one of the first studies of the material, by Chittick et.al.[3]. The major point is that the intensity dependence of the photoconductivity is neither linear nor square root in behaviour. The previous chapter has shown that the presence of discrete localised states in the mobility gap would cause linear and square root behaviour and one might have expected that models of a-Si:H using discrete states would have been rejected early on, especially as disorder could be expected to broaden in energy any discrete state by at least kT. However there are certain reasons to expect features in the mobility gap of a semiconductor. By analogy from the crystalline case where well defined defects such as the divacancy cause discrete localised states to appear in the band gap, some workers, especially Spear's Dundee group have found such states to be present in non-crystalline materials from their interpretation of field effect data[6].

The following description of some of the reports in the literature on photoconductivity generally compares the two conflicting ideas of discrete and distributed states in the mobility

gap.

The early report on the properties of this material by Chittick et al.[3] describes a major problem in amorphous material technology, i.e. the exact properties of the material depended on the substrate temperature. Other parameters can affect the electronic properties of the material, such as electrode and vacuum chamber geometry. Therefore when comparing results from measurements on materials from two different laboratories, exact correspondence will never be obtained, even when the same method of deposition has been used.

4.1.2 Glow Discharge Material

4.1.2.1 Interpretations using Discrete States

The Dundee University group made early photoconductivity measurements[9, 10]. The first paper was mainly concerned with the characterisation of the material, taking high photosensitivity of the material as an indication of the low density of states in the gap, and attempting to use photoconductivity as a measure of optical absorption at low absorption coefficients.

Measurements of the temperature dependence of the photoconductivity were the major feature of the second paper. This followed the pattern described in the work of Simmons and Taylor[34] and in chapter 2 of this thesis. Spear's results are given in fig.4-1

An activation energy of about 0.2eV was obtained in the high

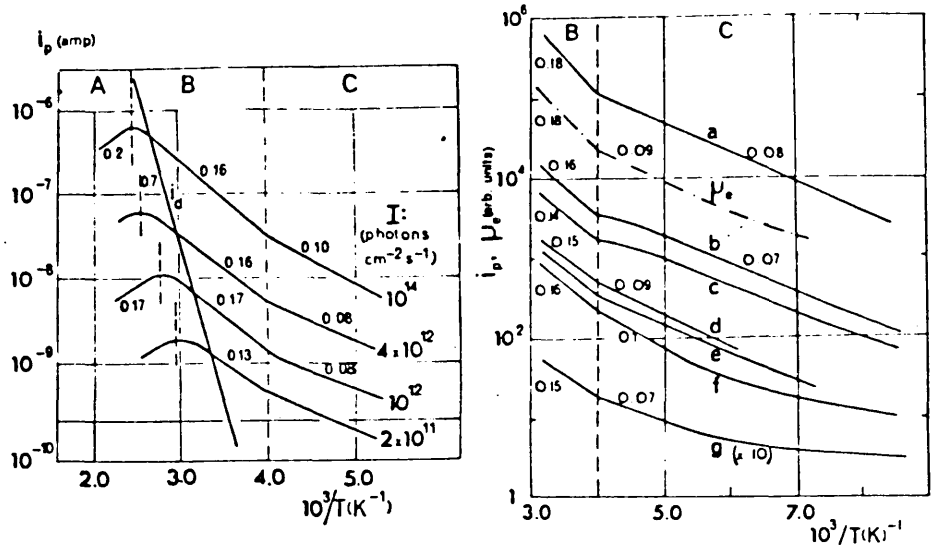

Figure 4-1: Photoconductivity data from Spear et al.[8]

temperature monomolecular region I, despite the difficulty of the photocurrent being smaller than the dark current. At intermediate temperatures, in region II, the photocurrent decreases with temperature, displaying a well defined activation energy of about 0.16eV, which is the same as for electron drift mobility studies [8]. For the lowest temperatures, a smaller activation energy was observed, 0.1eV. The break between region II and region III occurred at the same temperature for a number of different incident intensities, 250K. This was taken to imply a change in conduction mechanism at this temperature, from extended state transport to hopping.

Spear et al. also measured the intensity dependence of the photocurrent apparently at only one temperature, although this is not made explicit. The intensity dependence was expressed by eq.(1.23) where γ varied between 0.6 and 0.9.

In region I, as T is high, then conduction is in extended states. Assuming a transition between E_A and E_y in fig.1-5 to be the recombination path it is shown that monomolecular recombination would be accompanied by an activation energy of 0.2eV, if energy level values from earlier papers by the Dundee group were used.

Similarly, with the same energy levels, and because of the similarity of the activation energies in drift mobility and photoconductivity studies, an E_A to E_y transition is suggested for region II, but here the quasi Fermi levels are moved substantially from the equilibrium level. As the charge density is now higher than the dark charge density, recombination is bimolecular, and an activation energy of (E_C-E_A) is obtained.

The interpretation in the immediately preceeding paragraph only applies to high illumination levels in region II. At low illumination, a monomolecular recombination exists, and here the trapped charge is supposed to have condensed near the Fermi-level, so recombination is thought to occur between E_A and E_{fo}.

As the indices in eq.(1.23) were not exactly 0.5 or 1.0, the authors suggested that the recombination path would be a mixture of monomolecular and bimolecular recombination, whichever mechanism dominates depends on the conditions. This is thought to be possible as the photons are absorbed exponentially, see eq.(2.1), and there may be a transition from bimolecular to monomolecular recombination as the excited carrier density falls away with distance from the surface.

There are some objections to this interpretation. Firstly it is overcomplicated as the existence of distributed states gives a simpler interpretation of sublinear(but non-square root) behaviour. Secondly, as observed by Rose[17], the transitional behaviour could only be observed over a small range in intensity. As values of γ between 0.5 and 1.0 have been observed to be constant over several orders of magnitude of intensity (see the results section of this thesis), Spear's interpretation may not be valid.

When the results for region III were compared to electron drift mobility studies, it was concluded that a hopping conduction pathway was observed, and all recombination transitions would have to be between localised states, and bimolecular, with an activation energy equal to a hopping energy. No other author has interpreted photoconductivity at low temperatures as due to hopping, even at 10K, see e.g. Hoheisel[47].

In 1977, the Dundee group reported on photoconductivity measurements on doped material [14]. The results are mentioned here because the interpretation which is used may have implications for methods of changing E_f without doping, and also because the group now uses the presence of distributed states whose origin is from broadening of quasi-discrete localised states to interpret the data, i.e. the density of states from Madan et.al.[6].

The Fermi level position in a-Si was moved by substitutional doping. Photoconductive recombination was interpreted using the field effect density of states and similar models as in previous

papers by the group 9, 10.

Figure 4-2 shows the photoconductivity at 295K plotted against dark Fermi level position for variously doped samples, n-type, p-type, and undoped. n-type samples can be seen to be about 100 times more photosensitive than p-type. This is explained by consideration of the charge state of the localised states at the centre of the gap.

Anderson and Spear have extended the C.F.O. type idea of overlapping tail states by considering the overlap of states tailing from the quasi-discrete defect levels. States tailing from the E_y state near the valence band are depopulated and positively charged above E_{fo}, and likewise below E_{fo}, states from the E_x peak become negatively charged, as their occupation has changed, see fig.4-3.

In the undoped material, as in the normal C.F.O. model, the integrated positive charge density above E_{fo} must equal the negative charge below. In the n-type material, excess charge introduced from the donors has condensed between the old undoped material Fermi level and the new Fermi energy nearer the conduction band, and this reduces the overall density of positive charge, the origin of which is the overlap of the defect state tails. The amount of negative charge below the new Fermi level is correspondingly increased, and overall charge neutrality is maintained by the presence of positively charged ionised donors. As is usual in a-Si, it is assumed that the measured current is due to free electrons. Therefore, the reduction of positively charged electron traps

Figure 4-2: Anderson and Spear's results[14].

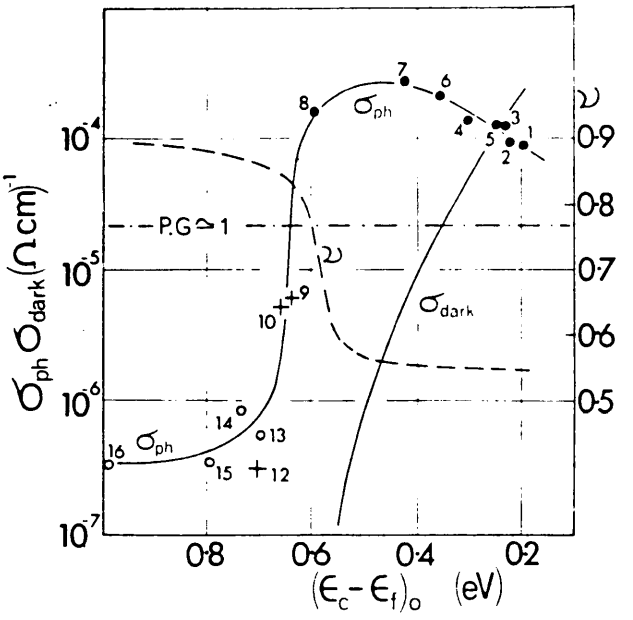

Photoconductivity at 295 K plotted against $(\epsilon_c - \epsilon_f)_0$, the position of the dark Fermi level for phosphorus doped (●), undoped (+) and boron doped (○) specimens. The numbers refer to the table. The broken line represents the exponent ν (see right-hand ordinate) in the intensity dependence $\sigma_{ph} \propto I^{\nu}$. σ_{dark} is a typical dark conductivity curve. P.G.~1 refers to unit photoconductive gain at a field of 3×10^3 V cm^{-1}.

Figure 4-3: Charge Distribution in Variously Doped a-Si

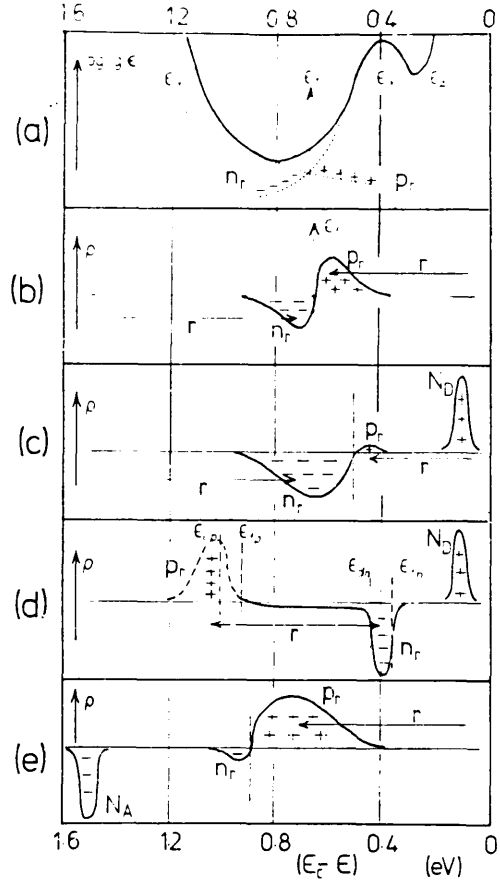

Diagrams for the discussion of the charge distribution in undoped and doped a-Si specimens. (*a*) Density of states $g(\epsilon)$ plotted against energy. The energy scale is normalized to ϵ_c. The position of the Fermi level is at $\epsilon_c - \epsilon_f = 0{\cdot}65$ eV, typical of an undoped specimen. p_r and n_r denote the densities of charged defect centres. (*b*) Charge distribution ρ in an undoped specimen at low light intensities. Recombination is monomolecular; the electron lifetime is determined primarily by transitions to the charged positive centres. (*c*) Charge distribution with moderate phosphorus doping in the dark or at very low light intensities, $(\epsilon_c - \epsilon_f)_0 \simeq 0{\cdot}5$ eV. Reduction in p_r rapidly increases electron lifetime. Recombination still mainly monomolecular. (*d*) Charge distribution in the doped specimen of diagram (*c*) illuminated with a higher intensity. Quasi-Fermi levels and demarcation lines are shown. $\epsilon_c - \epsilon_{fn} \simeq 0{\cdot}33$ eV so that most negative charge in the system lies in the peak at ϵ_x. Bimolecular recombination now takes place between the two regions of charge distribution. (*e*) Charge distribution in a lightly boron doped specimen at low light levels; $(\epsilon_c - \epsilon_f)_0 \simeq 0{\cdot}9$ eV. Increased density of p_r centres reduces the lifetime of the excess electrons which still carry most of the photocurrent.

reduces the capture rate of free electrons, increasing their lifetime, and the n-doped material is said to be photosensitised.

In the p-type material, the opposite happens; the new Fermi energy is below the undoped Fermi level and the resultant increase in trapped positive charge increases the rate of electron capture, reduces the electron lifetime, and the p-type material is said to be desensitised.

Observation of fig.4-2 shows that with sufficiently strong illumination, when the trap Fermi levels are outside the region where the band tails overlap substantially, the photoconductivity eventually saturates. Consideration of the Shockley-Read model of recombination, see fig.2-4, reveals that as illumination is increased, the concentration of excess trapped holes between E_{fo} and E^{p}_{ft} also increases. As these trapped holes act as recombination centres for electrons, saturation of the photocurrent eventually occurs for the n-type material. Note that this implies a change in recombination path from recombination involving initial capture of electrons into the upper part of the mobility gap, in the case of lower intensities, to capture into the lower part of the gap in the case of higher intensities. This change in pathway was given as the reason for the change in from 0.9 to 0.55 which is also shown in fig.4-2. A plot of photoconductivity and γ vs. (E_c-E_{fn}) showed this well. At the same time as the positive charge in the upper part of the gap (caused by the overlap of the donor-like and acceptor-like states) is removed, the quasi-Fermi level is believed

to approach the feature in the density of states at E_x, which will become occupied by a large density of electrons as predicted by the Shockley-Read model. Therefore Anderson and Spear have given the recombination path into the positive charge below gap centre as originating from E_x, not E_c. Again the not quite linear or square root intensity dependence of the photoconductivity is explained as a mixture of monomolecular and bimolecular recombination. This idea has been rejected above. In the discussion chapter of this thesis the author finds that when the quasi-Fermi levels move beyond their respective defect states, recombination becomes monomolecular, this is the opposite of the observations of Anderson and Spear.

Nonetheless the study illustrates how changes in recombination can be used to explain many of the results, particularly when the charge distribution is taken into account.

4.1.2.2 Interpretations using Distributed States

The papers just described and published by the Dundee group have shown how discrete-like states have been used along with other ideas on recombination to explain some of the experimental results. Most groups who have taken photoconductive measurements on a-Si:H have tended to use models involving the presence of distributed states, probably because this is the simplest reason for non-linear (but non-square root) behaviour of the intensity dependence of the photocurrent. The seminal study of Rose[17] has already been described.

Card et. al. [48] have calculated photoconductivity for a

semiconductor with symmetrical exponential tails of the C.F.O. type. E_f is thus in the middle of the gap. The overlap of the tail states continues throughout the gap and gives two types of recombination centre.

States originating from the valence band are donor-like, so are positively charged when empty and capture electrons at a greater rate in this charge state due to Coulombic attraction. Acceptor-like conduction band tail states are neutral when empty and should have a smaller capture cross section for electrons. This is an extension of the ideas put forward in a chapter 2 of this thesis where recombination involving two discrete states was discussed. Using the appropriate cross sections for the acceptors and donors and Shockley-Read statistics the authors demonstrated a sublinear dependence of the photocurrent as light intensity increased, as previously predicted by Rose. Unfortunately no analytical value for γ was given. This paper is not expected to provide the whole explanation for the photoconductive behaviour of a-Si:H as the idea of electron correlation in defect states has not been applied.

The remaining papers discussed in this section present the most modern ideas, and they especially attempt to explain why the observed features of the experimental results do not exactly follow Rose's model[17].

Evangelisti et. al. [49, 50] have made several interesting measurements. They were mostly concerned with the Staebler-Wronski effect, but several of their comments are of great interest in the

study of photoconductivity in amorphous silicon.

Calculation of how the quasi-Fermi level moved with intensity was compared to the expected variation using a purely exponential density of states, and a disagreement was obtained. This led Evangelisti et. al. to suggest that E_{fn} had to move through the minimum in the density of states.

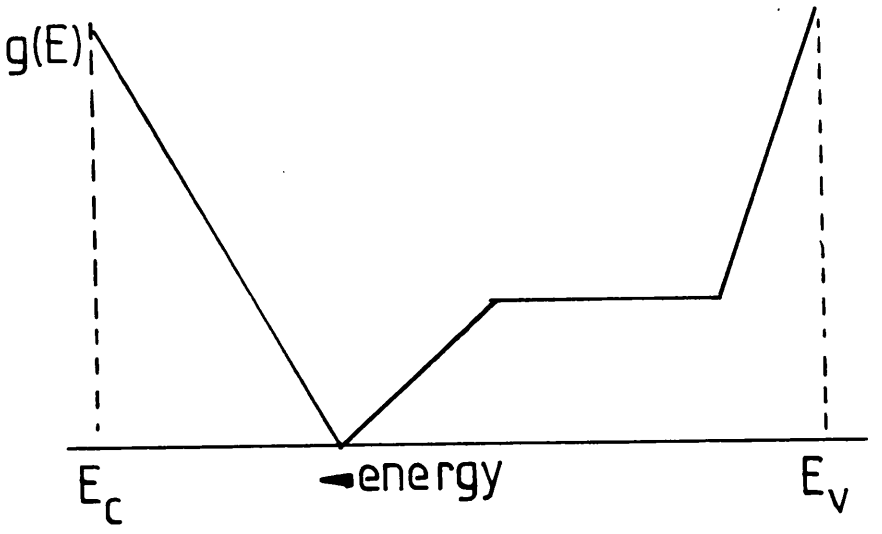

Figure 4-4: The Density of States used by Evangelisti[49, 50].

In the second paper[50] it was pointed out that a mixture of monomolecular and bimolecular recombination would only explain the power law indices for the intensity dependence of the photoconductivity in amorphous silicon over a very short range of intensities, which disagrees with the observation that a well defined γ exists over a large intensity range.

Using the density of states shown in fig.4-4 it was found that the characteristic temperatures of the exponential tails as inferred from photoconductivity measurements were higher than those

inferred from photon absorption measurements. It was speculated that the deeper states would contribute more effectively towards the recombination. All the measurements were at room temperature, so unfortunately the interesting variations of γ with temperature have not been used to confirm the model of the density of states.

The authors, using a more detailed argument than that of Rose[17] obtained the expression

$$G-C_n(n^2+N_T kT\ln(n/n_o))=0 \qquad (4.1)$$

and showed that the power law form of equation(1.23) could still be obtained if the second term in brackets was larger than the first. The symbols have their usual meanings, with N_T as the average density of recombination centres averaged between the dark and quasi-Fermi levels.

The equation reduces to that of Rose for exponential tails. With N_T as a fitting parameter one can only obtain an average density of states. A second feature of eq.(4.1) is that it shows that the intensity dependence is not independent of the dark carrier concentration, n_o, which would explain how values of γ can be erratic from film to film, as small variations in E_{fo} are known to exist. Furthermore the Staebler-Wronski effect [51] is known also to change values of n_o and small differences in light soaking from sample to sample may also have an effect on γ.

The density of states used by these authors is very useful as the additional states in the centre of the gap could now be identified with correlated electronic states.

So far many authors have interpreted γ values between 0.5 and 1.0 as evidence of exponential tails, but recently several authors have shown that other distributions of slowly varying densities of traps have the same property.

Bhattacharya and Narasimhan [52, 53] have shown that calculations on space charge limited current and steady state photoconductivity measurements show comparative discrepancies if an exponential tail is used. Furthermore they calculated γ values for non-exponential tails, and still obtained values of between 0.5 and 1.0.

Also as pointed out in the Rose analysis[17]

$$\gamma = T_c/(T+T_c) \qquad (4.2)$$

where T_c is the characteristic temperature of the exponential tail. In this case a plot of $1/\gamma$ vs. T will be a straight line which has a value of γ of 1.0 only at 0K. This is not found experimentally by Bhattacharya and Narasimhan, nor was it found in the present work as will be seen in the discussion and results chapter.

Hack, Guha and Shur [54, 55] have made calculations of the expected photoconductivity using the density of states in fig.4-5. The extra complication of the deep states was added to explain the results obtained from doped samples. All the states are described by exponential functions with the appropriate characteristic energies, and Shockley-Read statistics are used to give the trap occupation.

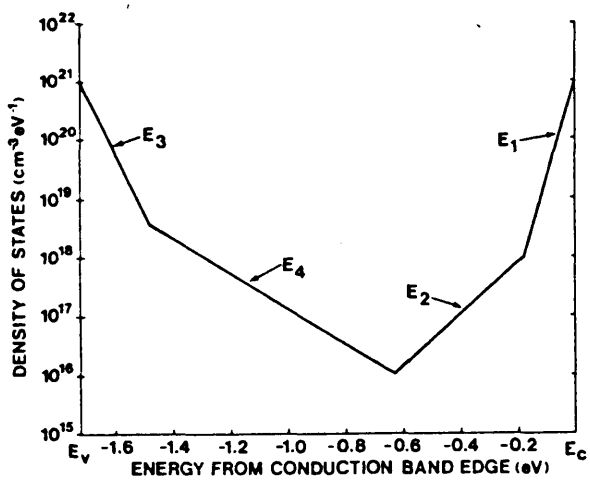

Figure 4-5: The Density of States of Hack et. al.

A plot of γ vs. E_c-E_f (which was changed by doping) at constant temperature and generation rate, gave similar results to Anderson and Spear[14]. As E_f was moved towards the conduction band mobility edge, a plateau was reached in the photoconductivity. The density of states model used by Hack et. al. is different from that of Anderson and Spear in detail, but the interpretation of the results is the same. The Hack model also explains the sensitisation with light n-doping as due to the elimination of positive charge at the cross-over of the deep state tails, and the eventual saturation of photoconductivity as due to an increase of positive charge in the lower half of the mobility gap due to the creation of positive charge in the normal Shockley-Read manner.

The model successfully predicts γ values of less than 0.5, as measured experimentally for strongly doped samples.

Kagawa et.al. [56]have made similar measurements, but modified

the Fermi level position by field effect. They used a model which contained two exponential tails with a quasi-discrete set of defect state in the middle of the gap to act as recombination centres.

Again a γ value of less than 0.5 was obtained for small E_c-E_f values (large band bending). However the γ value varied monotonically with Fermi level position, unlike the abrupt change from 0.9 to 0.55 as found by Anderson and Spear[14]. It was explained that the abrupt change is caused by a change in the density of states as a result of the doping, an effect which is not observed when E_f is changed by band bending.

4.1.2.3 Interpretations using Electron Correlation

The first studies of the effects of electron correlation on the photoconductive behaviour of a-Si:H have been made by Okamoto et.al.[57, 58, 59]. The details of the analysis are too long to include in this thesis, but the density of states used for the case of positive correlation energy is given in fig.4-6.

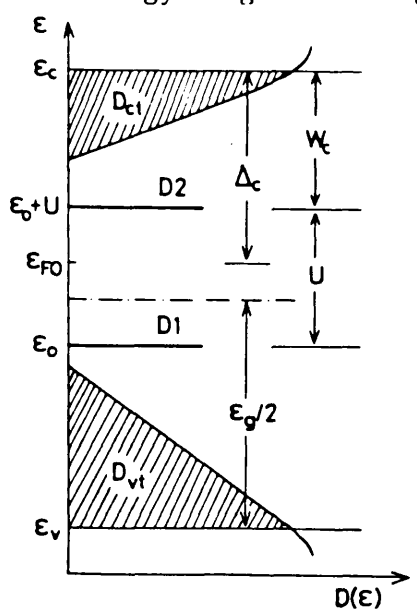

Figure 4-6: The Density of States of Okamoto[59]

The model incorporates uncorrelated "one electron" exponential tail states, and a discrete correlated state. The analysis shows how different values of γ are obtained as the quasi-Fermi levels are made to move through different sections of the localised states.

At low intensities or high temperatures the response is successfully predicted to be monomolecular. At the lowest temperatures or highest intensities, the response is predicted to be bimolecular. At intermediate temperatures or intensities two regimes are possible, depending on whether a critical parameter with units of temperature is exceeded. For this work only one region is considered. For this regime a γ value of between 0.5 and 1.0 is predicted, and an activation energy is predicted for the temperature dependence. This can be considered as a consequence of the discretisation of the correlated states. As intensity is increased, the extra "injected" negative charge changes D^0 states to D^-, and the density of recombination centres is reduced. This causes γ to be less than 1.0.

This model could be regarded as the most complete density of states model considered so far, as band tail states are included with correlated defect states. However a well defined activation energy is not always observed in a-Si:H, see the results section of this work.

4.1.2.4 How Correlation can explain Sensitisation, intuitively

A major consequence of including electron correlation with positive Hubbard energy, U, is that as the quasi-Fermi level is

moved towards the conduction band edge, the density of D^- states is increased at the expense of the other D states. By Coulombic considerations this will seriously reduce the rate of electron capture, and the material will be sensitised. Desensitisation of p-type material can be explained in the same way. Therefore the concept of electron correlation can be used to explain the results of Anderson and Spear[14] or Hack et.al.[54, 55]. Saturation of the photoconductivity with doping could be explained as due to eventual saturation in the density of D^- states.

Okamoto's prediction of bimolecular recombination for the positive U case at the lowest temperatures is in disagreement with the γ value of 1.0 reported in the results section of this thesis.

4.1.2.5 Summary

The above is an attempt to describe all the important models of the photoconductivity of a-Si:H published to date. They all need simplifications to make the analysis possible. As a full explanation of all the observed properties of the material has not yet been published due to the difficulty of the analysis, it is tempting to suggest that computer modelling could lead to a better result. However it seems that even this powerful tool is limited in that an unreasonable amount of computer power would be needed to account for every possible parameter imaginable. This is further discussed in the relevant section of this work. It seems that results for photoconductivity need to be considered along with results from other experiments before a full picture of the properties of the material will be obtained and the subject of the

density of states of a-Si:H remains controversial.

4.1.3 Sputtered Material

It cannot be said that the study of photoconductivity in sputtered a-Si has led to any fundamental changes in the understanding of recombination in amorphous materials. Therefore this section is used as a comparative review of the properties of sputtered and glow-discharge a-Si where they differ.

Historically, films of amorphous silicon made by glow discharge decomposition of silane could be made to have "good" electrical properties before those made by r.f. sputtering of the pure material. a-Si films sputtered from a pure target in argon gas were characterised by a high density of states, could not be doped and were not highly photoconductive.

Following on from experiments on amorphous germanium[60, 61] the Harvard group prepared hydrogenated sputtered amorphous silicon by mixing hydrogen with the argon gas. They proved that the material could be doped and prepared p-n junctions[62] by adding PH_3 and B_2H_6 to the hydrogenated argon.

They also measured the photoconductivity as a function of hydrogen content and substrate temperature[63]. These measurements showed that there was an optimum substrate temperature of about 250°C. As for the hydrogen concentration, it had a photoconductivity peak at two values of H concentration. The peak for the substrate temperature was interpreted to be due to hydrogen

escaping from the sample during high temperature deposition, and that for the hydrogen concentration as due to a change in the valence band structure due to the impurity atoms.

Most important is the idea that the incorporation of hydrogen in the films compensates the dangling bonds, which when optimised with the structural network reorganisation caused by the best substrate temperature, results in a sufficiently low density of states in the sputtered material to make substitutional doping possible. Nonetheless, either because the glow-discharge technique is at a higher stage of development, or because the best glow discharge material is better than the best sputtered material, sputtered material has been a commercial failure.

Moustakas[64, 65] reviews the properties of this material. As found by Anderson and Spear, and Hack et.al., sputtered material also shows photoconductive sensitisation of the n-type material, and desensitisation of the p-type material. The temperature dependence of the photoconductivity was also reviewed, and can be seen to be typical for amorphous silicon.

A review by Paul and Anderson [66] also gives the photoconductive properties of the sputtered material, which also has a dependence on intensity given by equation (1.23). The value of γ is not systematic with temperature.

The properties of sputtered amorphous silicon hydride do not differ fundamentally from those of the glow discharge material,

however examination of the literature reveals a large scatter in the results for values such as room temperature photoconductivity at one intensity for different samples produced in the same preparation chamber, e.g. see Paul and Anderson[66] p298. Variations such as those are presumeably due to differences in the detailed density of states between different samples. This difficulty in control over the properties of the sputtered material is probably the cause of the commercial failure of the material, despite the theoretical easiness and comparitive safety of the method, which does not require the use of the pyrophoric silane. An indication of the higher density of states of the sputtered material is that the Staebler-Wronski effect does not appear to be very marked.

Chapter 5

Photoconductivity with one Defect with Correlation

5.1 Introduction

The mid gap defect in amorphous silicon has been identified as a dangling bond by many authors, mainly due to the e.s.r. signal found in the material as a consequence of unpaired electron spins. The presence of the unpaired spins implies that amorphous silicon posesses a positive correlation energy because (as is described in Chapter 1) eq.(1.25) is endothermic. It costs the correlation energy, U, to add the second electron as the repulsion of the first electron has to be overcome. The effect of this correlation on photoconductivity is not intuitively obvious, but in this section it will be shown for the first time that the effect of correlation on a system with one dangling bond gives a photoconductive response very similar to the two level Shockley-Read-Hall system described previously. In Chapter 8 of this thesis, a distributed localised state model is used to explain the photoconductive properties of undoped a-Si. The analysis is done using one electron states, but the similarity of the results from the two level Shockley-Read-Hall system and the single level correlated state system has been extended to the case of distributed localised states. This similarity has been used such that the distribution of one electron states implied by the analysis is interpreted as due to the presence of correlated states.

5.1.0.1 **Energy Level Diagram**

Figure5-1 shows the energy level diagram for the correlated dangling bond system for the case of positive U only.

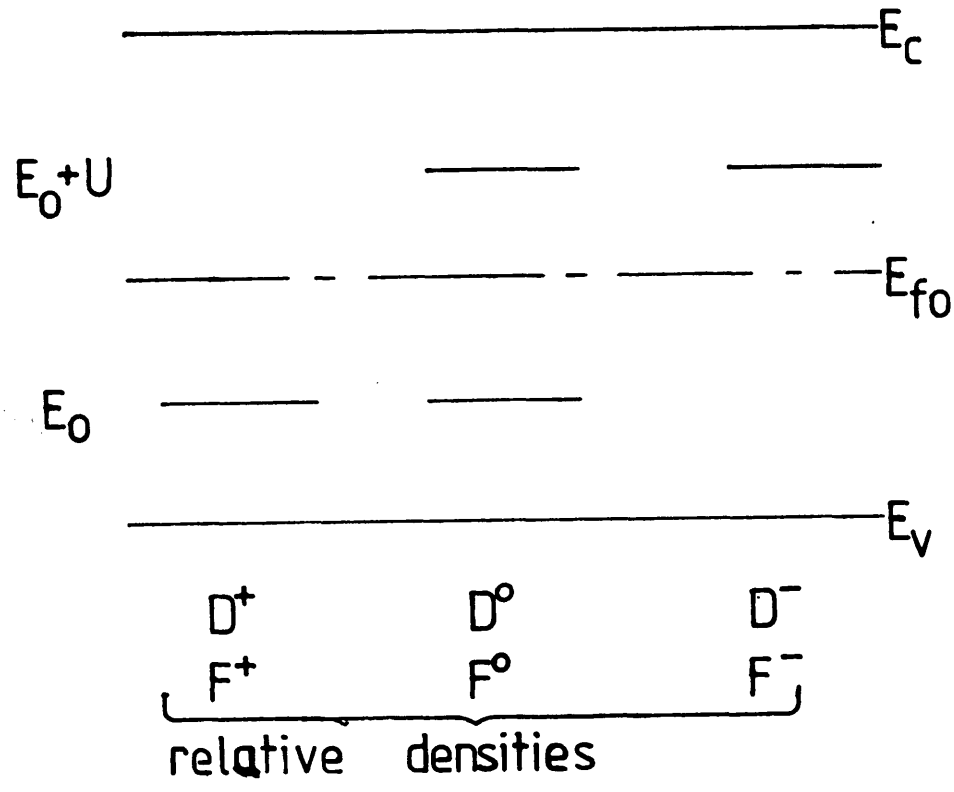

Figure 5-1: Energy Level Diagram with Correlation

The D^+ level is drawn at E_o as energy E_o-E_v is required to excite an electron from the valence band to the defect to form a D^o. The discussion is simplified if E_v is set at zero. The D^- defect is situated at E_{o+U}, as U represents the extra energy required due to the electronic repulsion as the second electron is added to the defect. D^o can be effectively located at two energies, but not of course at the same time. E_o represents the energy released when the electron drops to the valence band, forming D^+; E_{o+U} represents the energy released when the D^- reverts to D^o by electron emission; so

the level used on the diagram depends on the spin status of the defect.

5.1.0.2 Occupation

As Fermi-Dirac statistics only refer to a one-electron system (E_f is the energy required to add one electron to the solid) it is necessary to use the relative densities, F^+, F^o, F^-, which refer to the defects D^+, D^o, and D^- respectively. The use of the occupancy functions are such that

$$F^+ + F^o + F^- = 1 \qquad (5.1)$$

The interpretation of the F functions are that if the density of the defect is N, the density of D^o states at thermal equilibrium is NF^o.

5.1.0.3 Transition Probabilities

Spin degeneracy has an effect on the emission probabilities of localised states. If the states have density N_d, where the subscript defines the state as donor-like, then the density of spin states needs to be $2N_d$, and using the Boltzmann approximation

$$n_d = 2N_d \exp[-(E_d - E_f)/kT] \qquad (5.2)$$

where n_d is the density of occupied donors.

Fig.5-2 shows the donor communicating with the nearest band, as the other transitions have been shown in the previous section to be negligible. Detailed balance is now used to find the emission probabilities, which is justified later. Capture rate into one state equals release rate, if detailed balance is used, which gives

$$n_o C_n N_d = n_d e_n \qquad (5.3)$$

where the symbols have their usual meanings. Substituting eq.(5.2) gives

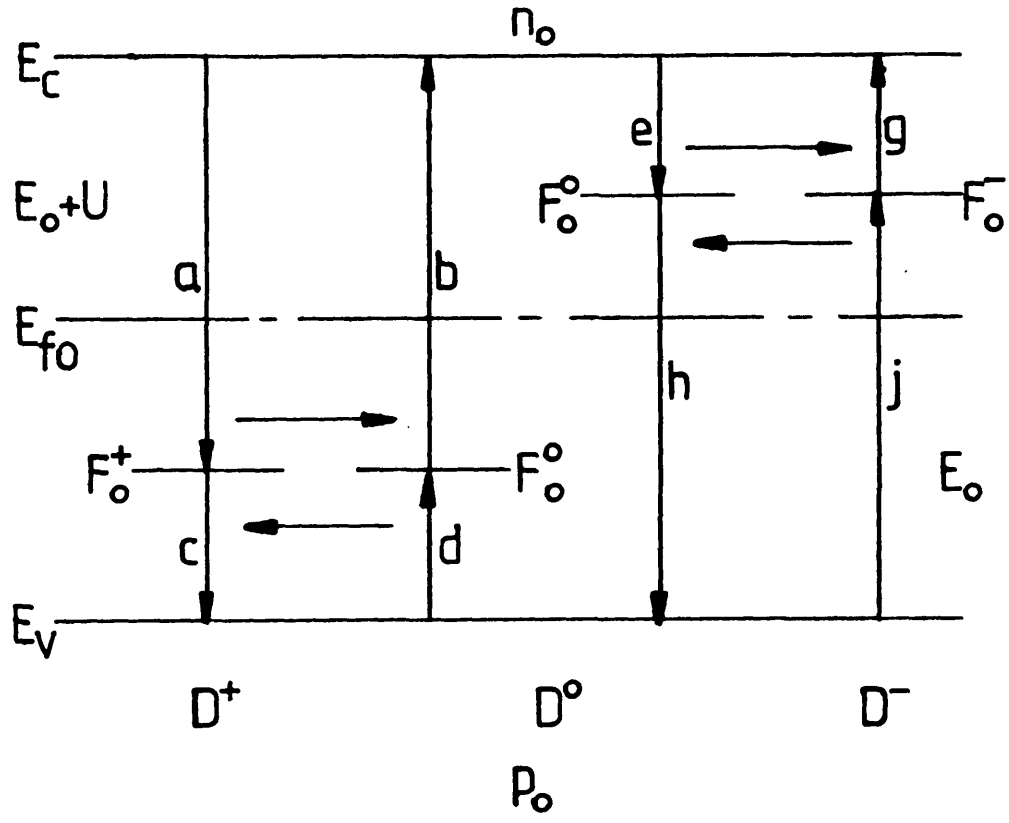

Figure 5-2: Detailed Balance with Spin Degeneracy

$$e_n = 1/2 . C_n N_c \exp[-(E_c - E_d)/kT] \tag{5.4}$$

and as

$$e_n = C_n n_1 \tag{5.5}$$

then

$$n_1 = 1/2 . N_c \exp[-(E_c - E_d)/kT] \tag{5.6}$$

Using similar arguments

$$p_1 = 2 N_v \exp[-(E_d - E_v)/kT] \tag{5.7}$$

which has a factor of two rather than a half.

5.1.0.4 Occupation under Thermal Equilibrium

In thermal equilibrium, one uses the occupancy functions,

$$F_o^+ + F_o^o + F_o^- = 1 \tag{5.8}$$

The various possible transition probabilities(not rates), are

$a = nC_n^+$, electron capture by $D^+ \rightarrow D^o$
$b = n_1^+ C_n^+$, hole capture by $D^o \rightarrow D^+$

$c = p_o^o C_p^o$, hole release by $D^+ \rightarrow D^o$
$d = p_o C_p^o$, hole capture by $D^o \rightarrow D^+$

$e = nC_n^o$, electron capture by $D^o \rightarrow D^-$
$g = n_1 C_n^o$, electron release by $D^- \rightarrow D^o$

$h = p_1^- C_p^-$, hole release by $D^o \rightarrow D^-$
$j = p_o C_p^-$, hole capture by $D^- \rightarrow D^o$

where the transitions are illustrated in fig.5-3.

The 'emission densities', taking spin degeneracy into account are

$$n_1^+ = 1/2 . N_c \exp[-(E_c - E_o)/kT] \tag{5.9}$$

$$n_1^o = 2N_c \exp[(E_o + U - E_c)/kT] \tag{5.10}$$

$$p_1^o = 2N_v \exp[(E_v - E_o)/kT] \tag{5.11}$$

$$p_1^- = 1/2 . N_v \exp[(E_v - E_o - U)/kT] \tag{5.12}$$

Note that the n_1^o and p_1^- terms involve acceptor-like states and will need different capture coefficients than the donor-like states. By inspection it can be seen that

$$n_1^+ p_1^o = n_1^o p_1^- = n_i^2 = n_o p_o \tag{5.13}$$

5.1.0.5 Transition Rates

Given a particular transition probability, the transition rate is given by the product of state density, occupation probability and transition probability. Assuming detailed balance to be valid, then rate a = rate b, so

$$n_o C_n^+ F_o^+ N = n_1^+ C_n^+ F_o^o N \tag{5.14}$$

and

$$F_o^+ / F_o^o = n_1^+ / n_o \tag{5.15}$$

The subscript [o] on the occupancy fraction F denotes the existence of thermal equilibrium. Likewise, rate c = rate d, so

$$F_o^+ / F_o^o = p_o / p_1^o \tag{5.16}$$

Rate e = rate g, so

$$F_o^o / F_o^- = n_1^o / n_o \tag{5.17}$$

Rate h = rate j, so

$$F_o^o / F_o^- = p_1^- / p_o \tag{5.18}$$

It must be the case that

$$F_o^+ + F_o^o + F_o^- = 1 \tag{5.19}$$

Rearranging this for F_o^- and substituting this into eq.(5.17) gives

$$F_o^o = \frac{[1 - F_o^+] n_1^o / n_o}{1 + (n_1^o / n_o)} \tag{5.20}$$

Similarly, appropriate substitution gives

$$F_o^+ = \{1 + n_o / n_1^+ + n_o^2 / n_1^+ n_1^o\}^{-1} \tag{5.21}$$

If this is rewritten by substituting for the emission densities and carrier densities, one obtains

$$F_o^+ = \{1 + 2\exp[(E_{fo} - E_o)/kT] + \exp[(2E_{fo} - 2E_o - U)/kT]\}^{-1} \tag{5.22}$$

By similar arguments

$$F_o^o = F_o^+ 2\exp[(E_{fo} - E_o)/kT] \tag{5.23}$$

and

$$F_o^- = F_o^+ 2\exp[(2E_{fo} - 2E_o - U)/kT] \tag{5.24}$$

These equations are identical to those obtained from analysis by statistical mechanics[23], providing confirmation of the validity of the assumption that detailed balance still applies to the

condition of thermal equilibrium in semiconductors where spin degeneracy and correlation need to be taken into account.

The position of the Fermi energy under the regime of positive correlation energy, U, is found by assuming that

$$F_o^+=F_o^- \ll 1, \quad F_o^o \simeq 1 \tag{5.25}$$

this is justifiable as the $\exp[(E_{fo}-E_o)/kT]$ term is the largest term. Charge neutrality implies that

$$-n_o+p_o-F_o^-N+F_o^+N=0 \tag{5.26}$$

If most of the charge is assumed to be trapped, n_o and p_o can be ignored, and using equations (5.22), (5.24) and (5.25) gives

$$E_{fo}=E_o+U/2 \tag{5.27}$$

which can also be obtained by statistical mechanics.

5.2 Steady State Photoconductivity

When the above ideas on correlation are applied to the steady state photoconductivity of amorphous materials, the photoconductive behaviour is shown to be similar to the Shockley-Read system described previously.

5.2.0.1 Occupation under Illumination

As the occupation of the localised states must change under illumination it is necessary to use the non-equilibrium occupation functions of equation(5.1). As in the Shockley-Read-Hall case, it is assumed that the highest transition rates occur between the relevant defect and the nearest band. Figure5-3 illustrates that rates a & b and h & j are small compared to the more likely transitions c & d and e & R_1 and R_2 indicate that two possible recombination paths are possible. R_1 represents a hole capture by a

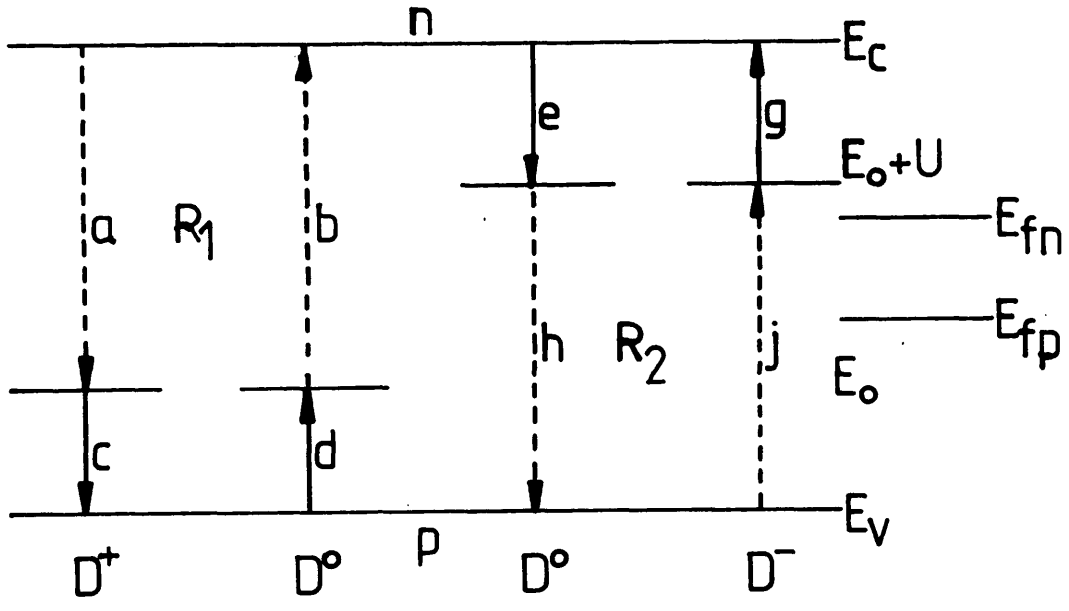

Figure 5-3: Energy Level Diagram Showing the Probable Transitions under Illumination

D^o state, which results in the formation of a D^+ state; recombination occurs when the D^+ state captures an electron to form a D^o state. R_2 describes rapid electron capture by a D^o followed by hole capture. Processes c & d and e & g control the distribution functions, even if the lower rate processes cause recombination in a manner analogous to the Shockley-Read case, if the quasi-Fermi levels are further away from the relevant bands in energy than the transition energies. This is the regime of low and intermediate light intensities. Care should be taken when two competing rates are compared, the absolute value of the capture coefficient is important, a D^o state may have a lower hole capture cross section than the D^+ electron cross section.

Using the preceeding approximations, rate c = rate d, and

$$p_1^o C_p^o F^+ N = p C_p^p F^o N \tag{5.28}$$

or

$$F^+/F^o = p/p_1^o \tag{5.29}$$

Also, as rate e=rate g,

$$F^o/F^- = n_1^o/n \tag{5.30}$$

This last equation is solved for F^o, using

$$F^- = 1 - F^o - F^+ \tag{5.31}$$

to give

$$F^o = [\,1 + n/n_1^o + p/p_1^o\,]^{-1} \tag{5.32}$$

The other two occupancy fractions are obtained by assuming that most of the charge in the sample is trapped, so again by charge neutrality

$$F^- = F^+ \tag{5.33}$$

Equations (5.29) and (5.30) are set so that

$$F^o/F^+ = F^o/F^- \tag{5.34}$$

and

$$p_1^o/p = n_1^o/n \tag{5.35}$$

so eq.(5.32) becomes

$$F^o = (1 + 2n/n_1^o)^{-1} \tag{5.36}$$

and the occupancies of the defect levels can be easily found if the free carrier densities are known.

5.3 Recombination

For low and medium excitation, trapping and release with the nearest band controls the distribution function. Fig.5-3 therefore shows the two possible recombination mechanisms.

Path1, with rate R_1, has rapid trapping by a hole by a D^o

state to form a D^+ state followed by the rate limiting step of electron capture, which dominates the overall recombination rate by path 1. As usual, the slow transition rate is responsible for the electron-hole annihilation. Path2, rate R_2, has rapid electron trapping followed by rate limiting hole capture. As in the Shockley-Read case one pathway is assumed to be dominant.

The recombination rate for path1 is again the difference between electron capture and release, so

$$R_1 = nC_n^+ NF^+ - n_1^+ C_n^+ NF^o \tag{5.37}$$

The approximations for F^+ etc. given earlier assume equality of these two rates, but we now require to find the small difference between the two, the recombination 'leak'. The full expressions are found in Appendix I, and one finds that

$$R_1 = (np - n_o p_o).N/F^o.\left(\frac{n}{C_p^o} + \frac{p_1^o}{C_n^+}\right)^{-1} \tag{5.38}$$

If the same procedure is done for path2, then the total recombination rate is given by

$$R = (np - n_o p_o)N/F^o.\left\{\left(\frac{n}{C_p^o} + \frac{p_1^o}{C_n^+}\right)^{-1} + \left(\frac{n_1^o}{C_p^-} + \frac{p}{C_n^o}\right)^{-1}\right\} \tag{5.39}$$

if the approximate value for F^o is used. Equation (5.35) holds for non-equilibrium steady state conditions, but as in the dark $p=p_o$ and $n=n_o$ it must also be valid. Thus, in thermal equilibrium

$$p_o = n_o p_1^o / n_1^o \tag{5.40}$$

Substituting this equation and (5.35) into (5.39) gives

$$R = p_1^o/n_1^o (n^2 - n_o^2) N F^{o-1} \left\{\left(\frac{n}{C_p^o} + \frac{p_1^o}{C_n^+}\right)^{-1} + \left(\frac{n_1^o}{C_p^-} + \frac{p}{C_n^o}\right)^{-1}\right\} \tag{5.41}$$

5.4 Low Light Intensities

Here we assume $\Delta n < n, \Delta p < p$. Equation (5.41) can now be rewritten

$$R=G=p_1^o/n_1^o 2\Delta n n_o N F^{o-1}\left\{\left(\frac{n_o}{C_p^o}+\frac{p_2^o}{C_n^+}\right)^{-1}+\left(\frac{n_1^o}{C_p^-}+\frac{p}{C_n^o}\right)^{-1}\right\} \quad (5.42)$$

by expanding the first term in the brackets. Simplifying gives

$$R_{tot}=G=2n_o\Delta n p_1^o N/n_1^o.\left\{\left(\frac{n_o}{C_p^o}+\frac{p_2^o}{C_n^+}\right)^{-1}+\left(\frac{n_1^o}{C_p^-}+\frac{p}{C_n^o}\right)^{-1}\right\} \quad (5.43)$$

the first reciprocal term in the brackets refers to recombination via path1 and the second to path2.

5.4.0.1 Path1

If path 1 dominates, then path 2 is ignored, and

$$R=G=2n_o\Delta n\,\frac{p_1^o N}{n_1^o}\left(\frac{n_o}{C_p^o}+\frac{p_2^o}{C_n^+}\right)^{-1} \quad (5.44)$$

which can be rearranged to give

$$\Delta n=G\left\{\left(C_p^o 2\frac{p_1^o}{n_1^o}N\right)^{-1}+\left(C_n^+ 2\frac{n_o}{n_1^o}N\right)^{-1}\right\} \quad (5.45)$$

The rate of recombination depends on the capture transition with the slowest rate. The first term corresponds to transition d, the capture of a hole by a D^o state, and the second term corresponds to transition a, the capture of an electron by a D^+ state. As transition a involves a greater energy loss than transition d, it is ignored for reasons given previously. This argument only applies if the energy levels E_o and E_o+U are approximately symmetrical in the band gap, which may not be the case in a-Si:H if D^+ is near mid gap as according to some authors[67]. Ignoring the second term, and solving for n gives

$$\Delta n=G\,n_1^o/C_p^o 2 p_1^o N \quad (5.46)$$

which is monomolecular in G. Substituting for the temperature dependent terms gives

$$\Delta n\propto\exp[2(E_{fo}-E_{fi})/kT] \quad (5.47)$$

where E_{fi} is the intrinsic Fermi level, defined as mid gap. This has a positive activation energy for a-Si:H when $E_{fi}<E_{fo}$.

5.4.0.2 Path2

Now path1 is ignored. Equation(5.40) eliminates p, and after rearranging

$$\Delta n = G\left[\frac{(n_1^\circ)^2}{C_p^- 2n_o p_1^\circ N} + \frac{1}{2NC_n^\circ}\right] \qquad (5.48)$$

The first term in the above equation involves capture of a hole by a D^- state, transition j, the second term involves capture of an electron by a D^o state, transition e. As the first term is larger, then

$$\Delta n = G(n_1^\circ)^2 / 2n_o C_p^- N p_1^\circ \qquad (5.49)$$

which has an activation energy given by

$$\Delta n \propto \exp([2(E_{fo}-E_{fi})+U/2]/kT) \qquad (5.50)$$

which will be positive.

This analysis shows that the low intensity region 1 of the photoconductive response has a positive activation energy and a monomolecular response to light intensity.

5.5 Medium Light Intensities

In this circumstance, $\Delta n, \Delta p > n_o, p_o$, and the quasi-Fermi levels are still between the relevant defect levels, so $\Delta n \ll p_1^\circ$ and $\Delta n \ll n_1^\circ$. Ignoring the lower terms mentioned in the previous paragraphs gives

$$R = \frac{\Delta n^2 p_1^\circ N}{n_1^\circ}\left\{\frac{C_n^+}{p_1^\circ} + \frac{C_p^-}{n_1^\circ}\right\} = G \qquad (5.51)$$

if equation (5.35) is substituted for p, and $n_o p_o$ is ignored. The first term is path1 which represents electron capture by a D^+ state as the first step, whereas path2 represents hole capture by D^-

5.5.0.1 Path1

Ignoring path2, and solving for Δn gives

$$\Delta n=(Gn_1^o/NC_n^+)^{1/2} \tag{5.52}$$

which is bimolecular in form. Substituting for the temperature dependent term gives

$$\Delta n \propto exp[-[E_c-(E_o+U)]/kT] \tag{5.53}$$

which describes a negative activation energy.

5.5.0.2 Path2

Ignoring path1 and solving for Δn gives

$$\Delta n=(G[n_1^o]^2/p_1^oNC_p^-)^{1/2} \tag{5.54}$$

which is again bimolecular in G. Using the temperature dependent terms gives

$$\Delta n \propto exp-([E_c-(E_o+U)]-1/2.(E_o-E_v))/kT \tag{5.55}$$

which is again negative.

Thus both paths give for region 2 of the photoconductive response negative activation energies and bimolecular intensity dependence.

5.6 High Light Intensities

Since this regime is defined to be such that the quasi-Fermi levels are "outside" the relevant defect levels, the emission terms can be ignored and only capture processes need be considered. Appendix I shows that

$$F^o \simeq 1 \tag{5.56}$$

and due to charge neutrality considerations, $F^+=F^-$.

Ignoring the emission terms, and using $np \gg n_o p_o$, with $\Delta n=n$, $\Delta p=p$, then using appendix I, $\Delta p=C_r \Delta n$ gives

$$R=G=\Delta n(1/C_p^o+1/C_n^o)^{-1} \tag{5.57}$$

which solved for Δn gives

$$\Delta n=G/N.(1/C_p^o+1/C_n^o) \tag{5.58}$$

For both paths the photoconductive response in region 3 is temperature independent and linear in intensity.

5.6.1 Conclusion

Examination of the table in fig.5-4 will show that the results from the Shockley-Read-Hall system of recombination, applied to a two level system are very similar to a system using a single level but including the effects of electron correlation. In the discussion section of this work, this result is extended to the more difficult case of recombination centres distributed in energy. The analysis is done for a one electron model, but it is then assumed that this similarity allows one to identify the recombination centres with correlated states.

Figure 5-4: Comparison of the Results for the Two Level Shockley-Read-Hall system and the Single Level System with Electron Correlation

Intensity Regime	2-level system	Correlated system
LOW	path 1 $\Delta n \propto \exp\left[\frac{2(E_a - E_f) - (E_f - E_d)}{kT}\right]$ path 2 $\Delta n \propto \exp\left[\frac{(E_a - E_f)}{kT}\right]$ monomolecular recombination	$\Delta n \propto \exp\left[\frac{2E_{fo} - E_{fi}}{kT}\right]$ $\Delta n \propto \exp\left[\frac{2(E_{fo} - E_{fi}) + U/2}{kT}\right]$
MEDIUM	path 1 $\Delta n \propto \exp\left[\frac{-2(E_c - E_a) + (E_d - E_v)}{2kT}\right]$ path 2 $\Delta n \propto \exp\left[\frac{-(E_c - E_a)}{2kT}\right]$ bimolecular recombination	$\Delta n \propto \exp\left[\frac{-(E_c - [E_o + U])}{kT}\right]$ $\Delta n \propto \exp\left[\frac{-(E_c - [E_o + U]) - \frac{1}{2}(E_o - E_v)}{kT}\right]$
HIGH	path 1 $\Delta n = \frac{G}{C_{na} N_a}$ path 2 $\Delta n = \frac{G R_d}{C_{nd} N_d}$ monomolecular recombination	$\Delta n = \frac{G}{N\left(\frac{1}{C_p^o} + \frac{1}{C_n^o}\right)}$

Chapter 6

Computer Modelling

6.1 Introduction

As has been previously mentioned, the analysis of the steady state or transient photoconductivity of a system with an arbitrary density of states is too complicated for straightforward mathematical analysis without severe simplification. A suitable solution for this problem is to use computer simulation.

Simulations of both steady state and transient measurements have been done in this study using programs originally devised by Dr. C. Main, the supervisor of this study. Modifications of the programs have been made by the author of this thesis to suit particular cases; while he cannot claim these programs to be his original work, he has made extensive use of them as research aids and has gained insights into the processes being modelled by their use. A brief description of the methods is felt to be necessary, and this follows.

The programs were used with the worker as part of a closed loop. A "first guess" for the density of states and trapping parameters was within the appropriate section of the computer program, which was then run on the DECSYSTEM-20 mainframe digital computer, and the result of the simulation was obtained, usually graphically. After inspection, changes were made to the relevant parameters until the simulated result was identical to the experimental result, either within experimental error, or within the

limits of the computer model. The programs were checked to see if they were physically reasonable by using them on exponential densities of states that were TROK-like and an exact correspondence with the TROK analysis was obtained[68].

6.2 Density of States

A semiconductor with an arbitrary density of states possesses a continuous finite density of states throughout the band gap. For the purposes of computer modelling this continuum is easily represented by a quasi-continuous discretised set of j+1 levels spaced at energy intervals dE. If a gap of width E_g is to be divided into j spaces, then

$$dE=E_g/j \tag{6.1}$$

j is chosen so the magnitude of dE does not put discretisation errors into the simulation, but, typically, reducing dE below kT in width made no further improvement.

For a C.F.O. type model we have acceptor like conduction band tail states and donor like valence band tail states, where the density of states for both tails is,

$$g_a(E)=Gexp(-(E_c-E)/E_a) \tag{6.2}$$

and

$$g_d(E)=Gexp(-E/E_d) \tag{6.3}$$

where E_a and E_d are the characteristic energies of the conduction and valence band tails, and G represents the band edge densities, set to be equal for simplicity. The units for g(E) are cm-3eV-1. The discretised densities are written

$$g_a(j)=dE*Gexp(-(E_c-j*dE)/E_a) \tag{6.4}$$

and

$$g_d(j)=dE*Gexp(-j*dE/E_d) \tag{6.5}$$

with units now of cm^3. This approach is approximate to the integration of the continuous density of states over the energy range dE.

G is related to the effective density of states at the band edge by

$$N_c=G*kT \tag{6.6}$$

For each energy there are two seperate density of states functions, both of which are considered seperately for convenience.

6.3 Simulation of the Steady State Photoconductivity

6.3.1 Trap Occupation at Thermal Equilibrium

The equilibrium Fermi level, E_{fo} needs to be found so the equilibrium carrier densities n_o and p_o can be used to calculate the excess densities. The Fermi-Dirac function, $f_o(E)$, is used to find the electron occupation, and for hole occupation $[1-f_o(E)]$ leads to errors in numerical precision for the states below E_f, so

$$\bar{f}(E) = \frac{exp\left(\frac{E-E_{fo}}{kT}\right)}{1+exp\left(\frac{E-E_{fo}}{kT}\right)} \tag{6.7}$$

is used.

Now we have

$$n_o=N_c*f_o(E_c) \tag{6.8}$$

and

$$p_o=N_v*\bar{f}_o(0) \tag{6.9}$$

as the valence band edge is arbitrarily set to zero in energy.

Charge neutrality considerations are such that

$$-n_o + p_o - \sum_j g_a(j) \times f_o(j) + \sum_j g_d(j) \bar{F}_o(j) \qquad (6.10)$$

So for computation, this needs to be solved for E_{fo} by iteration, after suitable values have been substituted for all the parameters.

The result of the iteration in the programs used in this study is that E_{fo} for an undoped sample lies close to the cross over of the exponential tails in a C.F.O. type model, because of the electric charge at either side of E_{fo}.

6.3.2 Occupation under Illumination

As has been shown previously, occupation under illumination is given by Shockley-Read statistics, eq.(2.28). The emission terms can be written

$$n_1(j)=N_c\exp(-(E_c-j*dE)/kT) \qquad (6.11)$$

and

$$p_1(j)=N_v\exp(-j*dE/kT) \qquad (6.12)$$

for the discretised set of states. Again electron occupancy is used for the conduction band tail and hole occupancy for the valence band tail. It has to be taken into account that the species ratio, R, will be different for the two tails, R_a=0.01, R_d=100, due to their charge/occupancy natures. This gives

$$f_a(j)= \frac{R_a n + p_1(j)}{R_a n + p_1(j) + R_a n_1(j) + p} \qquad (6.13)$$

for the electron occupation and

$$f_d(j) = \frac{R_d n_1(j) + p}{R_d n + p_1(j) + R_d n_1(j) + p} \tag{6.14}$$

for the hole occupation. The charge neutrality condition is now

$$-n+p-\sum_j g_a(j) f_a(j) + \sum_j g_d f_d(j) = 0 \tag{6.15}$$

6.3.3 Method of Solution

The charge neutrality condition apparently has two implicit unknowns, n and p. However n and p are interdependent. The method used is to assume a value for n, say $10*n_0$, and then iterate the charge neutrality equation to find the value of p which gives a zero net charge for this value of n.

6.3.4 Recombination Rate

Once n and p are found, the trap occupations are easily found using eq.(2.28). Now the recombination rate needs to be found, since this equals the excess generation rate. Note that this will give the intensity dependence of the steady state photoconductivity. It has been shown previously that the excess generation rate for one discrete state is the difference between electron capture rate from the conduction band and the emission rate into the conduction band. Put into the discretised form for the simulation, we have

$$R = G = \sum_j C_{na} g_a(j) \left\{ \frac{np - n_0 p_0}{R_a(n+n_1) + p + p_1} \right\} \tag{6.16}$$

$$+ \sum_j C_{nd} g_d(j) \left\{ \frac{np - n_0 p_0}{R_d(n+n_1) + p + p_1} \right\}$$

This gives the excess recombination rates directly for each tail, as the thermal equilibrium values for n and p included within the calculation will give zero recombination due to detailed balance.

The whole procedure can be repeated for several chosen values of total electron density, $n=1.1n_o$; $n=2n_o$; etc. Electron correlation could also be included, but due to the lack of time this has not been proceeded with.

This is the method used in the steady state photoconductivity simulation computer program, STEADY, which is included in appendix 2.

6.4 Computer Modelling of the Transient Photoconductivity

6.4.1 Introduction

The steady state case is easy to calculate as Shockley Read statistics will always give the full occupation values for the model at steady state after sufficient time for iteration has been allowed. For the transient case the occupations for each discretised state needs to be known for each discretised value of time over which the simulation is set to run. The smallest time step involved needs to be somewhat less than one trapping time, otherwise instability may occur in the solution. At each time step, a different set of occupation statistics will be required as the excess carriers thermalise down the band tails. This means that much more calculation is needed for the transient case, which would soon lead to inconveniently long C.P.U. times unless simplification

was used. Due to the format of the relevant equations for transient measurements, matrix transformation techniques are ideal for this application.

6.4.2 Basic Equations for the Linear Case

If the j_{th} trap has a density of $N_t(j)$ and a trapped electron occupation density of $n_t(j)$ then at any instant

$$dn/dt=-\sum_j nC_n(j)N_t(j) + \sum_j n_1(j)C_n(j)n_t(j) \quad (6.17)$$

where the first term represents trapping and the second release. Also

$$dn_t(j)/dt=+nC_n(j)N_t(j)-n_1(j)C_n(j)n_t(j) \quad (6.18)$$

The trapping is normalised so that the overall trapping time is 1.0, i.e.

$$\tau_{t=1}=1/\sum_j C_n(j)N_t(j) \quad (6.19)$$

and $N_c=1$.

Time steps are produced in the following manner. In the short time δt, the changes in electron densities δn and $\delta n_t(j)$ are

$$n=-\sum_j nC_n(j)N_t(j)\delta t + \sum_j N_1(j)C_n(j)n_t(j)\delta t \quad (6.20)$$

and

$$n_t=+nC_n(j)N_t(j)\delta t -n_1(j)C_n(j)n_t(j)\delta t \quad (6.21)$$

So, if we go from step i to step i+1, then

$$n^{i+1}=n^i+ n \quad (6.22)$$

and

$$n_t^{i+1}(j)=n_t^i(j)+ n_t(j) \quad (6.23)$$

The calculation for all states can be given in matrix form as

$$[n^{i+1}]=[A][n^i] \quad (6.24)$$

Figure 6-1: The Transition Matrix

$$
\begin{bmatrix}
1-\Sigma C_n(j)N_t(j)\delta t & n_1(j)C_n(1)\delta t & \cdots & n_1(j)C_n(j)\delta t & \cdots & n_1(n1)C_n(n1)\delta t \\
C_n(1)N_t(1)\delta t & 1-n_1(1)C_n(1)\,t & \cdots & 0 & \cdots & 0 \\
\vdots & & \ddots & & & \\
C_n(j)N_t\delta t & 0 & 0 & 1-n_1(j)C_n(j)\delta t & \cdots & 0 \\
\vdots & & & & \ddots & \\
C_n(n1)N_t(n1)\delta t & 0 & 0 & 0 & \cdots & 1-n_1(n1)C_n(n1)\delta t
\end{bmatrix}
$$

where [A] is the transition matrix, illustrated on fig.6-1. Note that only row 1, column 1, and the diagonal elements are present. The time steps can be accelerated as

$$[n^{i+2}]=[A][n^{i+1}]=[A][A][n^{i}] \tag{6.25}$$

so

$$[ni]=[A]^{i}[n^{0}] \tag{6.26}$$

where $[A]^{i}$ is the i^{th} power of matrix [A] and $[n^{0}]$ is the initial condition.

This gives rapid generation of long time steps without instability as the transform matrix is squared each step, and it is further convenient as most transient results are plotted in double logarithmic form, so the size of the time step can be adjusted so that suitable intervals are plotted. Continued squaring of [A] leads to the steady state stationary solution when $t\rightarrow\infty$, although small truncation errors can arise. In practice this is not observed, and this program could be used to give steady state solutions, as can be seen from the section on the step response in Chapter 7.

The required solutions can be read from the matrix at any required time interval to give the transient response which can be plotted conveniently by a graphics routine. Whichever transient is to be simulated depends on the initial conditions and the matrix $[n^{o}]$. For the flash response we have

$$[n^{0}]= \begin{bmatrix} 1 \\ 0 \\ 0 \\ \vdots \\ 0 \end{bmatrix} \tag{6.27}$$

By including other elements in matrix [A], monomolecular recombination can be included. Similarly a constant generation can also be modelled.

The programs can also be modified to include any required density of states or capture coefficient, but as these two occur as products the effect of either cannot be distinguished from the other, as the transient response will be slow for high capture rate by localised states whether this is caused by one or the other parameter. This program is listed in the appendix 3.

An extension of this method allowing trap filling and bimolecular recombination(non-linear effects) was used in the transient photoconductivity computer simulation TRANS, here the matrix is updated as the transient proceeds. This program was used in the interpretation of the experimental results, as described in Chapter 7, and the program is listed in appendix 4.

Chapter 7

Experimental Method

7.1 Preparation of Samples

The samples used in this study were produced by two methods. Firstly sputtered material was used, then glow discharge decomposition material.

7.1.1 Sputtered Amorphous Silicon

r.f. sputtering is a useful technique to prepare amorphous silicon. In this technique, an r.f. field is set up between two electrodes, one of which is earthed and onto which the substrates that will receive the deposited material are mounted. The other electrode is the target which holds the material that is to be deposited. When this electrode is in the negative half cycle of the r.f. field, the positive argon ions in the plasma are accelerated onto the target and collide with sufficient force to dislodge some of the target atoms which find their way to the substrates. The presence of hydrogen in the chamber causes the silicon to react with it, and as is well known, the electronic properties of the a-Si are vastly improved by the incorporation of the small atom, as described in chapter 4.

The plasma is not uniform, and there is a reduction in the ion concentration near the target; if the plasma is examined a dark space can be seen which extends for a few millimetres from the target. As this is the most resistive region of the plasma, due to the reduction in density of ionised material, most of the voltage

drop of the r.f. field occurs here, and the volt drop in this region accelerates the plasma ions directly onto the target. This voltage of acceleration is called the d.c. bias, and it is indicated on the sputtering machine, as it is a measure of how energetic the target collisions are. A value of 0.8kV is a typical figure.

Fig.7-1 shows the configuration of a typical sputtered sample, with undoped hydrogenated amorphous silicon deposited onto evaporated aluminium gap cell electrodes.

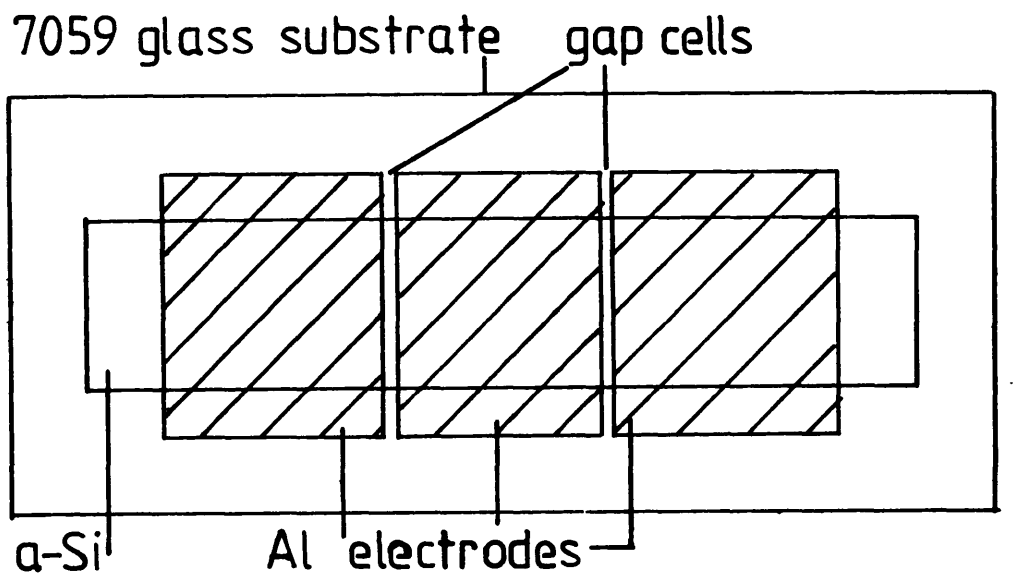

Figure 7-1: Sputtered samples

The sputtered hydrogenated amorphous silicon was prepared in the Nordiko r.f. sputtering system in Dundee College of Technology. As shown in fig. 7-2 the system has the following features. The vacuum chamber is evacuated by an Edwards 19E vacuum system, which consists of a rotary pump and a 9 inch diffusion pump. This is used to

Figure 7-2: Schematic diagram of the Nordico bias sputtering system.

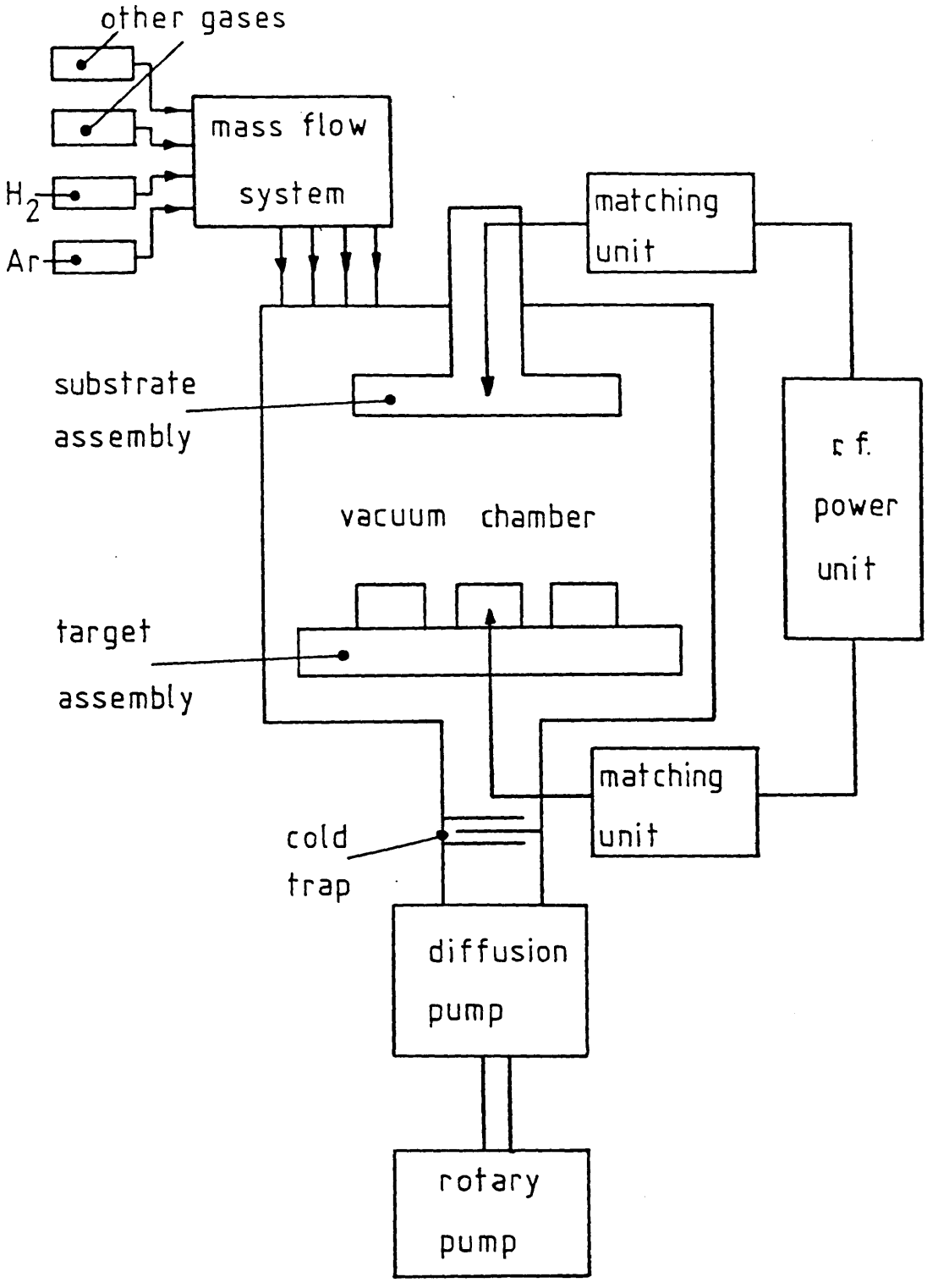

evacuate the system to its ultimate vacuum of about 10^{-5} torr to ensure that contamination by out gassing of material adsorbed on the inside of the system is negligible.

The sputtering target was a 4inch disk of poly-crystalline silicon.

Corning glass substrates were mounted onto a circular copper substrate holder which held up to eight glass slips disposed radially 10cm. above the target. A copper-constantan thermocouple junction was screwed to the substrate holder. A heater in good thermal contact with the holder allowed the substrate temperature to be varied. As the r.f. field interfered with the thermocouple signal, the heater current had to be at a pre-set value and the ultimate temperature measured before the r.f. field was switched on. This took a considerable time (at least four hours) as the thermal inertia of the system is high. A substrate temperature of 240 C produced the best films from this system[69]. A table of the conditions used in the sputtering system is given in fig.7-3.

Temperature	240 C
r.f. power	0.64 watts/cm2
D.C. bias	0.8kV
Overall pressure	15μmHg
Ar:H_2	2.75:1
Sputtering time	17 hours
Sample thickness	1.3μm

Figure 7-3: Sputtering parameters

Hydrogen and argon gases were introduced to the system by a mass flow apparatus which regulated the overall pressure with a M.K.S. Baratron 260 series pressure sensor and control system which automatically varied the rate of gas flow to maintain a constant chamber pressure. The desired ratio of hydrogen to argon remained fixed at the value in fig.7-3.

The a.c. sputtering field was produced by a Nordiko r.f. generator which operated at a frequency of 13.56 MHz, impedance matched to the generator.

Substrates, on which suitable aluminium electrodes were already deposited by vacuum evaporation, were mounted into the sputtering machine and had the thermocouple attached. The silicon target was rotated to a position below the substrates, and the target cooling water was turned on.

When the conditions inside the chamber were suitable, a plasma was then initiated by turning on the r.f. field, and perhaps momentarily increasing the gas pressure to ease plasma formation. The reflected r.f. power was tuned out and the plasma was left for eight hours to sputter the target surface clean. After this the substrate cover was removed and the hydrogenated amorphous silicon was deposited until an appropriate thickness was obtained. Finally the system was purged of gasses, cooled down to room temperature, and the samples removed.

7.1.2 Glow Discharge Decomposition Amorphous Silicon

This material is prepared by causing a plasma to decompose silane gas SiH_4 at low pressures. Because the starting material is already hydrogen rich the material so produced is already hydrogenated. The samples in this study were supplied by Philips Research Laboritaries, Redhill, Surrey. Fig.7-4 shows the arrangement of the interdigitated gap cell arrangement used by Philips.

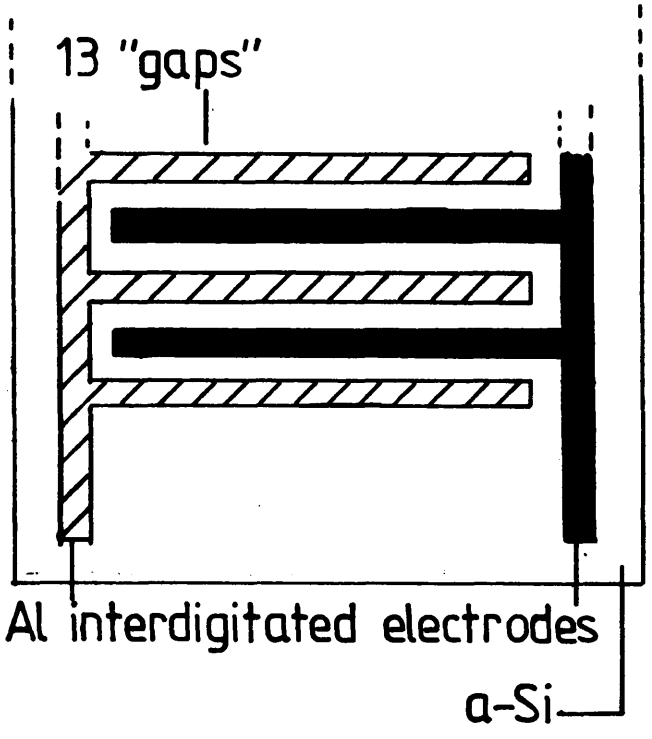

Figure 7-4: Glow Discharge Samples

Chapter 4 describes how this glow discharge method has often produced material with better electrical properties for use in device manufacture than any other method. This is not a fundamental property, as the Harvard group has produced good device grade material by sputtering, however in this work, it is shown later that the glow discharge material was the superior. The automatic

inclusion of hydrogen into the a-Si reduces the spin and localised state densities in such a controllable manner that glow discharge decomposition of a-Si:H is the basis of a multi-million dollar industry, whereas sputtered a-Si is not produced in large quantities commercially.

7.2 Experimental Apparatus

As measurements of photoconductivity need to be made at temperatures lower than $0^{\circ}C$, the samples need to be measured under a vacuum, or water vapour would condense on the sample and holder. Consequently, the samples were stuck to a brass holder with silicon grease, and the holder was screwed to a stainless steel finger, fig.7-5. The finger was attached to a stainless steel flange which formed one of six detachable sides to a stainless steel cube. Each face of this cube could be given a purpose. The lower end of the finger was immersed in liquid nitrogen to allow the sample temperature to be reduced, and the electrical connections to the sample were on this flange.

Electrical connections to the sample were made with silver DAG suspension on the thin(60μm) aluminium wires. These wires were in turn put on to p.t.f.e. insulated copper wires which led the sample current to B.N.C. connectors on the flange.

A platinum resistance thermometer sensor was placed in a hole in the brass sample holder within 2mm of the sample. This allowed the temperature of the sample to be fixed by an Oxford Instruments D.T.C.2 three-term temperature controller. Furthermore, the sample

Figure 7-5: The Sample Holder

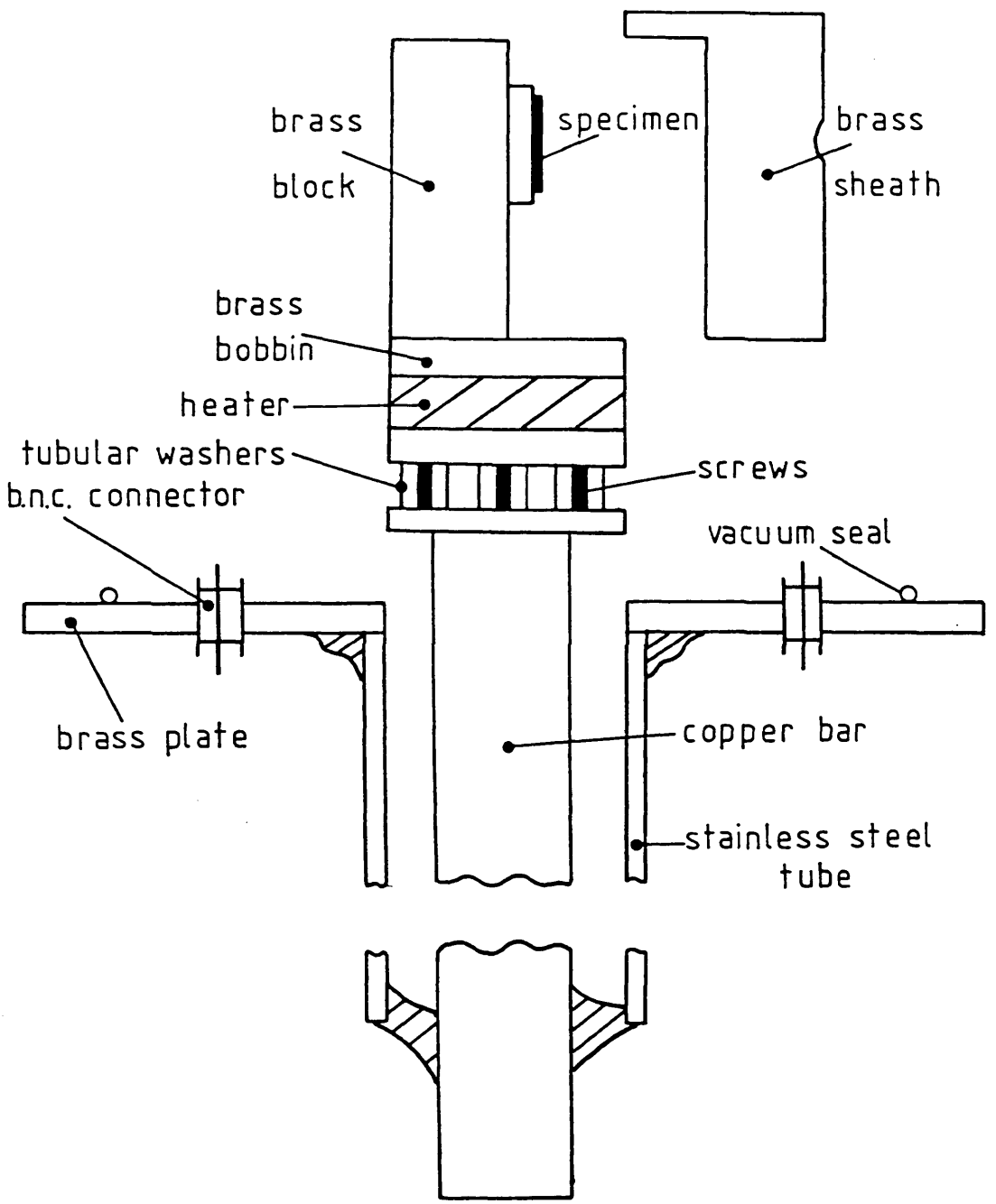

holder was bolted to a non-inductively wound 30 Ohm heater, which was on a brass bobbin screwed to the cold-finger, so the temperature could be varied at will by using the temperature controller to balance the heater against the heat loss caused by the liquid hydrogen.

At very low temperatures, to avoid heating the sample by black body radiation from the vacuum chamber, two brass and copper jackets surrounded the sample and were mounted to the cold finger and heater to ensure that it faced an environment similar to its own.

The samples were illuminated by two methods. Firstly by a L.E.D. fitted to the end of a plastic or silica glass light pipe. The latter had an arrangement by which the sample end of the pipe could be moved to traverse the sample and facilitate the alignment of the beam. The wavelength of this source was changed by the selection of the appropriate L.E.D.fig.7-6

green	555nm
yellow	570nm
red	660nm
infra-red	940nm

Figure 7-6: L.E.D. light sources

The light pipe was put through a face in the vacuum chamber, and it fitted into the holes in the two sample jackets.

Secondly, the samples were illuminated by nanosecond pulses

from a Laser Science Inc. VSL-337 dye laser. This was operated at 580nm. with an output of 5kw for 10ns, i.e. a pulse of $1.5*10^{14}$photons.

A thermopile was used to calibrate a p-i-n diode to relate the light output of the L.E.D.s to the diode current. The L.E.D. sources could be operated at a higher current than the normal steady state maximum of 20ma. for short times in the step response measurement. A p-i-n diode with a fast response amplifier was used for this, with which only high outputs could be measured. This output was measured on a C.R.O. using a measuring resistor.

The laser was calibrated using a Scientech 362 power energy meter, which gave the energy of the pulse directly when the pulse was allowed to fall onto the detector. Only maximum intensity measurements were performed with the laser.

The oscilloscope used was a Textronix 7623A storage scope, which when used on the FAST setting could store pulses with the time base set at least at 20ns/division. A 7B53A dual time base could be used to compensate for triggering delays at such short times. For high currents at short times, typical in flash decay measurements, a 7A15A amplifier with a 50MHz bandwidth allowed measurements down to 40ns where "ringing" in the measurement system was observed, at long times, when the current was perhaps one millionth of the early values, a 7A22 differential amplifier was used which had a larger gain than the 7A15A, but only a 1MHz bandwidth. This balance could not be achieved for the step response, so methods involving

amplification were necessary. They are described below in the section on transient measurements.

7.3 Experimental Method.

7.3.1 Steady State Measurements.

7.3.1.1 Dark Conductivity

All samples were characterised by the measurement of the dark conductivity. With the sample in a vacuum, a d.c. power supply was used to apply an electric field of about $10^4 Vcm^{-1}$ to the sample. This field was chosen to minimise any high field effects. The dark current was measured by a Keithley 610C electrometer on which the lowest current measureable was 10^{-13}amps.

7.3.1.2 Photoconductivity

The sample was illuminated as described above. Under illumination conditions two methods were used, depending on the relative magnitudes of the dark and photocurrents.

Firstly, the low temperature/high intensity regime. Here the photoconductivity is very much higher than the dark conductivity, and a direct measure of the total current using the 610C is sufficient.

Secondly, when the photocurrent is less than about 100 times the dark current, a "back off" system, fig.7-7, was used, where approximately equal dark currents from two gap cells oppose each other. Only one gap is illuminated so an electrometer or a C.R.O. measuring across a series resistor, directly read the photocurrent. Unfortunately, due to small differences in the detailed properties

of each half of the double gap cell system, the balance point changed significantly with temperature, so the measuring instrument had to be set at a suitable datum with the sample in the dark, then the light was turned on and the deflection of the instrument display was recorded. As the electrometer did not have a sufficient back-off range, the measurements at the highest temperatures had to be taken with a C.R.O. with a differential amplifier input panel and the system was limited by the noise introduced by this to about 1% of the dark current at that temperature.

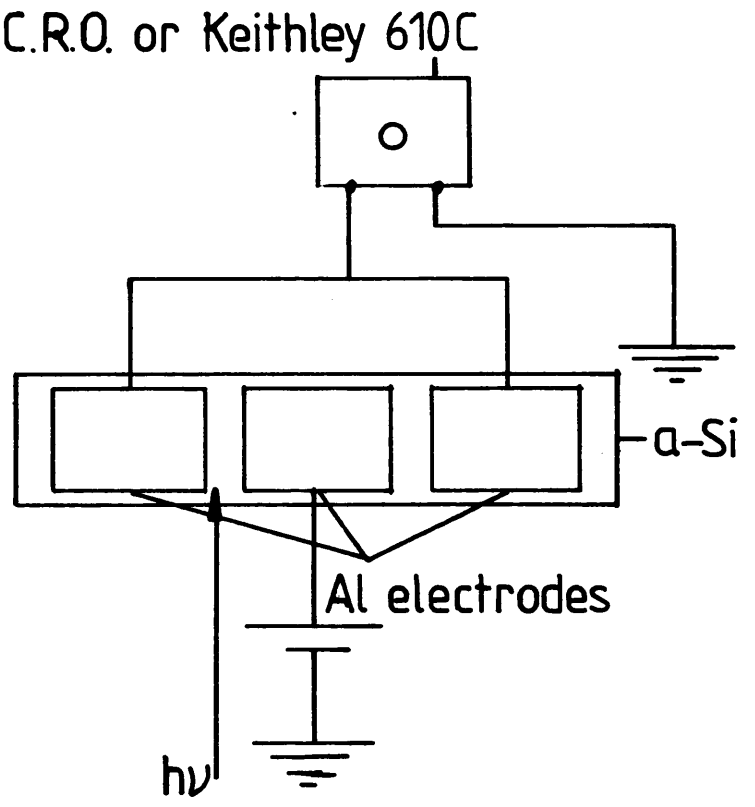

Figure 7-7: The Circuit for Steady-state Measurements

If a precision lock-in amplifier could be used, this 1% limit would be removed, but the available lock-in amp. needed to detect a

chopped square wave signal, which had to be at a frequency of above 5Hz. Unfortunately the material in this study did not have a short enough response time to allow it to be used.

There were two main steady-state experiments. Firstly, the temperature dependence of the photoconductivity at a fixed intensity of illumination. Secondly, at a temperature fixed by the temperature controller, the intensity dependance of the photocurrent was measured.

7.3.2 Transient Measurements

The transient rise of the photoconductivity in response to step illumination was measured. A signal generator was used to supply the pulse to the L.E.D., the current in which was measured on a C.R.O. to control the photon flux as described above. The photocurrent was detected on a C.R.O. by measurement of the signal across a suitable measuring resistor in series with the sample, sometimes after suitable amplification. The current transient was read from the stored display on the CRO.

Secondly, the transient photocurrent decay was measured. As the current is high at short times, a small measuring resistor can be used and the RC time constant can be smaller than in the case of the transient rise experiment, and shorter measuring times can be achieved. CRO triggering can be from the signal pulse itself, or externally from the LASER trigger, as convenient. Again the pulse was displayed by the storage facility of the oscilloscope.

Chapter 8

Results and Discussion

8.1 Glow Discharge Material

8.1.1 Characterisation

8.1.1.1 The Samples

Those samples used in this study which were produced by the glow discharge decomposition of silane were supplied as multi interdigitated samples on Corning 7059 glass substrates with aluminium electrode patterns which covered the entire surface of the slide. This was because the electrode configuration was similar to that used in thin film transistors, but with no gate or gate insulator to allow photoconductivity measurements. Consequently it was not possible to perform optical absorption measurements on the same film to obtain information about the optical gap or dielectric constant (from fringe analysis). Also the thickness of the samples. 9μm was too large for measurements at high α, which could cause difficulty in finding E_{opt} from the plot of $(\alpha h\nu)^{1/2}$ vs. $h\nu$. The only other available samples were 0.3μm thick. but at this thickness surface effects would have disallowed bulk measurement as the charge screening length is of the same order of magnitude as the thickness. Therefore a typical value of 1.8eV is used for E_g, and α for the red light illumination used in the experiments (660nm, 1.8eV) is taken to be $10^4 cm^{-1}$, [10].

8.1.1.2 Dark Conductivity

Characterisation of the samples was done by measurement of the dark conductivity, and a typical result is shown in fig.8 1.

Figure 8-1 Dark Conductivity of GD a-Si

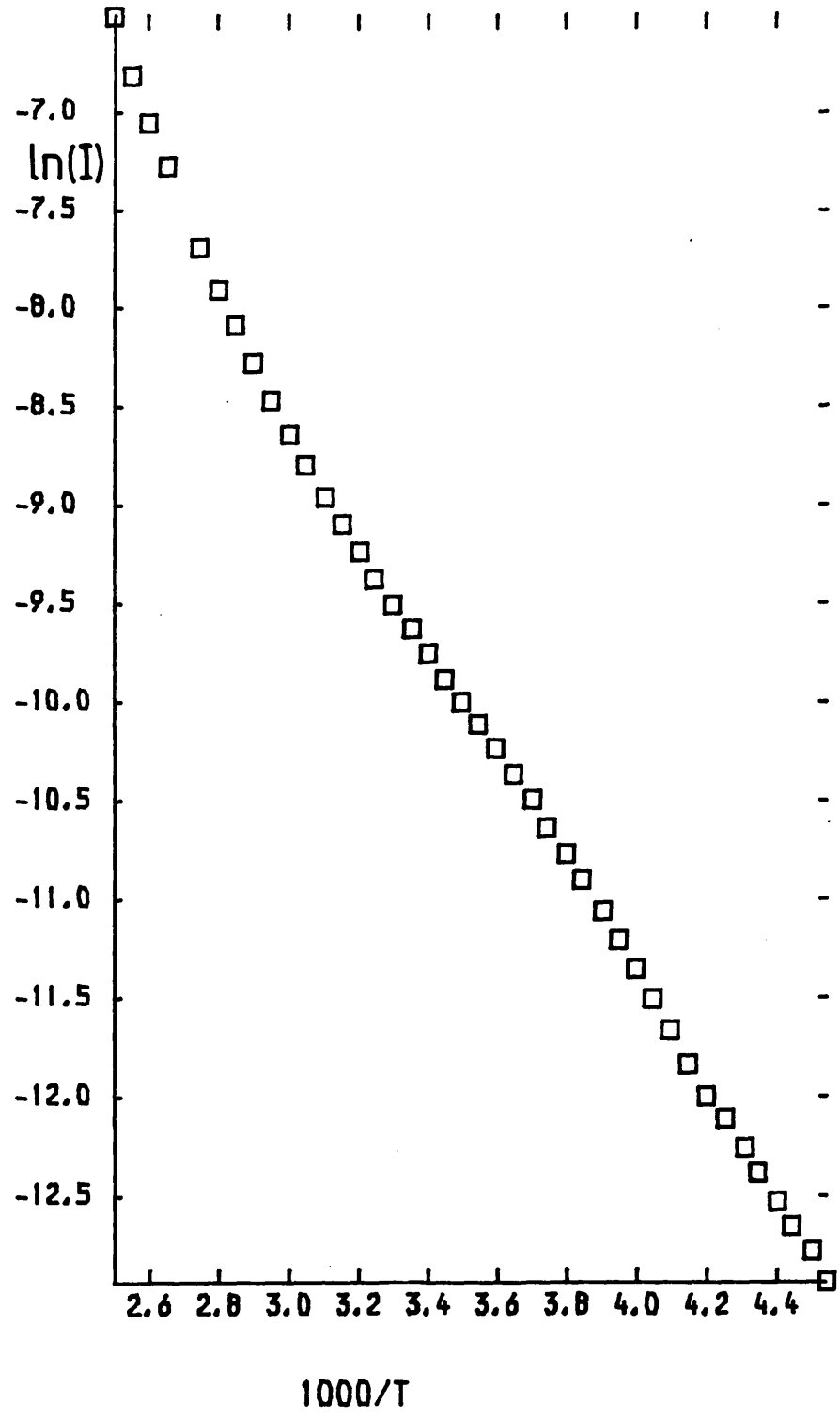

The activation energy for the dark conductivity is 0.84eV which is high[70] for undoped material. As light soaking increases the dark conductivity activation energy[71] all the measurements on the GD material may be on the light soaked state, although dark conductivity measurements were always performed before strong and steady illumination was applied. Furthermore, the absorption depth of the red light is about 1μm and the samples were 9μm thick so the reduction in conductivity in the top allegedly light soaked, layer would be dominated by the layer beneath. Unfortunately the samples were rendered useless if the temperature was raised above 373K, so they could not be annealed properly An increase in noise was the most obvious effect of overheating, so as a-Si should be able to withstand 500K[72], it is suggested that contact effects are causing the problem. Hepburn [73] has seen that application of a high voltage after annealing restores the original properties on F E.T. samples produced by the same manufacturer, possibly because this re-establishes the contacts.

The increase in the activation energy could be caused by band bending at the semiconductor surface, but this implies a charge screening length approximately the same as the sample thickness of 9μm, which is too high for a-Si[6].

The dark conductivity was remeasured throughout the photoconductivity meaurements, but no change in activation energy was observed. This implies that the samples were received in the light soaked state, possibly due to excitation during deposition.

The value of σ_o was calculated to be $820(\Omega cm)^{-1}$, a typical figure for extended state conduction.

8.1.2 Steady State Photoconductivity

8.1.2.1 Experimental Results

The temperature dependence of the steady state photoconductivity of glow discharge a-Si:H illuminated by a red L.E.D. is shown in fig.8 2. The dark conductivity is also plotted and this illustrates the first interesting feature of the results. Even when the photocurrent is only 1% of the dark current at the high temperature region, the slope of the curve of the photocurrent has still not turned over to become positive, as predicted by most theories. At the low temperature region, it can be seen that at both incident intensities, the photocurrent has become constant with temperature down to the low temperature limit of the measuring system.

These features are more clearly seen in fig.8 3 which shows the measured intensity dependence of the steady state photoconductivity at several temperatures, using the red L.E.D. as the source. The x-axis represents the bulk photogeneration rate, assuming that $\alpha = 10^4 cm^{-1}$ and that the generation is constant to the absorption depth of $1\mu m$. As is typical, the intensity dependence of the photocurrent is described by equation (1.23) over several orders of magnitude of intensity but the behaviour at low intensities and high temperatures is not typical for undoped material.

At high temperatures and low intensities one expects the

Figure 8-2: Temperature dependence of the steady state photoconductivity

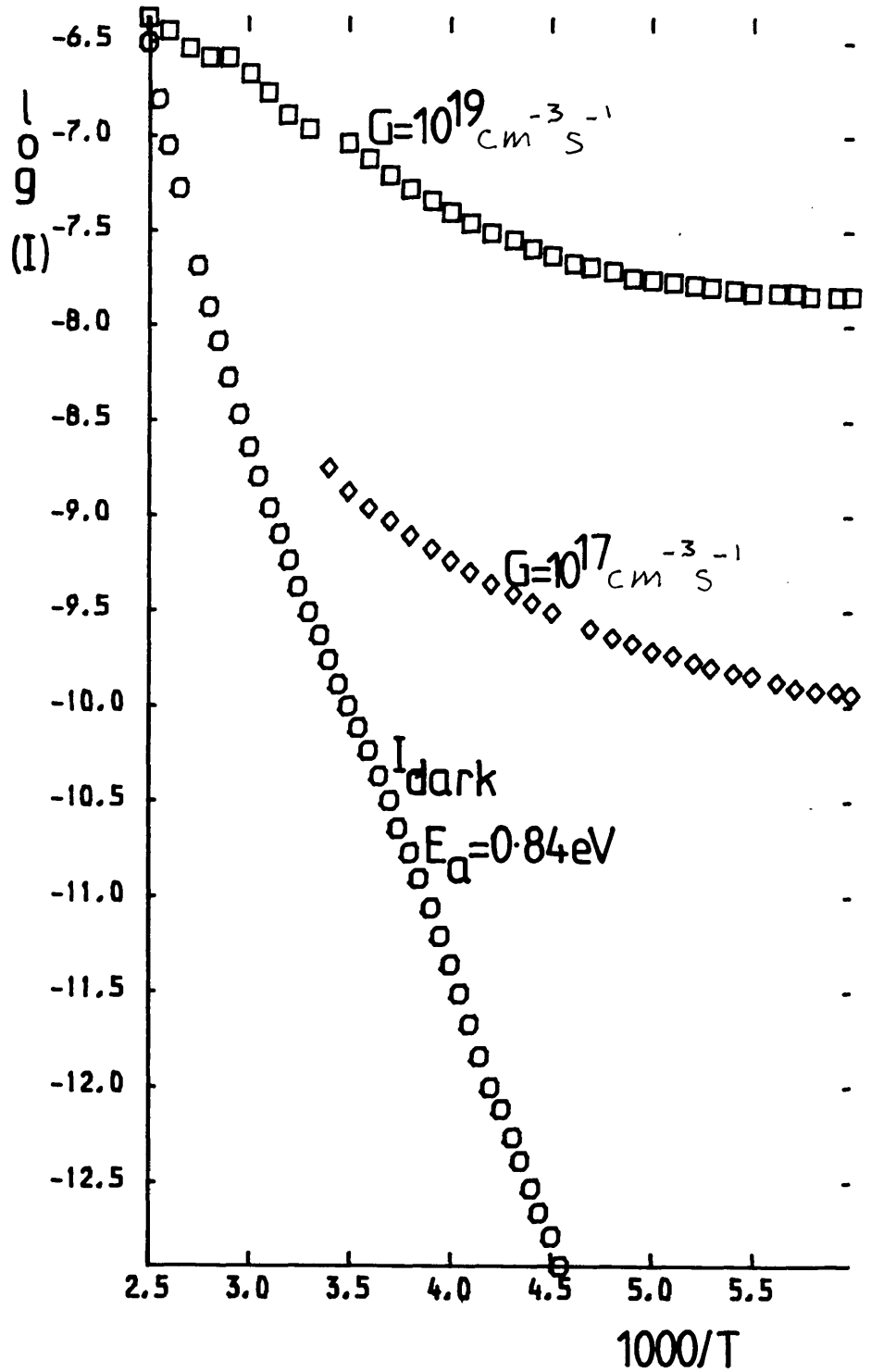

Figure 8-3: Intensity dependence of the steady state photoconductivity

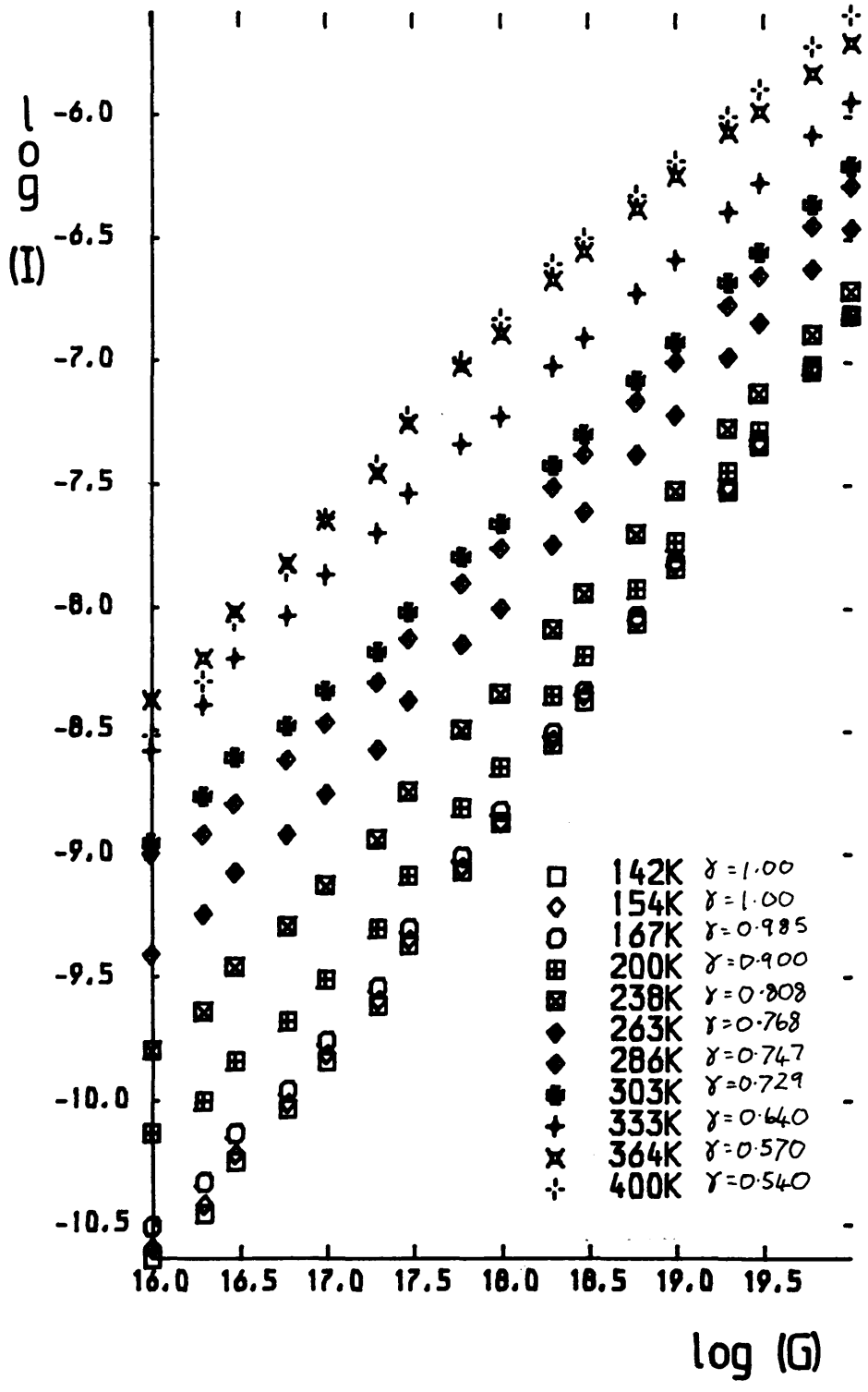

intensity dependence to become monomolecular when the photocurrent drops below the dark current. The positive slope of the temperature dependence should be evident in this figure in that below the break in the curve where it bends over to a gradient of 1.0, the curve should progress to points below those from curves taken at lower temperatures, i.e. a "crossover". However this was not observed experimentally; at 400K, γ changes from 0.54 to 0.78, as the intensity is decreased. The point at which the gradient changes is when the photocurrent is 25% of the dark current. At 364K a change in gradient occurs when the dark and photocurrents are almost equal. The arrangement of the curves on the graph indicates that at intensities below the experimentally achievable values, a positive slope to the temperature dependence of the photocurrent will be obtained, i.e. the curve for the higher temperature will drop below that of the lower.

At the lowest temperatures measured, the results are very interesting in that γ becomes 1.0, i.e. recombination is monomolecular. The results for 167K are scarcely distinguishable from those at 154K, and the points for 142K cannot be shown on the graph as they lie exactly on the same line as those at 154K. This is the keystone for the interpretation of the results.

8.1.2.2 Interpretation of the Intensity Dependence

For computational convenience, it is assumed in the following that the samples are evenly illuminated up to their absorption depth; this is only the case for weakly absorbed radiation, but as described previously, perhaps the diffusion coefficient is such as

to distribute the photoexcited carriers throughout the depth of the sample sufficiently quickly for this to be a reasonable assumption.

At low temperatures and high intensities, the quasi-Fermi levels are furthest removed from the dark Fermi level. Furthermore, monomolecular recombination occurs for a situation where there is a constant density of recombination centres. The simplest explanation of the gradual increase in γ as temperature is reduced until monomolecular behaviour is observed is that as the quasi Fermi level is moved away step by step from the thermal equilibrium position, at low displacements it is moving through a region of distributed localised states acting as recombination centres, hence $0.5 < \gamma < 1.0$, as the density of recombination centres is increasing with intensity Eventually the trap Fermi level moves outside the distribution of states and monomolecular recombination is observed. This restriction in recombination is necessary to explain the observed results, as otherwise a constant density of recombination centres, which is a necessary condition for monomolecular recombination, would not be obtained. The model put forward here is believed to be the simplest way of obtaining such a condition taking into account the expected features in the density of states in amorphous silicon, in particular the dangling bond, with which the recombination centres will be identified later in this thesis.

In real amorphous materials, one would expect that any density of states feature would be disorder broadened by at least kT. However in this interpretation, it is assumed for simplicity

that the distribution of states ends abruptly at a critical energy.

As a-Si:H is easily doped, this leads to the conclusion that the density of states is low near E_{fo}, if not at a minimum, so the density of states model used here involves a minimum in the density of distributed states at E_{fo}. a sharp reduction in the effective density of states at some critical energy in both band tails, and a rising density of states of exponential form between E_{fo} and the critical energy. An exponential form of the distributed states is used purely for simplicity. It is also assumed in the following that the measured photocurrent is due solely to electrons.

Taylor and Simmons [33] have shown that

$$\Delta n = G \int_{E_{fo}}^{E_{ft}^{n}} C_n(E) g(E) dE \qquad (8.1)$$

The occupation of each state is not involved in this equation because it was self cancelling in the derivation. In the integration the upper limit is the trap quasi-Fermi level, unfortunately it is difficult to calculate E_{ft}^{n} as n and p need to be known, however inspection of equations (2.31)and(2.34) reveals that E_{fn} is always less than E_{ft}^{n} by the amount

$$E_{ft}^{n} - E_{fn} = \ln([p/Rn]+1) \qquad (8.2)$$

which will not be very large in undoped a-Si, which is slightly n-type. So in the following argument, the free electron quasi Fermi level is used in equation(8.1) to replace the trap quasi-Fermi level as the upper limit of integration.

The capture coefficient is placed inside the integral in equation (8.1) because in a system where there are several fundamentally different types of localised state one would expect different values for C_n, especially when electron correlation is taken into account.

The theory of electron correlation and its effect on the photoconductivity has been discussed earlier, where it was shown that the behaviour of a single discrete correlated state (this state is shown at two energies in the energy level diagram, fig.5 1) was similar to that of a system using two discrete uncorrelated energy levels. So in the absence of a simple mathematical technique for distributed correlated states this analysis uses two uncorrelated sets of distributed states. As hole photocurrents are never observed in undoped a-Si, a further simplification is that the corresponding equation to (8.1) for holes does not need to be considered.

8.1.2.3 The Density of States Model

Calculations on the data, as given later, are consistent with an exponential density of states rising from a minimum at E_{fo}, which can be expressed as

$$g(E)=g(E_{fo})\exp(E/E_1) \qquad (8.3)$$

A value of $10^{17}cm^{-3}eV^{-1}$ is used for $g(E_{fo})$, which is a typical figure[6], and E_1 is the characteristic energy of the exponential tail for which a value of 0.05eV gave the best fit. The effective density of states is assumed to fall to zero at a critical energy of 0.23eV above E_{fo}. This is not necessarily the case, rather C_n may

drop substantially at this point, but which is the case cannot be ascertained with the available data.

8.1.2.4 Calculation of the Capture Coefficient

As

$$\Delta n = I/e\mu EA, \qquad (8.4)$$

Δn can be substituted into eq.(8.1) where the upper limit of integration is replaced by E_{fn}, but the value of E_{fn} is never allowed to exceed 0.23eV to produce the effect of restricting recombination within the critical range. If eq.(8.3) is used for g(E), then clearly eq.(8.1) can be solved for C_n. This is equivalent to assuming a constant capture coefficient for the states which control recombination in this model, which is a reasonable assumption for these states because they are envisaged as of the same origin and therefore fundamentally similar. Alternatively it can be taken to mean that the capture cross section varies more slowly than the density of states. Table 1 shows calculations of C_n for all of the temperatures and intensities at which the steady state photoconductivity was measured.

If the above model was totally correct, the calculated values of C_n would all be exactly the same. But the calculated values vary slightly, i.e. for 238K the calculated values for C_n fall slowly from $2*10^{-8}cm^3s^{-1}$ to $1.1*10^{-8}cm^3s^{-1}$ until E_f has been moved 0.23eV from E_{fo} when C_n rises to $1.4*10^{-8}cm^3s^{-1}$. However the calculated values for C_n do not vary more than a factor of two throughout the whole range of calculations, except for some of the low intensity measurements. These measurements are not expected to give such a

Figure 8-4: Table I

G ($cm^{-3}s^{-1}$)	Δn (cm^{-3})	ΔE_f (eV)	C_n ($cm^{-3}s^{-1}$)
167K			
10^{16}	$1.9*10^{6}$	0.3	$8.7*10^{-9}$
10^{17}	$1.1*10^{7}$	0.33	$1.5*10^{-8}$
10^{18}	$9.4*10^{7}$	0.36	$1.8*10^{-8}$
10^{19}	$9.7*10^{8}$	0.39	$1.8*10^{-8}$
10^{20}	$9.7*10^{9}$	0.42	$1.8*10^{-8}$
200K			
10^{16}	$4.6*10^{6}$	0.22	$5.5*10^{-9}$
10^{17}	$1.9*10^{7}$	0.24	$8.8*10^{-9}$
10^{18}	$1.4*10^{8}$	0.28	$1.2*10^{-8}$
10^{19}	$1.2*10^{8}$	0.31	$1.4*10^{-8}$
10^{20}	$9.7*10^{9}$	0.35	$1.7*10^{-8}$
238K			
10^{16}	$1.0*10^{7}$	0.12	$2.0*10^{-8}$
10^{17}	$4.5*10^{7}$	0.16	$1.8*10^{-8}$
10^{18}	$2.94*10^{8}$	0.19	$1.5*10^{-8}$
10^{19}	$1.9*10^{9}$	0.23	$1.1*10^{-8}$
10^{20}	$1.2*10^{10}$	0.27	$1.4*10^{-8}$
286K			
10^{16}	$7.5*10^{7}$	0.06	$1.15*10^{-8}$
10^{17}	$3*10^{8}$	0.1	$1.04*10^{-8}$
10^{18}	$1.4*10^{9}$	0.13	$1.15*10^{-8}$
10^{19}	$6.3*10^{9}$	0.17	$1.09*10^{-8}$
10^{20}	$3.1*10^{10}$	0.21	$0.85*10^{-9}$
10^{21}	$1.3*10^{11}$	0.24	$1.28*10^{-8}$

good fit, as the measurements were more difficult at such low photocurrents, and the Taylor and Simmons equation (3.1) applies to the medium and high intensity regimes, i.e. $\Delta n > n_o$. The average value of C_n is about $1.5*10^{-8}cm^3s^{-1}$. If v_{th} is assumed to be a typical $10^7cm.s^{-1}$, then $\sigma_n \simeq 10^{-15}cm^2$, which is reasonable for a neutral capture centre. Street[74] gives a value of $2.7*10^{-15}cm^{-2}$ for ballistic capture of an electron by a neutral defect. Therefore the recombination centres could be identified with the neutral dangling bond in a-Si:H, or if correlation is recognised to exist, the D^o states.

8.1.2.5 Computer Simulation of the Steady State Photoconductivity

The above analysis has given a reasonable model for the steady state photoconductive response of the a-Si used in this study. As explained below, an analytical model of the transient measurements is not so easily obtained, so for the sake of consistency a computer simulation of the steady state photoconductivity was performed, using the computer program STEADY. a simpler program than TRANS.

The parameters used were as follows. The conduction and valence band tails were exponential, with characteristic energies of 0.05 and 0.08eV respectively. These numbers were chosen to place E_{fo} in the upper part of the mobility gap; E_{fo} is within kT of the intersection of the band tails, also this value for the conduction band tail characteristic energy is the same as that used in the analysis in the last section. R was 100 and 0.01 for the donor like valence band tail and acceptor like conduction band tails

respectively, which is a typical figure for a coulombic/neutral capture ratio. The capture coefficients were $C_{na}=10^{-8}cm^3s^{-1}$ and $C_{nd}=10^{-6}cm^3s^{-1}$.

Figure 8 5 shows the best results for the computer simulation of the intensity dependence of the steady state photoconductivity. The recombination efficiency of states outside the critical energies, measured down from E_c as 0.45eV for the conduction band tail and 1.0eV for the valence band tail, was reduced to zero. The dependence of γ on intensity is shown on fig.8 6. The intensity dependence is similar to that of the measured data in fig 8-3, but γ is predicted to be 1.0 at very low intensities and high temperatures.

Fig.8-7 shows the measured variation of γ with intensity. This varies more sharply than the computer modelled version in fig.8 6, perhaps because the experimental gradient is taken from a series of points and the computer calculated one is an instantaneous value. Nonetheless the simulation successfully predicts qualitatively the general form of the response. The deviations from the experimental results are probably because the density of states model and simulation program are not sufficiently complex to model exactly the real situation.

8.1.3 Transient Rise

8.1.3.1 Measurements of the Step Response

Figures 8-8 to 8-11 show the double logarithmic plots of the measurements of the step response at different temperatures and

Figure 8-5: Computer Simulation of the Steady State Photoconductivity

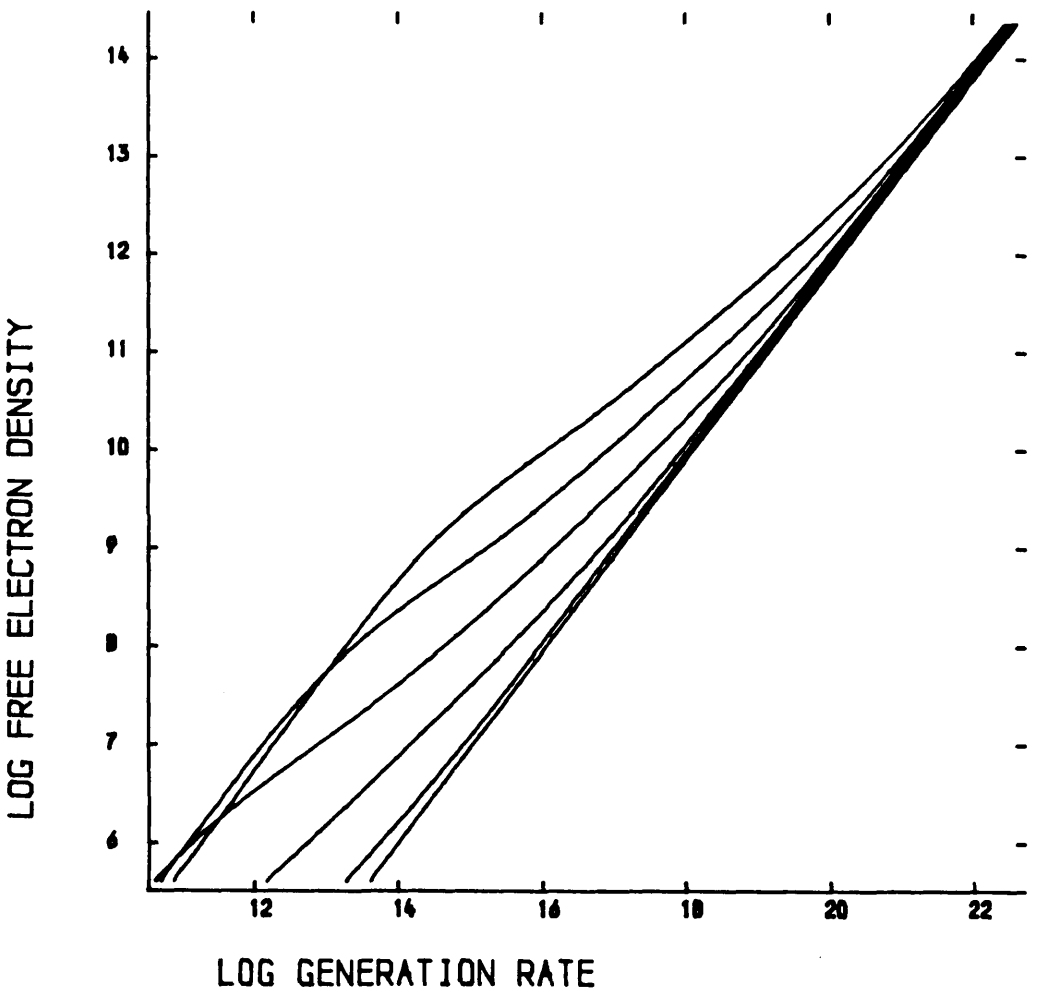

Figure 8-6: Computer Simulation of the Steady State Photoconductivity

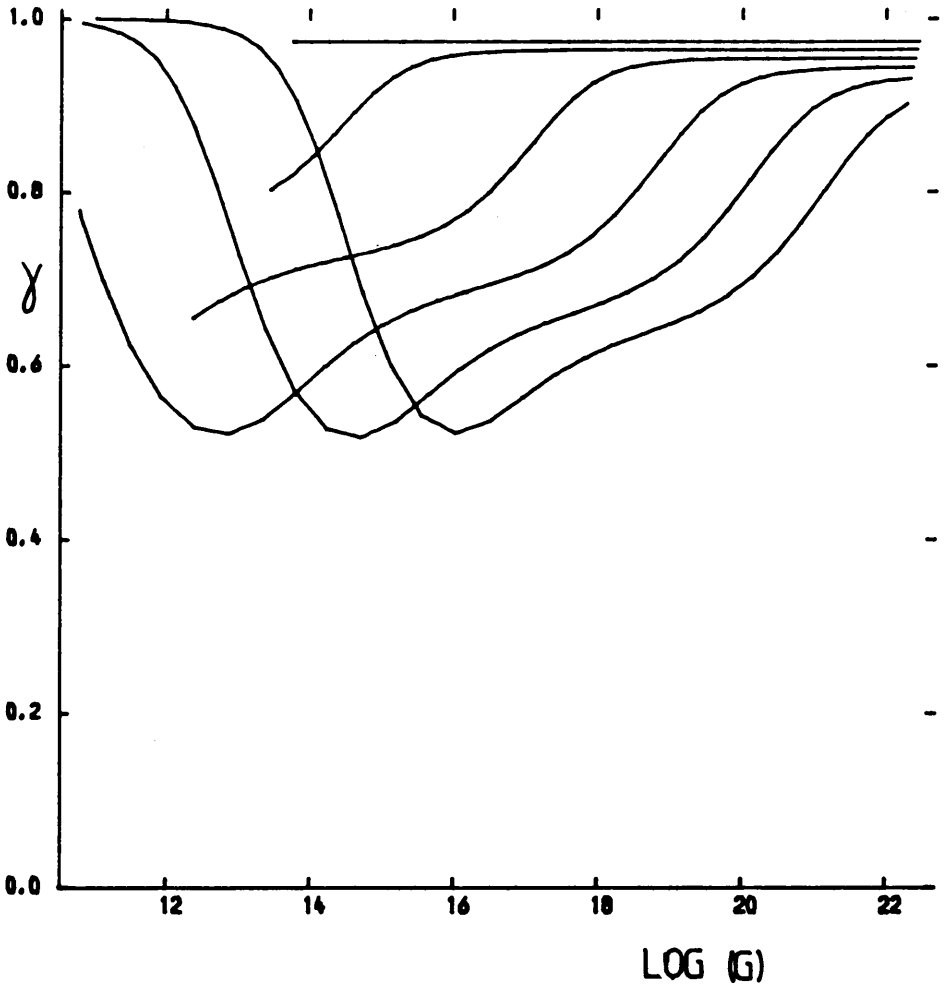

Figure 8-7: Measured Dependence of γ on Intensity and Temperature

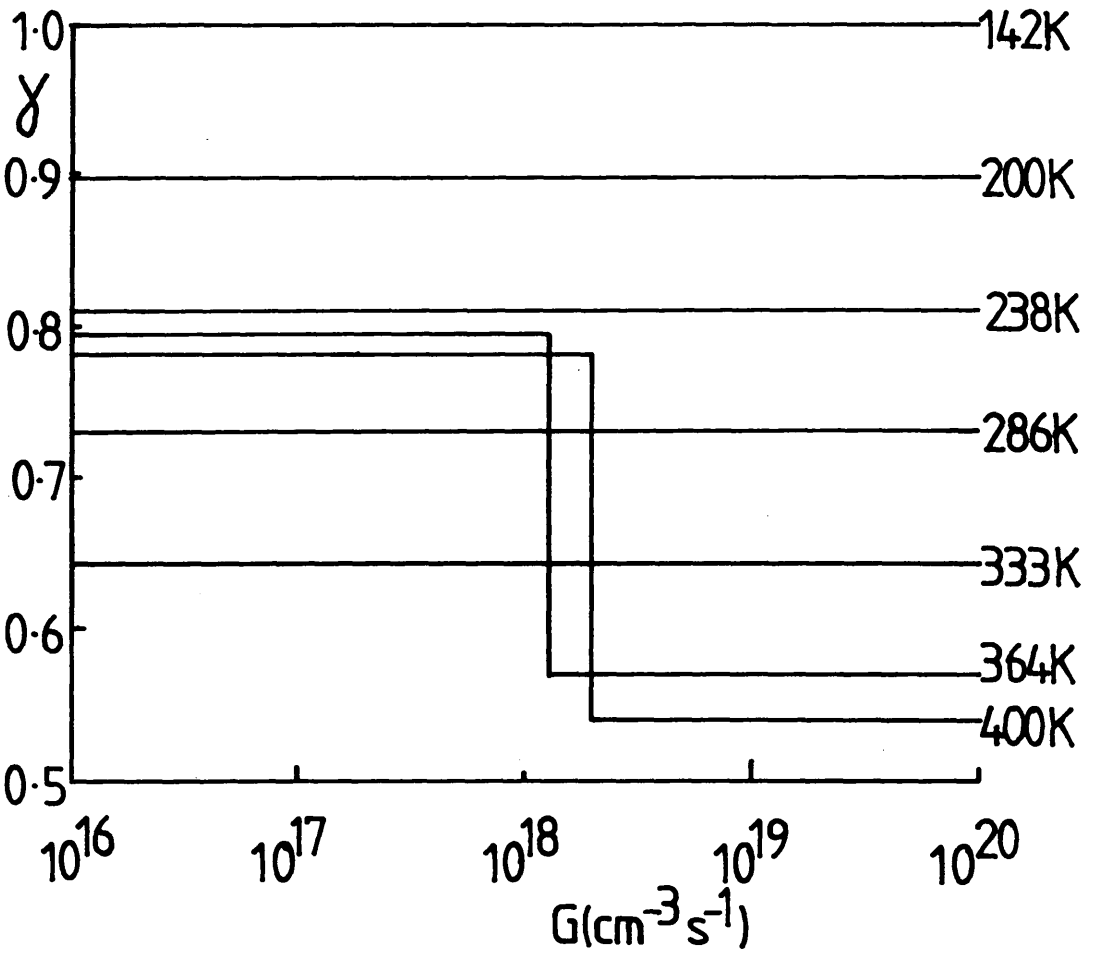

Figure 8-8: Transient Rise at 167K

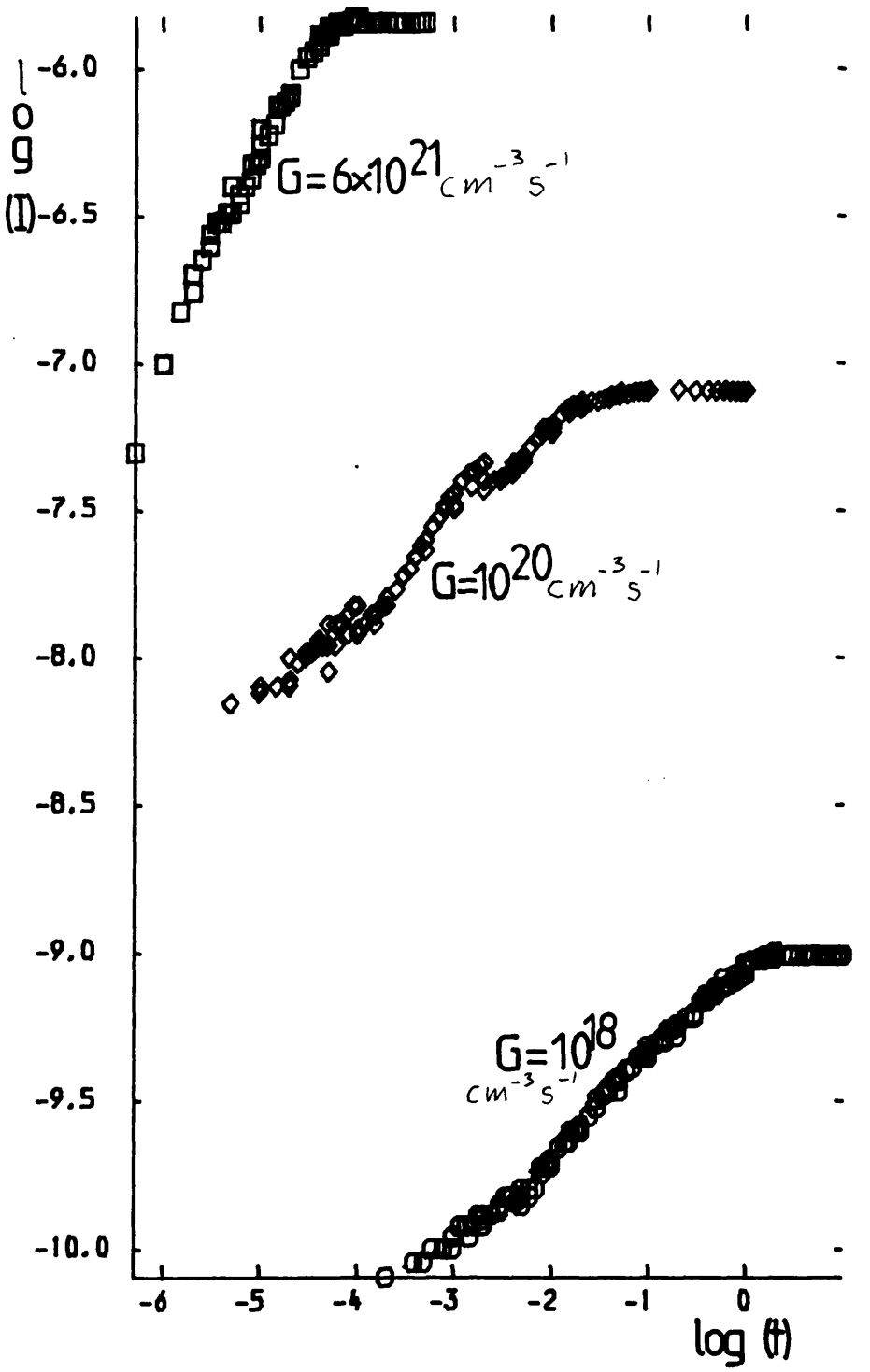

Figure 8-9: Transient Rise at 200K

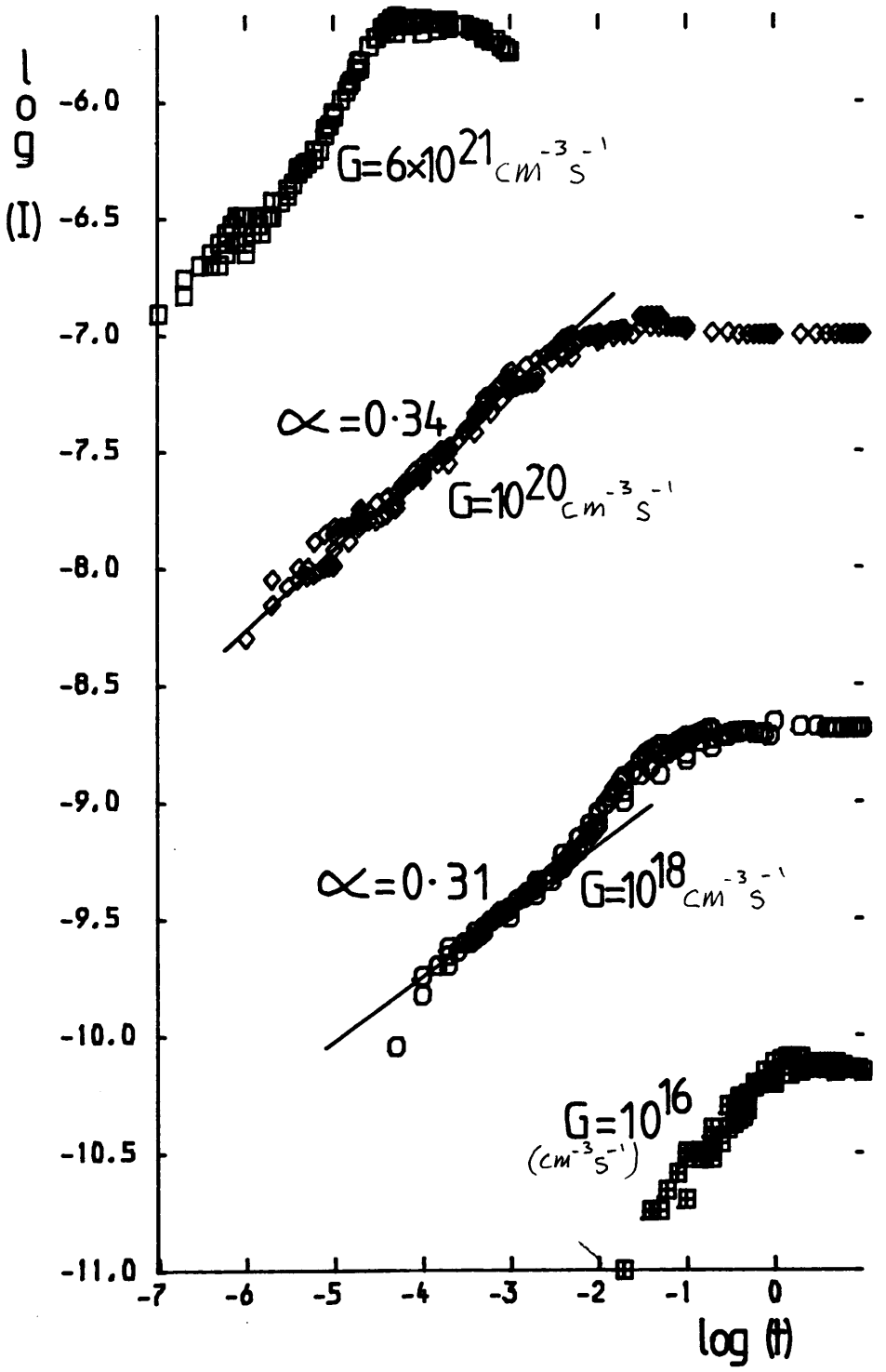

Figure 8-10: Transient Rise at 238K

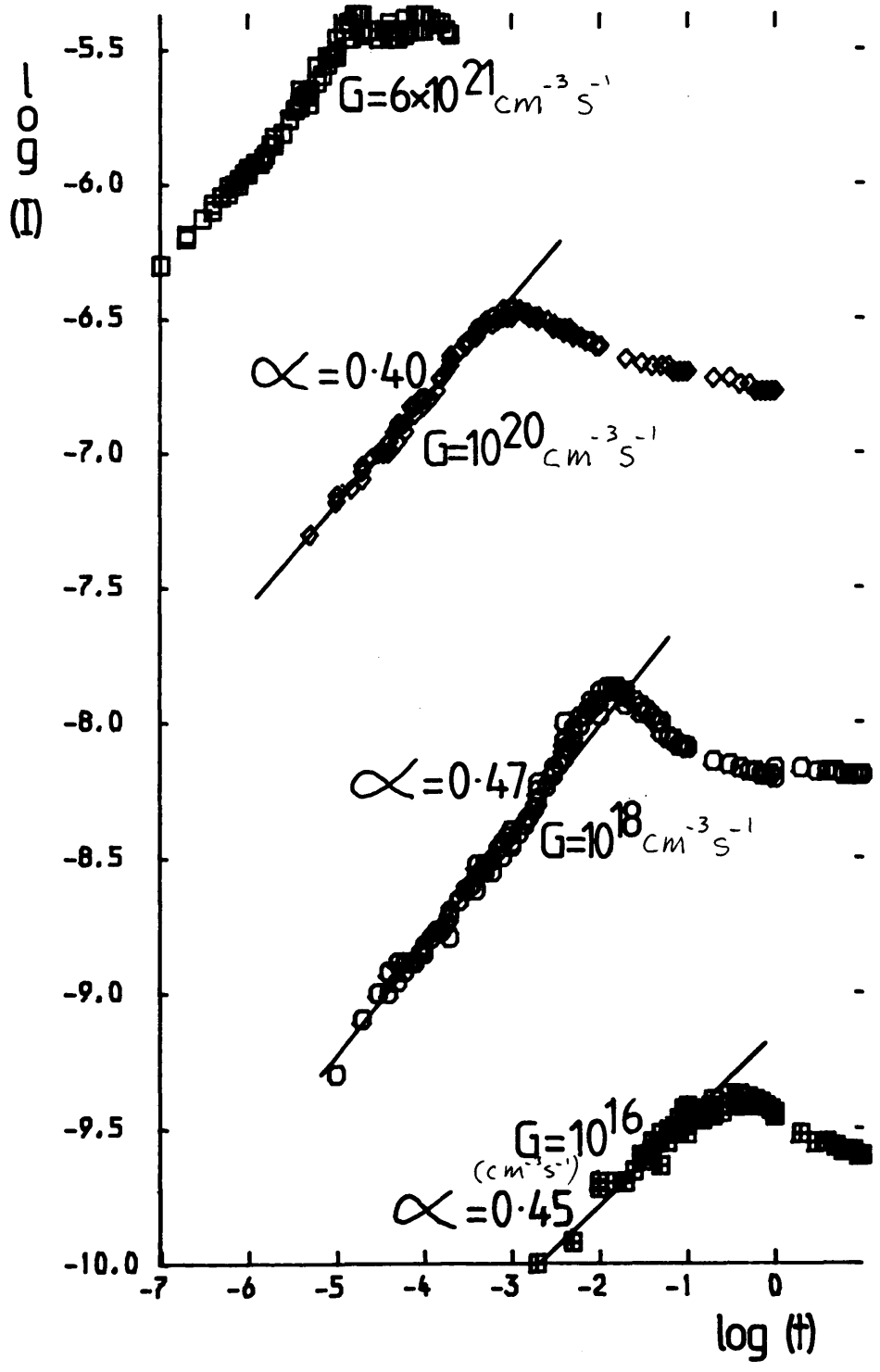

Figure 8-11: Transient Rise at 286K

G is in $cm^{-3} s^{-1}$

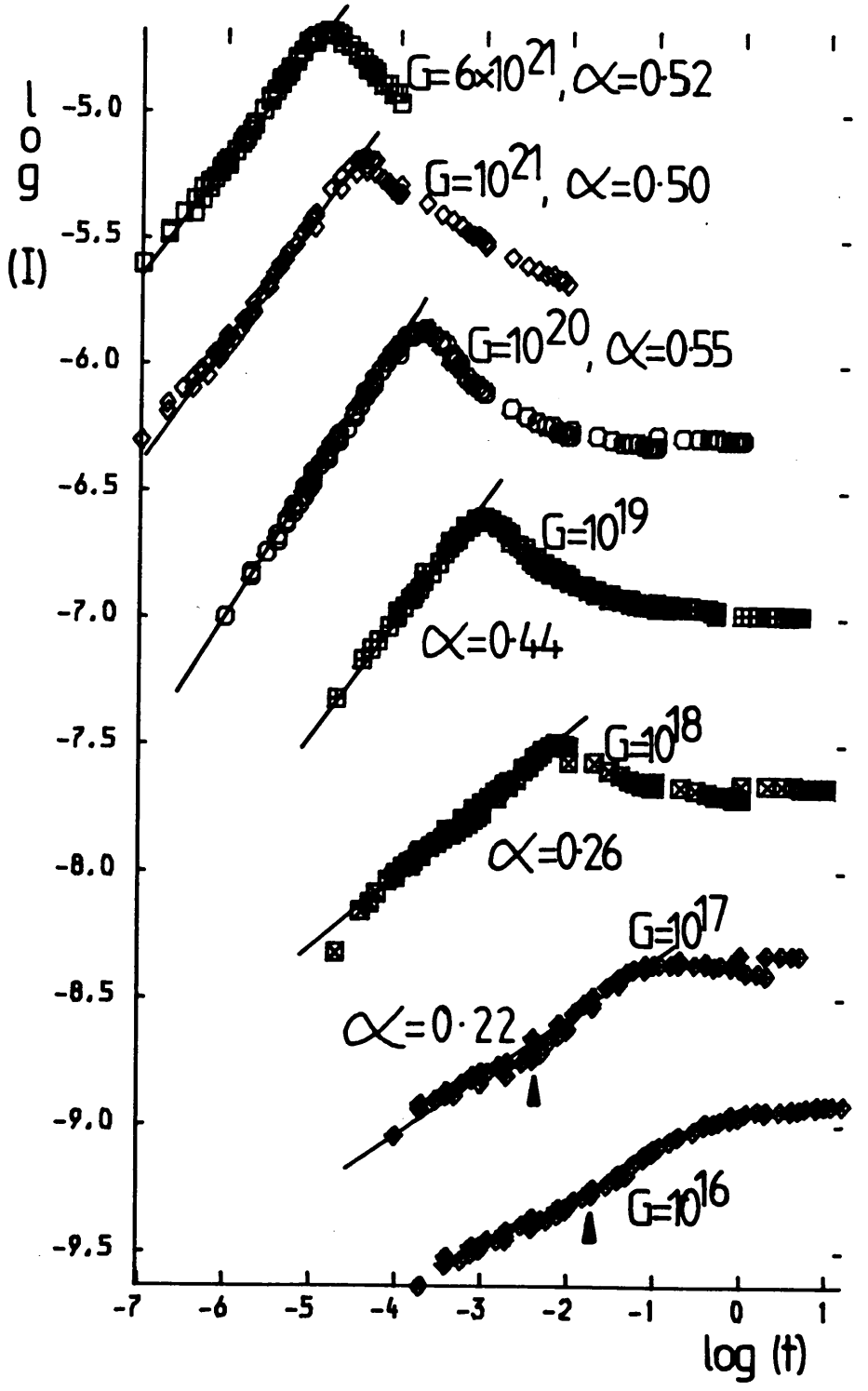

generation rates. The generation rates shown are bulk generation rates(units, photons m^{-3} s^{-1}), assuming $\alpha = 10^4$, i.e. an absorption depth of $1\mu m$, and uniform absorption for simplicity Using fig.8 11 which shows the response at room temperature as typical, the following features can be seen.

The initial part of the response rises approximately as a powerlaw. According to the TROK analysis of Kastner and Monroe [18] this would imply an exponential tail of characteristic α, equal to the ratio T/T_c. However this implies a constant slope for all illumination intensities whilst the results show a lower slope for intensities below $G=10^{20} m^{-3} s^{-1}$. Secondly the two lowest intensities, $G=10^{16}$ and $G=10^{17} m^{-3} s^{-1}$ show some structure in the curve near 20 and 2ms respectively. If this structure was to be considered as a perturbation of the TROK analysis caused by a feature in the density of states, it would be expected to be found at the same time for each intensity, as equation(3.2) is independent of illumination intensity.

A third feature of the results not explained by TROK is the non-universality of the curves, with scaling, at different intensities. The response at high illumination displays an overshoot, i.e. the photocurrent rises above the final value for a short time before falling to its steady state level. A straight line can be drawn through the positions of maximum photocurrent, as predicted by TROK, but again the two low intensity curves are anomalous, without detectable overshoot. One reason for this could

be that the Kastner-Monroe analysis is not valid at excess carrier densities lower than the free carrier densities, however fig8 1 shows that at 286K the dark current is $2.3*10^{-10}$amps. and fig8 11 shows that even for the two lowest intensities the photocurrents are always above this. Kastner and Monroe[18] give that a power law of T/T_c will be observed only when recombination is negligible, but the curve for $G=10^{18}cm^{-3}s^{-1}$ in fig8 11 shows a reduced power law from the earliest measurable times, i.e. before recombination is important.

To summarise, various features of the experimental results given in figures8-8 to 8-11 do not fit the TROK model exactly. Such deviations cannot be explained either as perturbations from the original model (such as features in the density of states) or as the breakdown of the model due to exceeding the limitations of the theory. For this reason, the TROK model is rejected, and a computer modelling procedure is then used to analyse the results.

8.1.3.2 Computer Simulation of the Step Response

The steady state results described in the previous section were interpreted using a model featuring distributed localised states. To account for the presence of monomolecular recombination at high intensities and low temperatures, it was postulated that the efficiency of the recombination centres would drop to zero at a particular energy. Then, when the quasi-Fermi level for electrons moved beyond this energy the density of recombination centres would become constant, which is the condition for the presence of monomolecular recombination. This idea was developed into a

computer simulation, where the transient decay program, TRANS, was modified such that the capture efficiency of states closer in energy to the relevant band edge than some user defined reference energy was reduced by a factor of ten. Recombination now occurs essentially between the reference energy and the dark Fermi energy. Figure 8 12 shows a suitable density of states picture used in the simulation. As the computer simulation calculates the overall capture rate at each discretised time step, i.e. the capture coefficient-density of states product defines the capture rate of a discretised localised state, it is not obvious whether a drop in g(E) or C_n is responsible for the reduction in recombination efficiency.

Figures 8 13 to 8 16 show simulations of the step response set at their respective temperatures. The characteristic energies of the exponential band tails were 0.05eV for the conduction band and 0.08eV for the valence band, which fixes the dark Fermi level at 0.7eV below E_c, the intersection of the exponential tails, assuming equal band edge densities. This implies a lower dark conductivity activation energy than that of the real sample, but E_{fo} needs to be somewhat removed from the gap centre, or an overshoot is not shown in the simulation. Also, the magnitude of the overshoot is underestimated by the numerical method. No recombination limit was applied to the valence band tail, otherwise the general shape of the experimental transients was not obtained, i.e. the reduction in slope of the transient, at longer times and lower intensities was not observed.

Figure 8-12: Density of States in the Computer Simulation

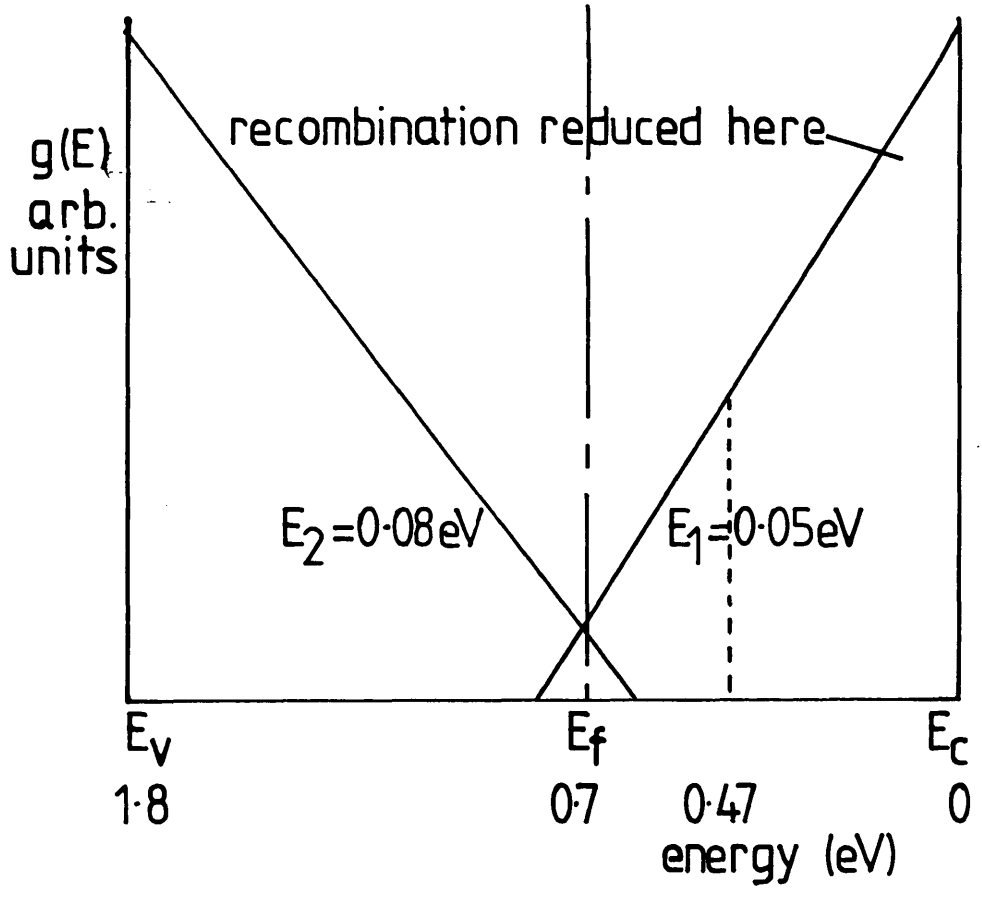

Figure 8-13: Transient Rise Simulation at 167K
(Recombination cut off only in the conduction band tail)

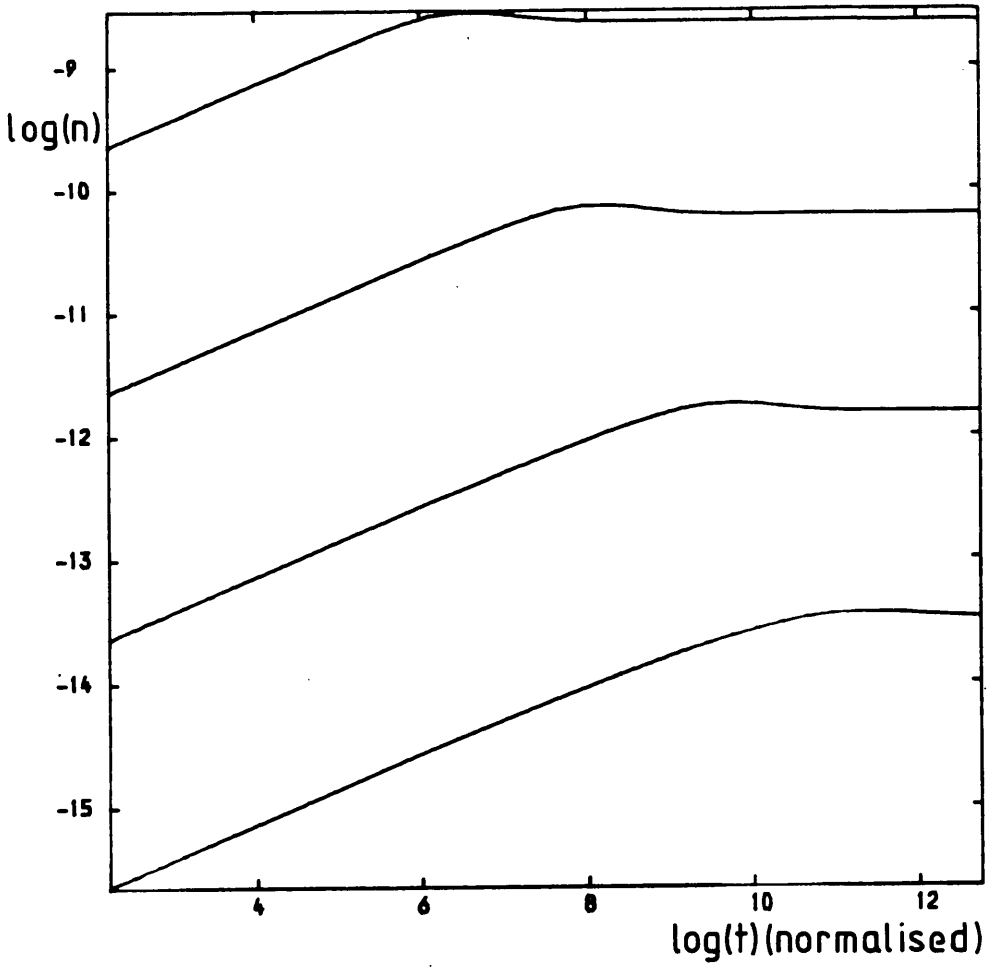

Figure 8-14: Transient Rise Simulation at 200K
(Recombination cut off only in the conduction band tail)

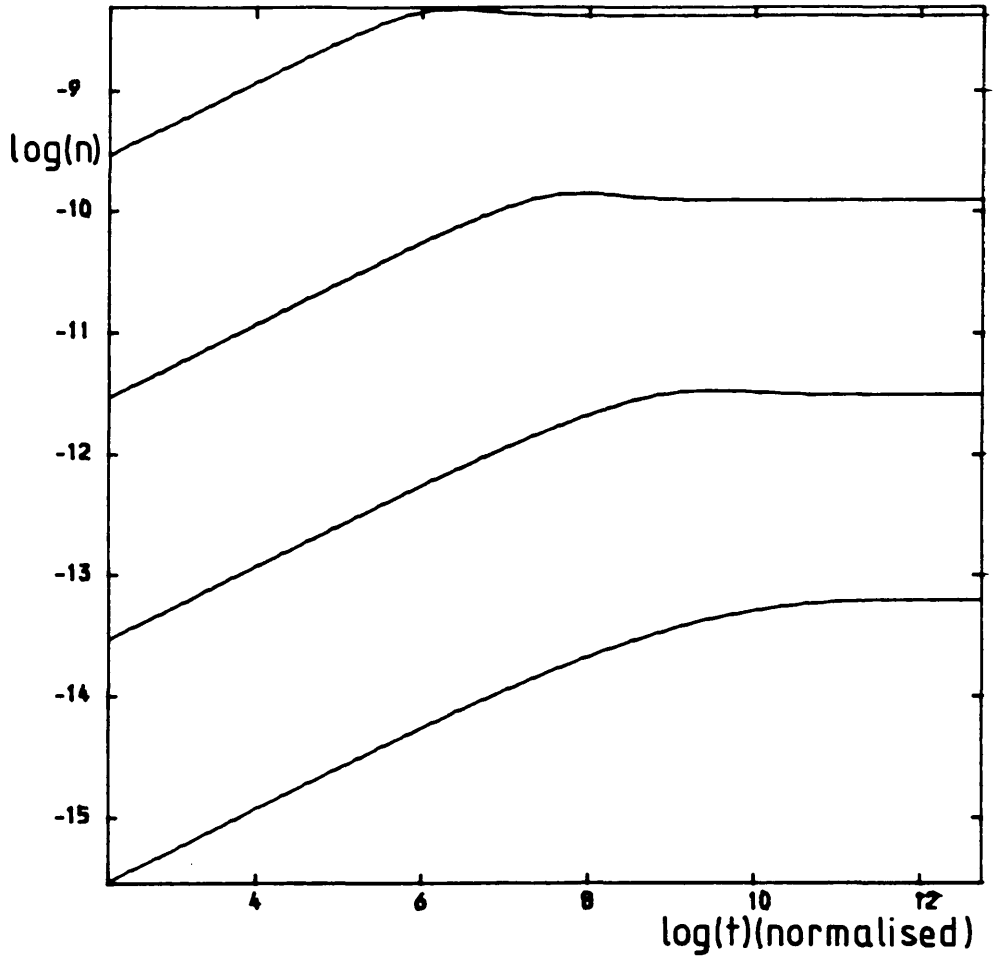

Figure 8-15: Transient Rise Simulation at 233K
(Recombination cut off only in the conduction band tail)

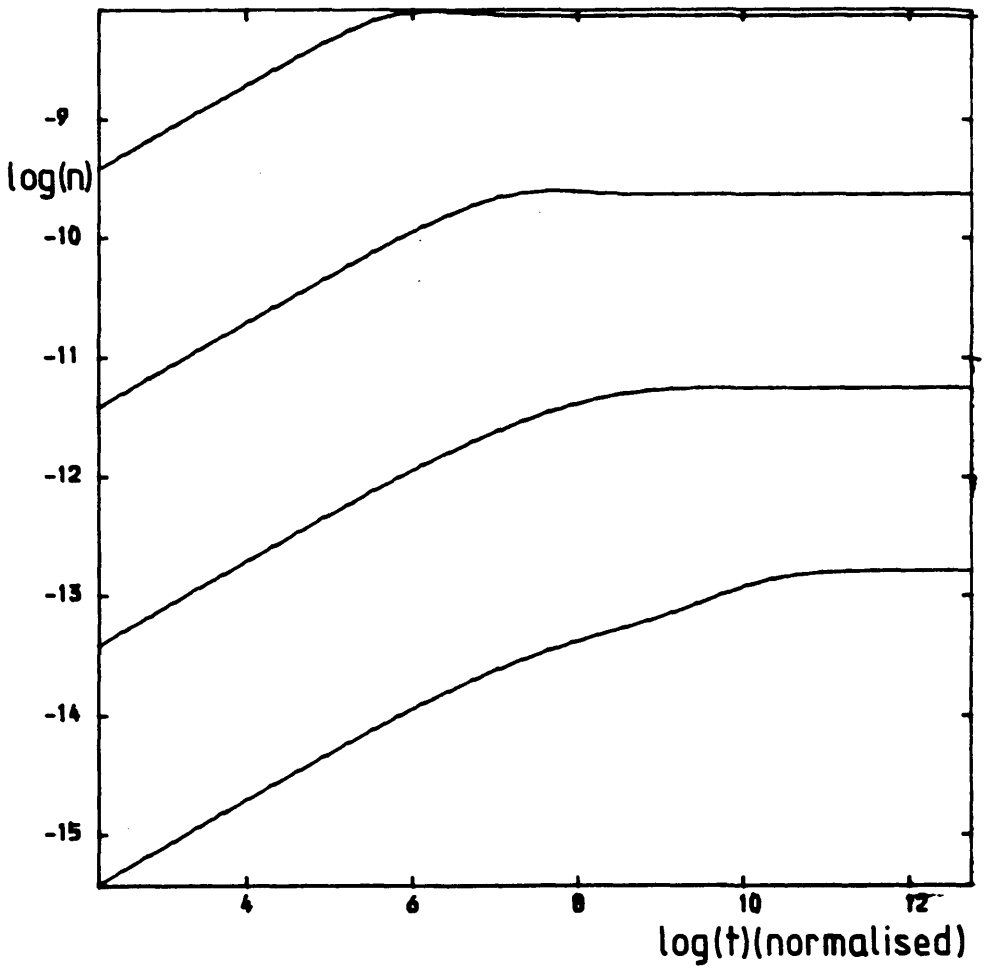

Figure 8-16: Transient Rise Simulation at 235K
(Recombination cut off only in the conduction band tail)

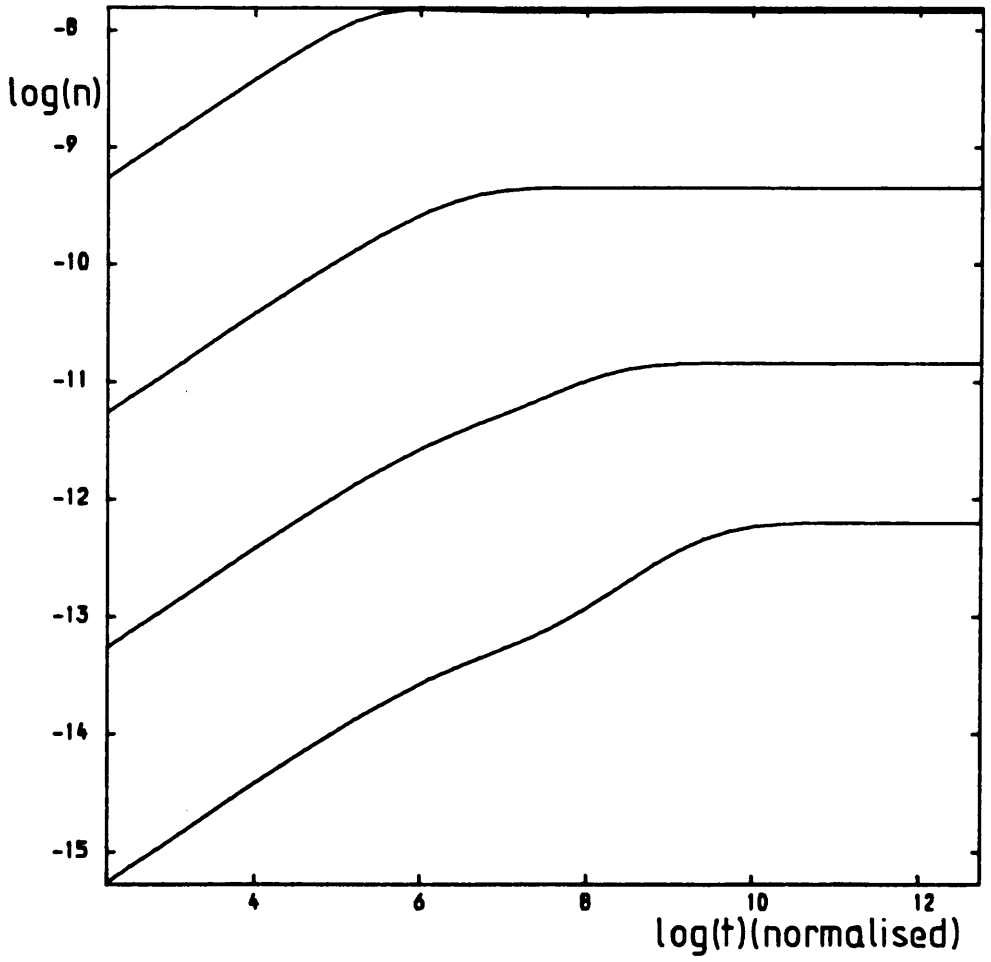

The simulation presents the time axis normalised to one trapping time, so, as the scale is logarithmic, zero represents one trapping time.

$$\tau_t = 1/\int C_n(E)g(E)dE \qquad (8.5)$$

The simulation uses a recombination edge to obtain the observed features of the step response, and this needs $C_n(E)$ to be inside the integral in the above equation, but practically $g(E)$ is so much smaller at the deep states that the effect of changes in $C_n(E)$ for these states can be ignored. The overall trapping time is weighted by all states, but for the same reason the contribution to it from the deep states is small, and can be ignored. Information about the initial trapping time is therefore relevant to the shallow states.

Solving eq.(8.5) for C_n gives

$$\omega = N_c C_n = N_c/\tau_t \int g(E)dE \qquad (8.6)$$

Since

$$g(E) = g(E_c)\exp(-(E_c-E)/kT_c) \qquad (8.7)$$

then

$$\int_{\mathcal{E}} g(E)dE = kT_c g(E_c) \qquad (8.8)$$

Using $N_c = g(E_c).kT$ gives

$$\omega = T/\tau_t T_c = \alpha/\tau_t \qquad (8.9)$$

As α is about 0.5, clearly the attempt to escape frequency is close to the reciprocal of the overall trapping time.

Figure 8-17 shows a step response simulation at one illumination intensity, but several temperatures. The region from log. time from -2 to just above zero represents region 1 in fig.3 2. At log. times near 0, the bend on the curve represents the linear

Figure 8-17: Simulation of Step Response
at Several Temperatures

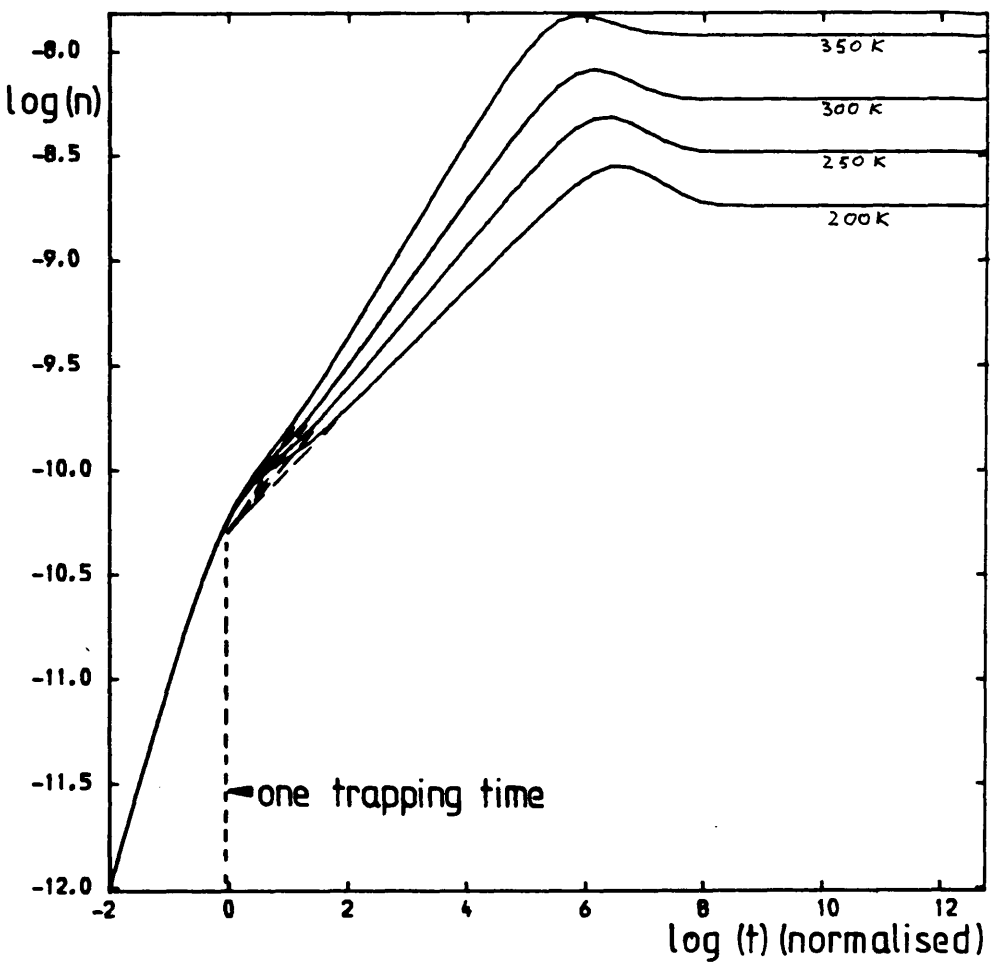

increase in free carrier density where only trapping is observed. The power law region where trapping and release are dominant before recombination becomes important is seen in the next time range. Note that before release is observed, the behaviour at all four temperatures is the same and they all lie on the same curve, i.e. capture coefficients vary slowly, or not at all, with temperature, but release parameters vary rapidly. Once release becomes important, the simulation clearly shows temperature dependent behaviour.

Note that the curves begin to deviate just above one trapping time. Indeed, if the power law regions are extrapolated into this region, they also all meet at a single point, also close to one trapping time. Figure8-18 shows experimental values obtained for the step response, measured at several temperatures, at two intensities, and the power law regions of the graphs have been extrapolated back to the crossing points. Within the accuracy of the extrapolation, τ_t is estimated as 10^{-12} to 10^{-10}s, which gives values of 10^{12} to $10^{10}s^{-1}$ for ν. These are reasonable figures. In the absence therefore of strong evidence to the contrary, a value of $10^{12}s^{-1}$ is used for ν below.

The ratio of electron to hole capture coefficients, R, was taken to be 100, a typical figure for coulombic/neutral capture. A simple interpretation of the origin of the recombination edges is, as mentioned in the steady state discussion, D^o and D^+ states in the conduction and valence band tails, respectively. The less effective

Figure 8-18: Measured Step Response
at Several Temperatures

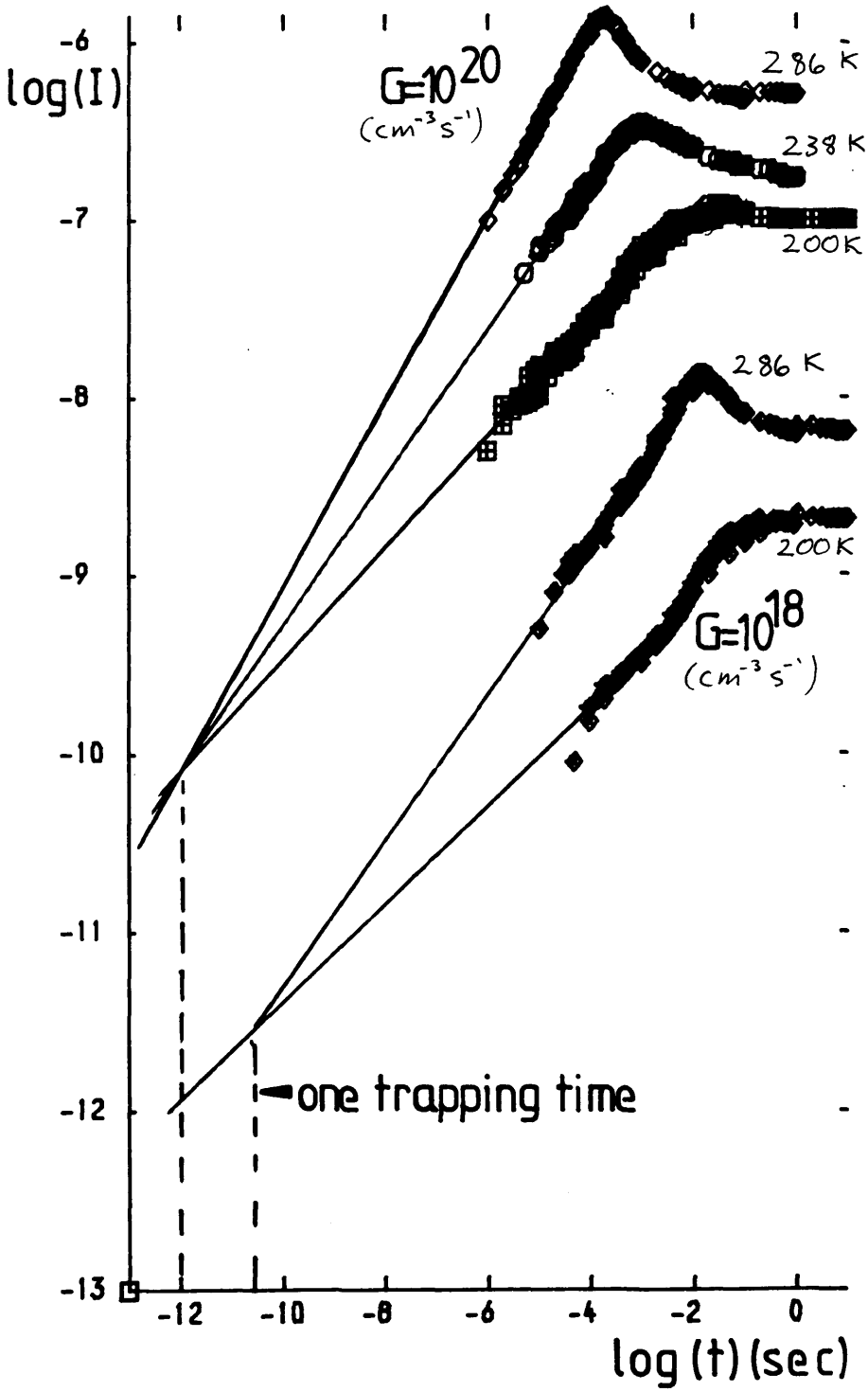

trapping centres nearer the appropriate band edges differ fundamentally, as their origin is disorder broadening of the band edges. For simplicity, the density of states functions used in the simulation are exponential, a form which would not necessarily be expected in real materials.

8.1.3.3 Physical Processes During the Step Response

In this section the physical processes occurring inside the sample are discussed in an empirical manner. Hard calculation is difficult for this type of process unless oversimplification, such as the TROK analysis, is used. This is precisely the reason for the usefulness of computer modelling.

Examination of the curves of figure 8-11 at short times shows that here a power law is observed, at least at high intensities, i.e. region 2 of fig.3-2. If a straight line is drawn vertically at a given time, the instantaneous transient photocurrent increases linearly with light intensity. This means that recombination is as yet negligible, and only trapping and release has occurred in these regions, even for the low bulk generation rate of $10^{17}cm^{-3}s^{-1}$ at $300\mu s$. When the curve drops below this power law line the rate of recombination is beginning to increase, and this represents region 3 of fig.3-2. At long times where the steady state is reached a factor of ten increase in generation rate produces a smaller increase in the transient current. This corresponds to the sublinear increase in steady state photocurrent with intensity.

What needs to be known is when does recombination eventually

equal generation, is it at the peak of the overshoot, or when the steady state level is finally obtained? Also, what are the physical processes necessary for the overshoot to be observed?

Figure 8-19 shows information from the TRANS transient photoconductivity simulation program, with trap depth plotted against electron occupation densities (units m^{-3}). Also shown is the exponential density of states used for this particular simulation.

As the X-axis represents electron density, the intercept of the electron density curve with the uppermost axis represents the free carrier density, as this line represents the conduction band.

Curve a represents the equilibrium, dark occupancies, which reflect the Fermi-Dirac statistic. The curve represents the f(E)g(E) product, and because we have a slowly varying density of states ($T_c > T$) it is an exponential in the region where Boltzmann statistics apply. At the bottom of curve a, it turns away from the exponential curve near E_{fo}, as does the Fermi-Dirac function.

At short times, the effect of illumination of the sample is shown to be an increase in electron density in the shallow states. The bulge in occupancy will occur near E_d, given by eq.(3.2). A consequence of the overall increase of electron density due to the creation of free carriers is that the intercept at the top axis is further to the right. This represents the increase in free carrier density in the region of the transient before recombination has

Figure 8-19: Simulation of State Occupancy

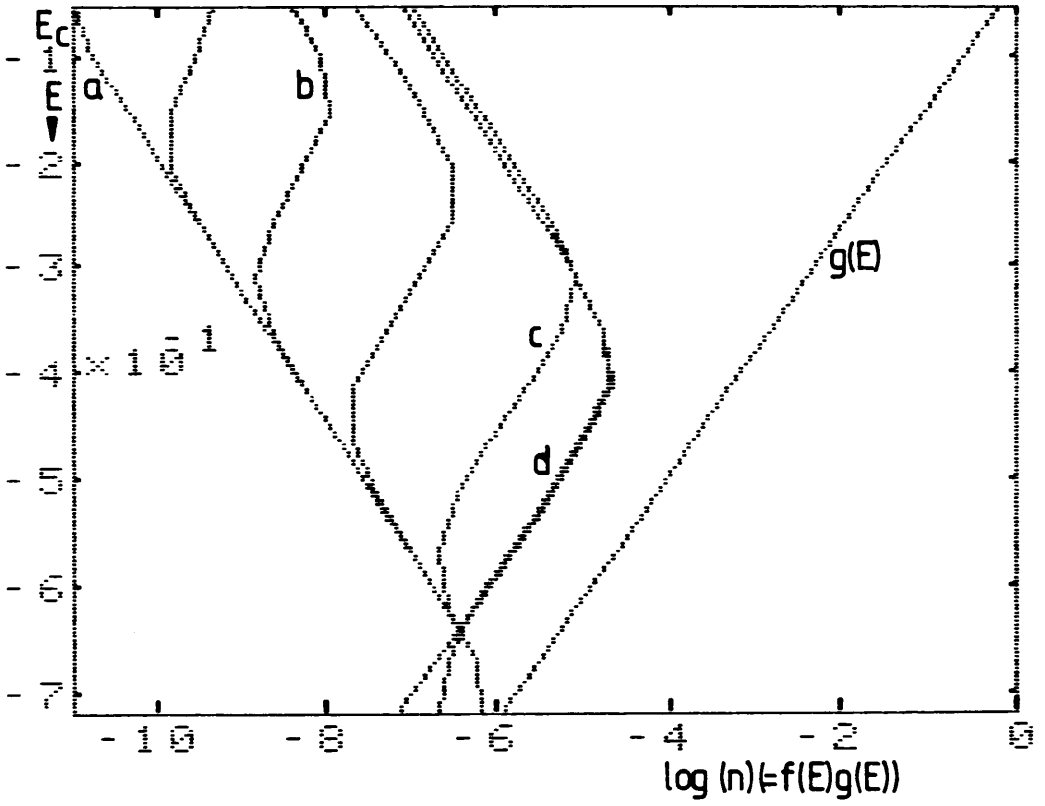

taken place, i.e. the region of the power law.

As time progresses, the area under the curve rises as illumination continues, and tne intercept representing the free carrier density moves further to the right, and the position of maximum density moves down in energy as E_d, curve b. Eventually recombination becomes non-negligible. Then the rise in area under the curve begins to slow down, and then stops. Curve c in fig.8 19 represent this stage. If overall rate of recombination is slow. then the deep states will become fully occupied before further thermalisation is impossible, and the free carrier density rises monotonically until equilibrium is reached. This is illustrated in fig.8 20. The first figure shows what happens when recombination proceeds at a noticeable rate before the deep states are saturated. This was done by suitable selection of the trapping parameters, the easiest of which is to make the conduction and valence band tails assymetrical. Now, the rapidly increasing rate of recombination reduces the increase in area under the curve which represents the density of electrons. Thermalisation becomes less likely than recombination at energies near E_d as electrons in states low in energy will be more likely to recombine than to be re-excited to the conduction band. The computer calculated free electron density now falls from some maximum level to the equilibrium level, and the overshoot in the step response is successfully generated. Curve d is instructive, as it shows the result obtained by Shockley-Read statistics, eq.(2.28). Between the trap Fermi levels, occupation is constant at Rn/Rn+p, and indeed the simulation shows electron

Figure 8-20: Transient Rise Simulation
with Slow Recombination

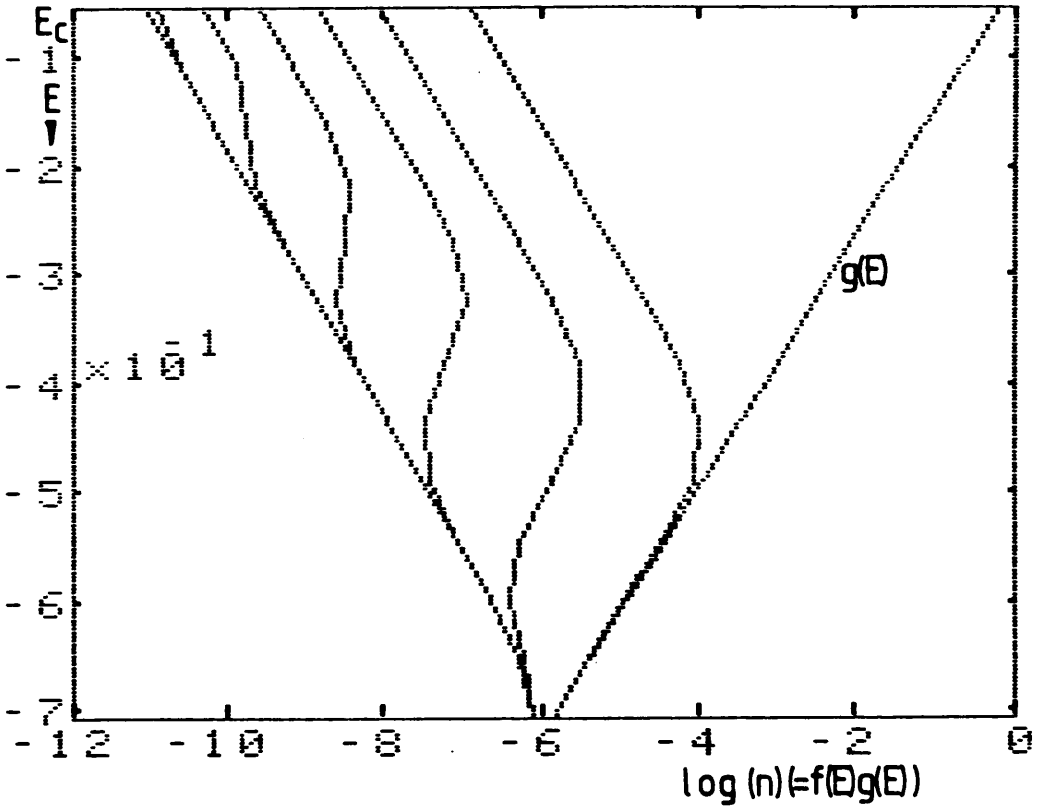

density in this range as parallel to the density of states curve, implying a constant occupation. Above E_{ft}^{p} the occupancy follows a Boltzmann like exponential function, and this is also illustrated as the curve follows a line parallel to the dark occupation curve.

To summarise, if the deep localised states become saturated and thermalisation continues until the onset of steady state equilibrium, then the simulation predicts that no overshoot will appear in the step response. However if recombination becomes important before the deep traps are fully occupied, the simulation predicts an overshoot.

8.1.3.4 Time to Reach Steady State

In steady state, occupation of the localised states is described by Shockley-Read statistics, and recombination occurs between the trap quasi-Fermi levels[31]. However the trap quasi-Fermi level position cannot be calculated readily for an unknown density of states as free carrier densities both for electrons and holes need to be known. In the following, E_d is calculated as the thermalisation energy attained at the end of the overshoot, when the steady state value is just reached, using $\nu=10^{12}s$. Table 2 compares this value with E_{fn}, the free electron quasi Fermi level, which is the more easily calculable. As given, the steady state is reached at an E_d value slightly above the free electron quasi-Fermi level. The difference in energies is not identical for all cases, but the difficulty in choosing the "steady state time" especially at the lowest intensities may explain this. It is suggested here that this energy difference can be identified with the necessary increase in

Figure 8-21: Table 2

G ($cm^{-3}s^{-1}$)	$E_{fn}-E_{fo}$ (eV)	E_c-E_{fn} (eV)	t_{ss} (s)	E_c-E_d (eV)
10^{16}	0.06	0.74	1.0	0.69
10^{17}	0.1	0.7	10^{-1}	0.63
10^{18}	0.13	0.67	10^{-1}	0.63
10^{19}	0.17	0.63	$2.4*10^{-2}$	0.59
10^{20}	0.21	0.59	10^{-2}	0.58
10^{21}	0.24	0.56	$9.0*10^{-3}$	0.57

energy of the trap quasi-Fermi level over the free carrier quasi-Fermi level, i.e. that in the transient rise, steady state is reached when the trapped carriers thermalise down to the trap quasi-Fermi level.

8.1.3.5 The Change in Slope of the Step Response

The computer simulation successfully predicts the reduction of the step response slope as observed for $G=10^{17}m^{-3}s^{-1}$ in fig.8.11, and at other temperatures, for moderately long times.

The physical explanation of this is as follows. If the density of states model is taken as a perturbation of the TROK model, then at short times the bulk of the charge is captured into shallow traps. We therefore observe a normal type of TROK transient, i.e. power law behaviour of gradient $\propto$ on a log-log plot. At longer times capture into the deep states becomes important although E_d has not progressed to this depth, and the TROK analysis becomes invalid. The greater relative capture rate of the deep states reduces the photocurrent to a value lower than that expected from TROK, and causes the slope of the curve to be reduced. This is not observed at high intensities because recombination becomes the dominant process before it can be observed. At very low temperatures and intensities, release is always at a low rate, and the TROK-like power law response is never dominant in the time regimes available from the experimental apparatus. The limits in the measurement system at small currents, due to the necessity for a high value measuring resistor cause the system to have a large RC time constant and hide the TROK-like region for many of the curves.

8.1.4 Transient Decay

8.1.4.1 Measurements of the Transient Decay

Figures 8-22 to 8-25 show the flash response of a Si:H at four different temperatures.

The important features of the results are firstly that the average slope of the curves is approximately -1.0 and secondly that a uniform straight line is not observed, i.e. the curves have structure.

8.1.4.2 TROK analysis of the transient decay

The TROK analysis[36, 37, 18] gives the slope of a featureless log-log transient decay plot as $-(1-\alpha)$. For a decay plot with some structure, if the TROK analysis is still valid, then equation (3.6) will give the density of states profile of the material. Figure 8-26 shows the result of the TROK analysis. The average slope of -1.0 of the decay implies an almost flat density of states profile, i.e. a high characteristic temperature. However, the deviations from linearity of the log-log plot show up as two distinct features in the density of states profile at about 0.3eV and 0.55eV below E_c. The important assumptions here are that the transient photocurrent is entirely due to electrons and the attempt to escape frequency is 10^{12}Hz. The positions of the peaks are dependent on ω by equation (3.2). Note that g(E) is on a linear scale in the figure.

As the TROK analysis appears to give a self-consistent density of states at several temperatures, and the highest peak density is no more than seven times the background density the lack

Figure 8-22: Transient Decay of a-Si:H at 238K

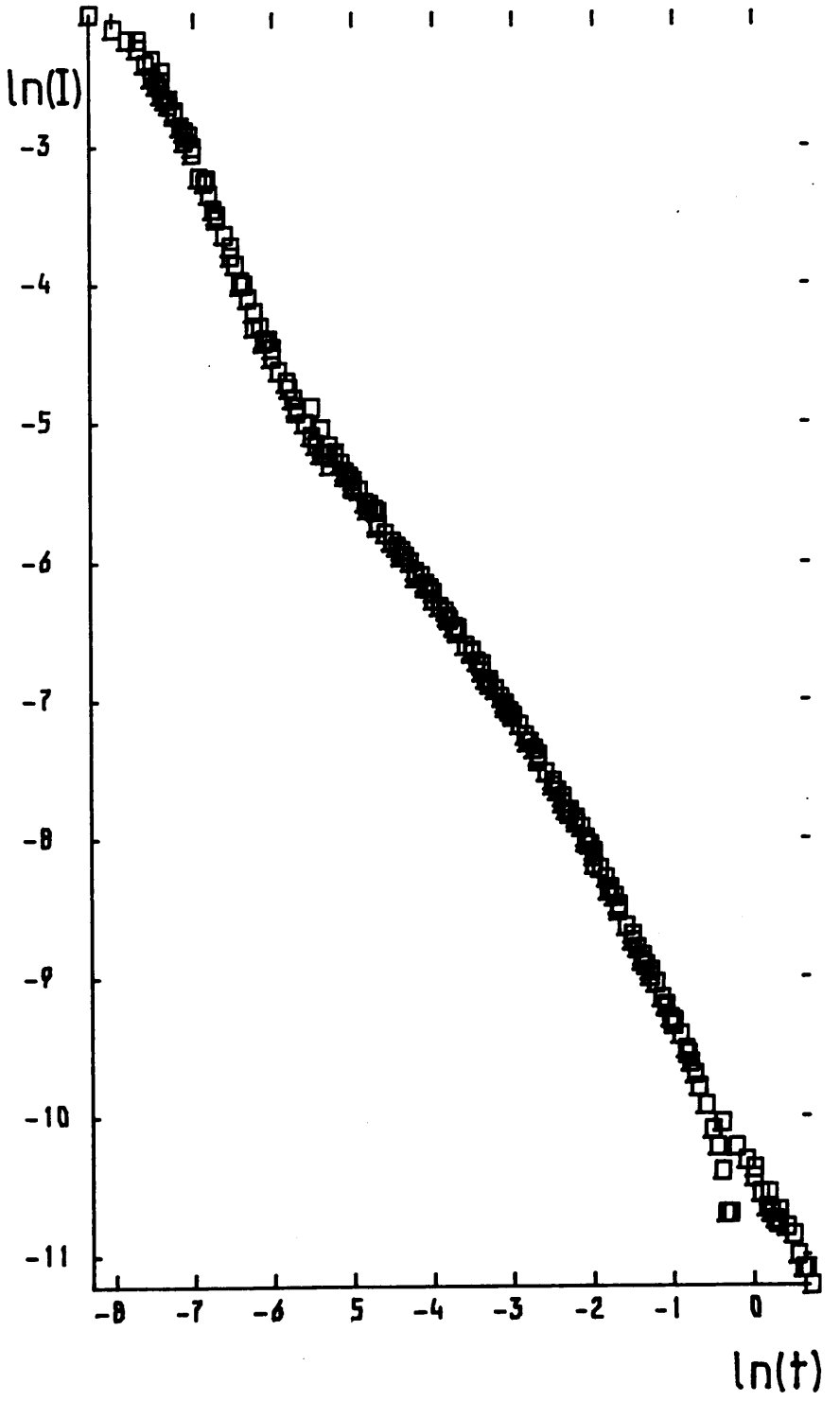

Figure 8-23: Transient Decay of a-Si:H at 263K

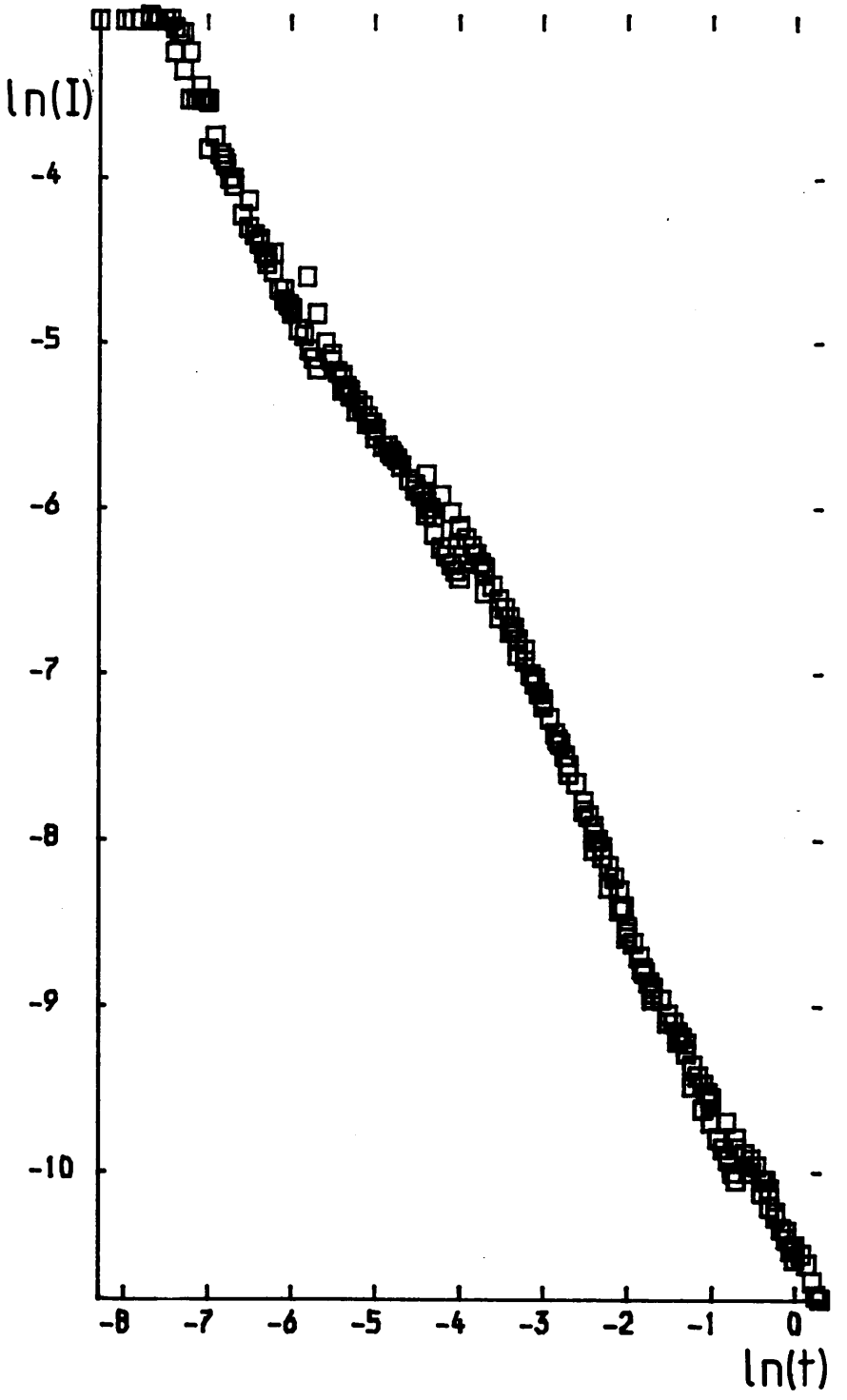

Figure 8-24: Transient Decay of a-Si:H at 286K

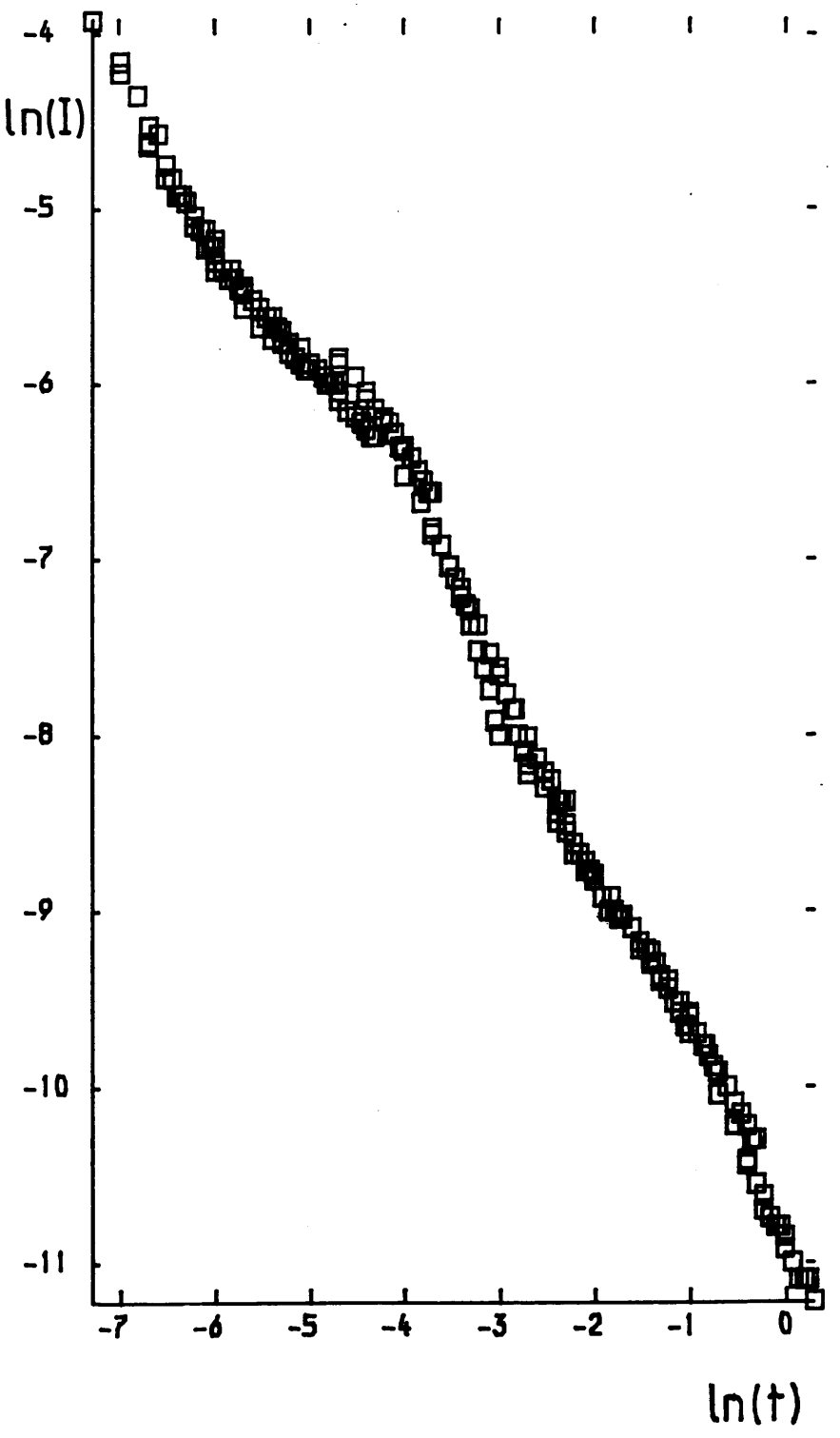

Figure 8-25: Transient Decay of a-Si:H at 333K

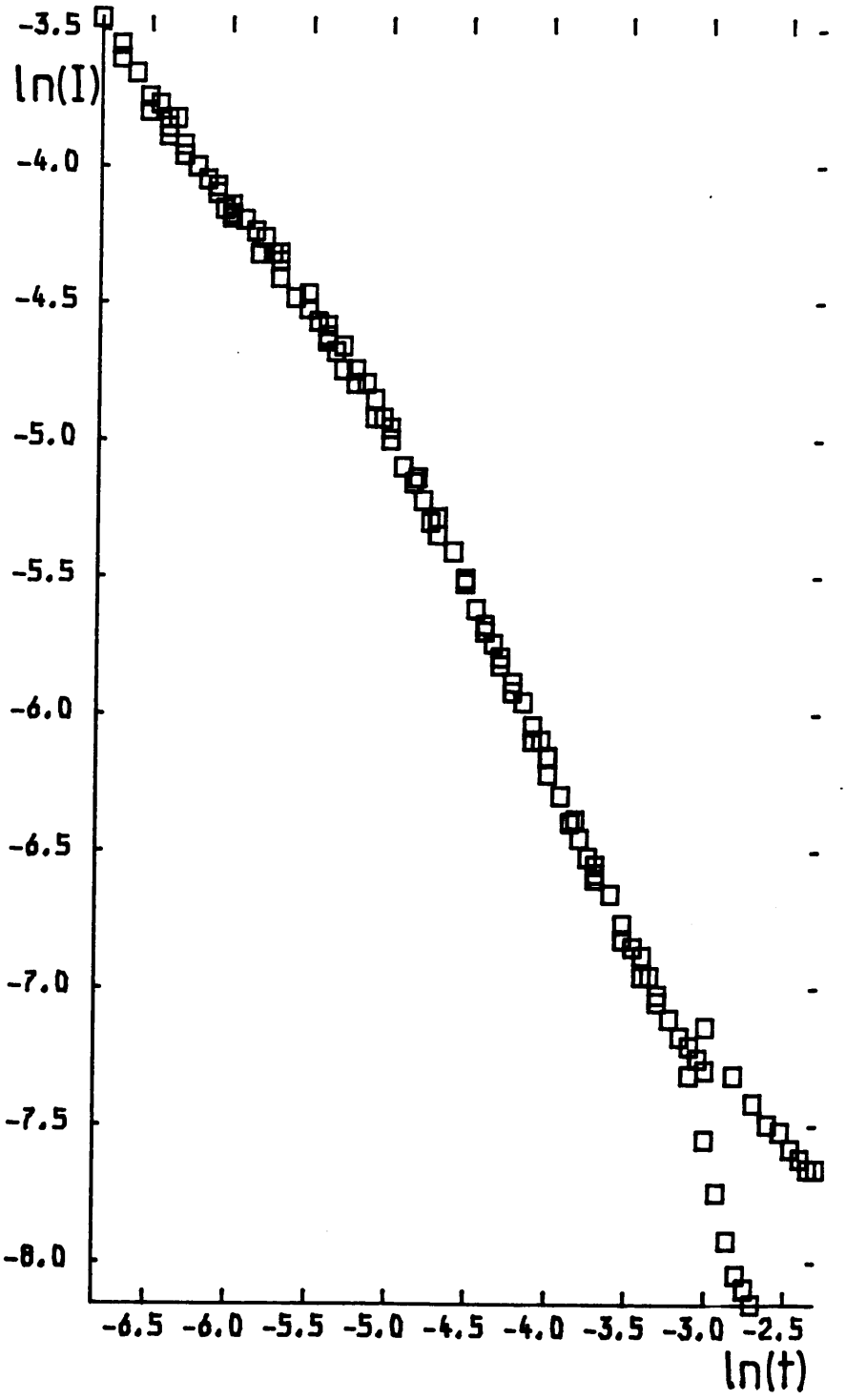

Figure 8-26: TROK analysis of the transient decay

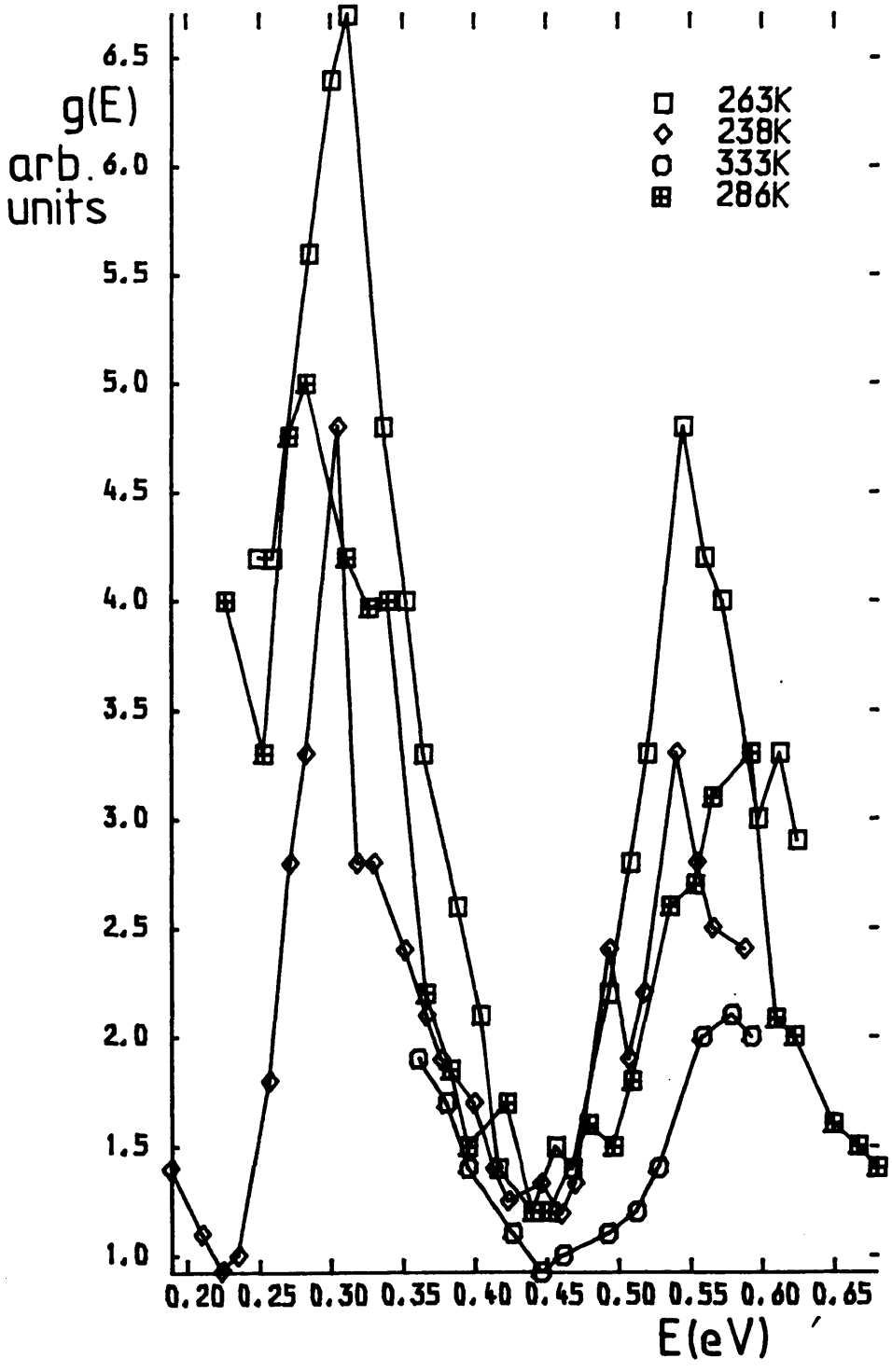

of structure in the transient decay could lead one to assume that the TROK model could be valid. However, the characteristic temperature needs to be about 2000K to explain the steep overall slope of the transient. As step response and steady state photoconductivity measurements have implied a characteristic temperature of about 550K, the TROK model has been rejected as incapable of explaining the transient decay of a-Si, and computer simulation has been used instead.

8.1.4.3 Computer Modelling

The major pitfall in the interpretation of the flash decay using computer modelling is that an explanation of the experimental decay is easily obtained.

Figure 8-27 shows a transient decay obtained by computer simulation using a density of states comprising an exponential tail of characteristic temperature 2000K with additional traps at 0.35 and 0.5 eV below E_c with densities above the exponential background of 5 and 3 respectively. Temperatures used in the simulation were 200K, 250K, 300K and 350K. The arrangement of the features of the deviations from the simple power law are very close to that of the experimentally measured curve, the "bumps" start off near log(time)=6 which implies approximately 1μs if $\nu = 10^{12}$Hz. The average slope of the graphs is not quite equal to 1.0, and this is a consequence of using a T_c of 2000K, rather than the infinite characteristic temperature needed to give a slope of -1.0.

Figure 8-28 shows another simulation, this time using a

Figure 8-27: Computer simulation:
TROK-like model for the transient decay

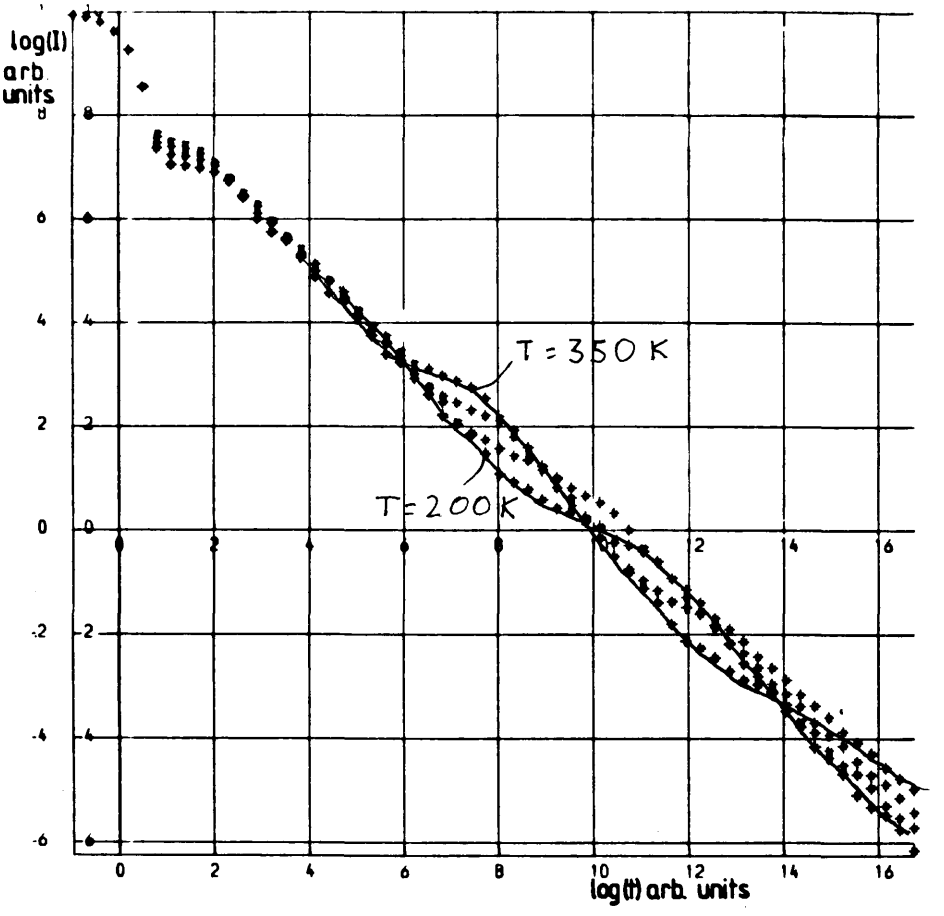

Figure 8-28: Computer simulation:
Three discrete levels model of the transient decay

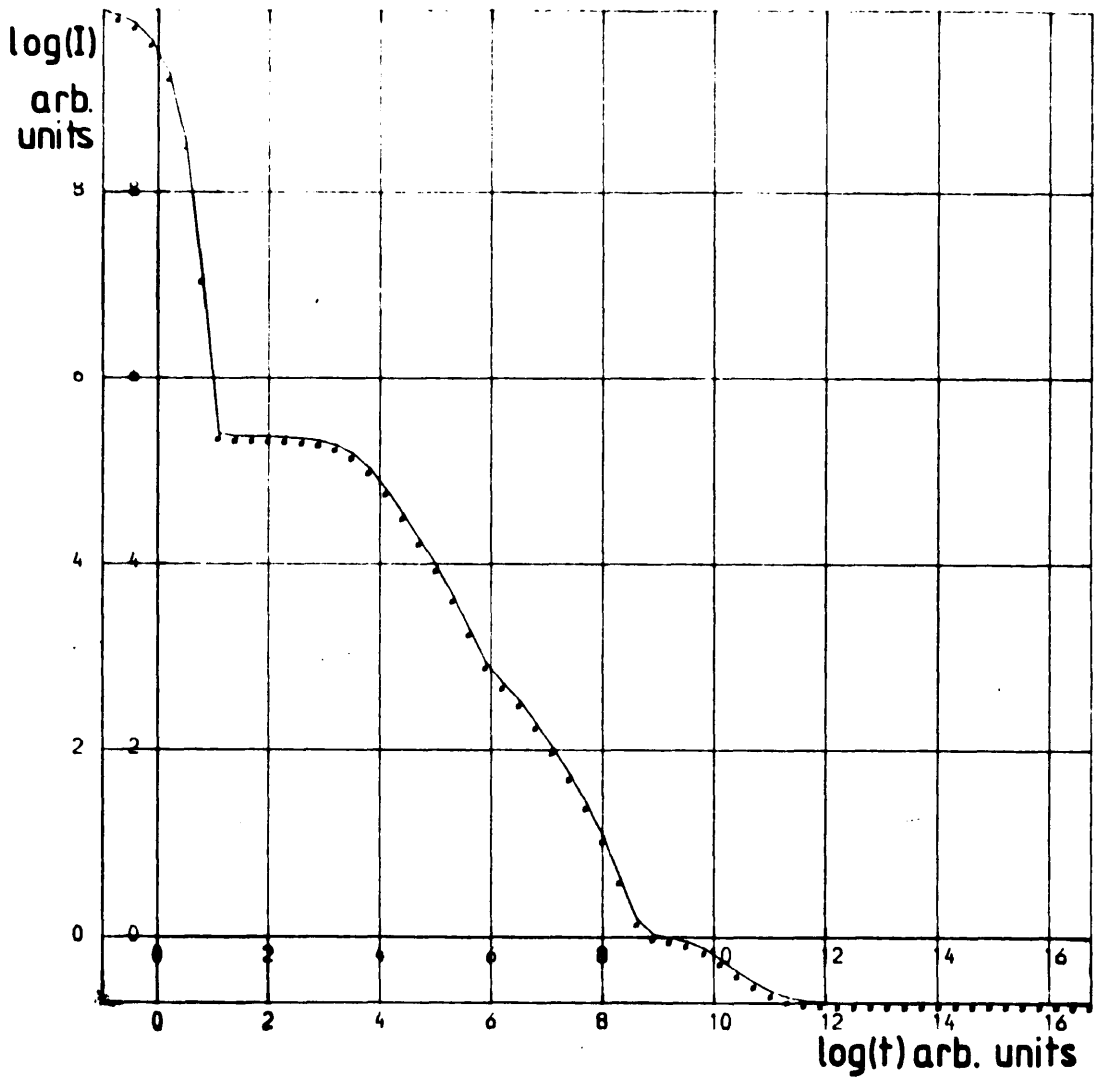

density of states comprising of three discrete levels. The energy positions of the upper two levels were selected to produce features in the decay at the same times as those found experimentally, these were at 0.35eV and 0.5eV. The localised state densities were obtained by inspection as 0.007 and 0.005 in arbitrary units. A third level at 0.7 eV, density 0.01, was included to absorb charge and thus simulate recombination. Only one temperature is used, corresponding to room temperature. The fit is not so good as the previous one as regards the "bumps" in the decay curve, but the overall gradient is better.

Although the fit obtained by these two very different density of states models is not ideal, without the use of a better model from other measurements such as the steady state and transient rise photoconductivity, it would be possible to view either of them as capable of explaining the measured results within experimental error. This implies that the calculated transient photodecay is relatively insensitive to the density of states model. Perhaps this is best illustrated by the prominence given to the mathematically simple TROK model in the literature, where a large body of work has been published interpreting the photodecay as due to the presence of exponential tails although other measurements have not been in agreement with this. Perhaps the steady state photoconductivity measurements on As_2Se_3 show this most strongly. as this material has long been known to display square root intensity dependence(a consequence of discrete localised states controlling recombination), but the transient decay has often been interpreted as due to

exponential tails.

8.1.4.4 High Intensity Simulation with Gap Centre Recombination

The previous two experiments, steady state photoconductivity and transient rise were both interpreted using a density of states model that rose exponentially from a minimum in the localised state density at E_{fo}. To explain the monomolecular behaviour of the intensity dependence of the steady state photoconductivity at low temperatures and the non-universality of the step response, it was necessary to make states near the gap centre more efficient at recombination than those near the band edges. Figure 8 29 shows a transient decay, from the TRANS program, with the same density of states as used for the step response, i.e. only those states within 0.23eV of E_{fo} on the conduction band side are more efficient than all the rest. Note that the overall slope of the decay curve is successfully predicted to be -1.0, but the curve is featureless because of the exponential nature of the density of states and despite the sharp reduction in the recombination efficiency at the critical energy. The easiest method of producing the observed features in the decay is by adding extra states until the simulated features reproduce those seen experimentally. Figure 8 30 shows the simulation result with states at 0.4eV below E_c given a higher density by a factor of ten above the exponential background density and the features caused by this in the transient decay occur at the correct times. Note that the energy of this feature is not the same as that used in earlier simulations. The temperatures used are the same as in the experimental study.

Figure 8-29: Computer simulation
exponential D.O.S. only

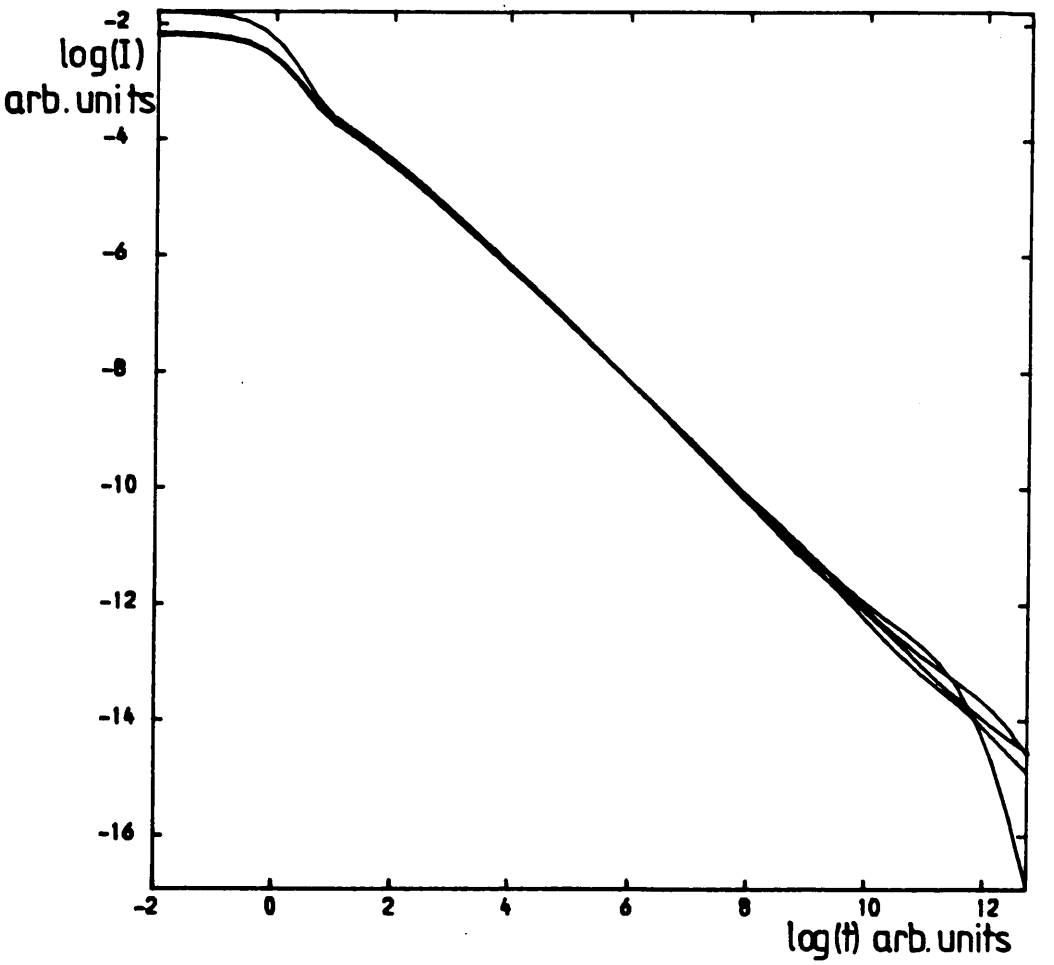

Figure 8-30: Computer simulation:
Restricted recombination with additional states

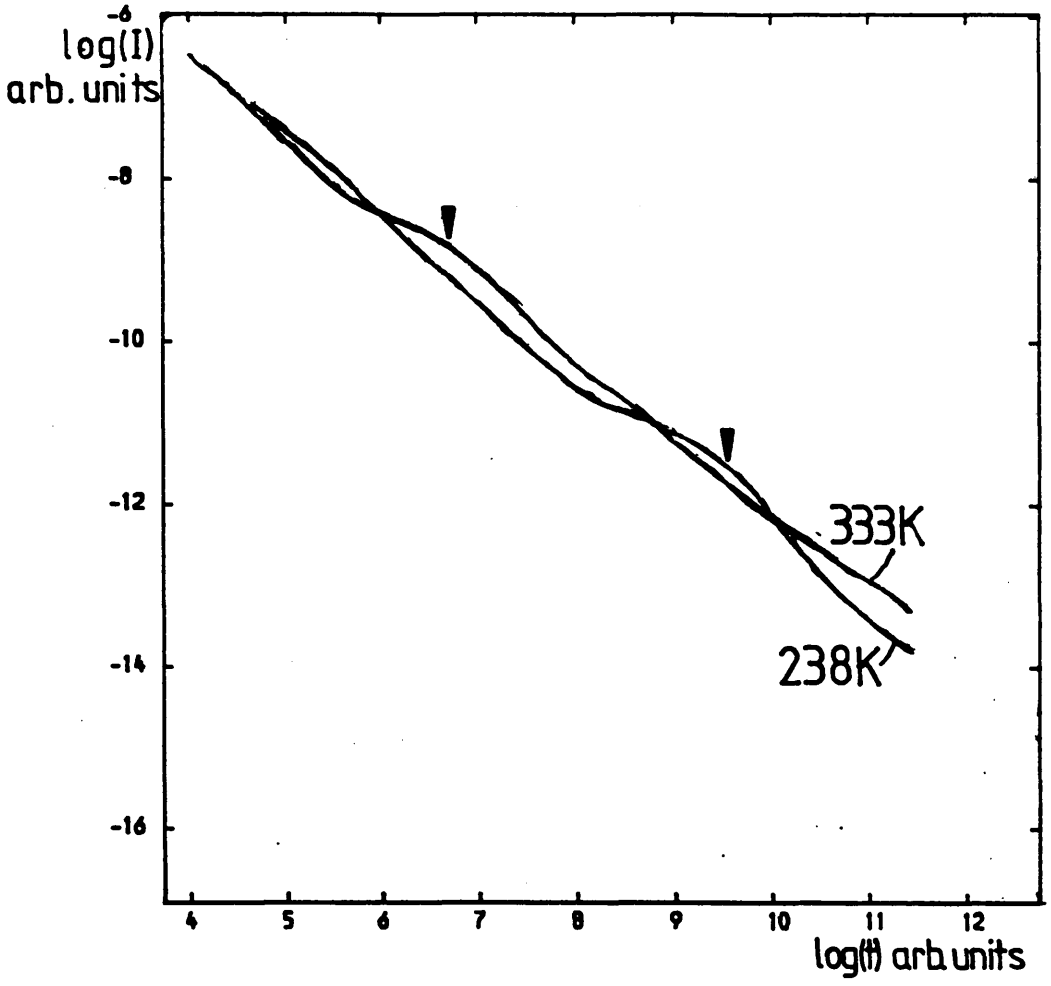

arrows show structure in decay due to states at 0·4eV

The pulse dye laser had an output of 5kw for 10ns. Assuming an absorption depth of 0.1μm for the yellow light, wavelength 530nm, $1.5*10^{14}$ photons were absorbed in a volume of $40\mu m*13*4mm*0.1\mu m=2.1*10^{13}m^{-3}$, or $7.2*10^{20}$electrons/cm^{-3} which represents the electron density before initial trapping. The electron current at this stage is given by

$$\Delta I=Ane\mu E \qquad (8.10)$$

and this is 480amps if a mobility of $10cm^2/Vs$ is used with an electric field of $10^4V/cm$. Examination of fig.8-29 shows that at the equivalent of 1μs the current is a factor of 10^7 down on the initial current, so here the instantaneous current will be $4.8*10^{-5}$amps. Examination of fig.8-22 shows the current here to be $6*10^{-5}$amps, so the initial estimate of the flash response strength is correct within experimental error. The overall gradient of -1.0 implies that the photodecay is in the high intensity regime of bimolecular recombination. At lower intensities, the simulation has an average slope similar to that of the TROK model, as shown in fig.8 31, which is for 286K. The characteristic energy of 0.05eV used in the simulation gives a slope of $-(1-\alpha)=0.5$. Note that the region of slope -0.5 extends to longer times as excitation intensity drops. Each curve differs from the other by a factor of one hundred in intensity. At the high intensities, the decays are seen to approach a common curve, that is any increase in excitation is accompanied by an equal increase in bimolecular recombination. Therefore it is easy to adjust the flash intensity to give the required drop in current between the time of the flash and some

Figure 8-31: Computer simulation:
Transient decay at different intensities.

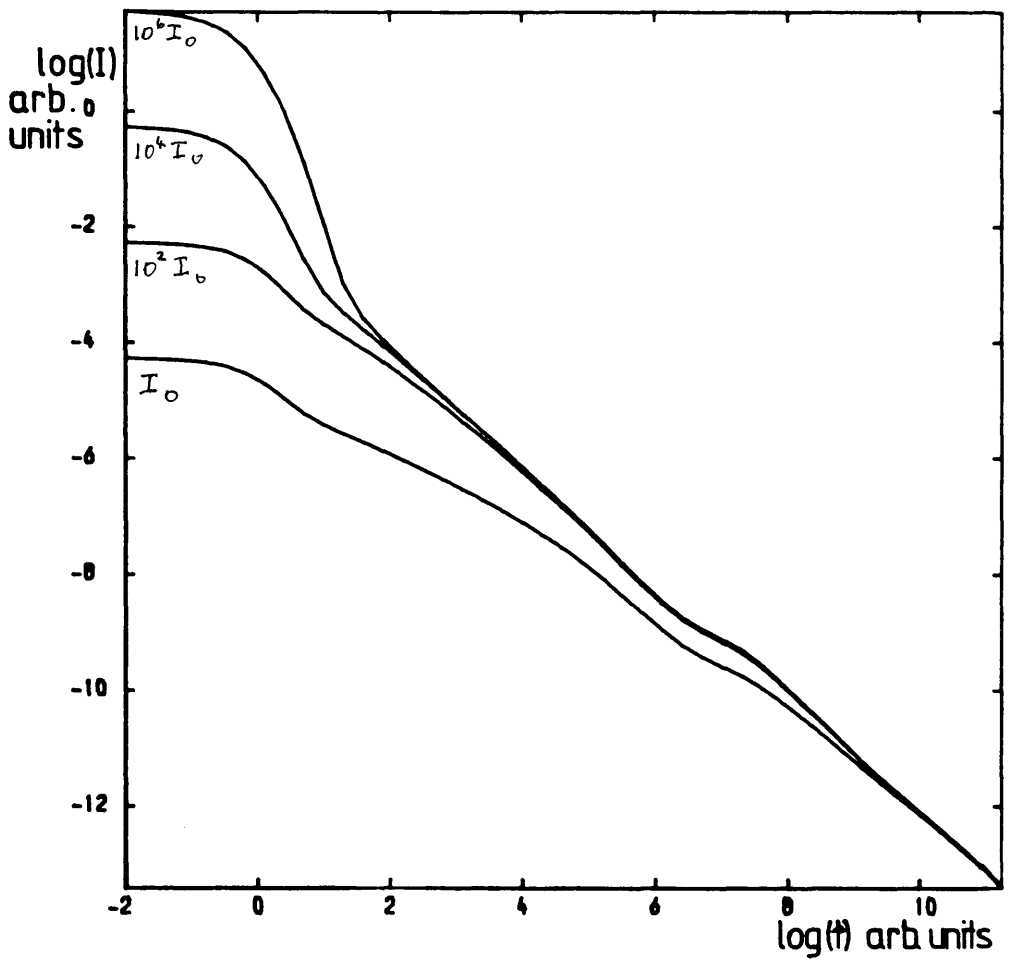

experimentally accessible time.

Figure 8-32 shows the density of states used in the simulation, including the discrete state at 0.4eV used to provide the features in the transient photodecay. A step response simulation was done with this extra discrete state included, but the curves obtained did not look like the experimental curves which did not show any features except those which could be explained by the recombination "cut off", so in this respect the interpretation of the results from the two experiments do not tie up so well. This may be because the yellow light used in the flash decay experiment has a small absorption depth, so all the excited carriers may be produced in a region where surface states dominate the recombination.

8.2 Sputtered Material

It was intended to measure both sputtered and glow discharge silicon to provide a comparison between the two materials. Unfortunately, as will be shown in this section, the sputtered material was considerably less photosensitive than the glow discharge material so the maximum Fermi level shift was smaller, and a high intensity monomolecular recombination regime was not observed; this meant that a critical energy for recombination could not be inferred in this material. Also it was not possible to obtain any useful information from transient rise measurements as short times could not be observed due to the higher RC time constant associated with the sputtered samples.

Figure 8-32: Density of states used in the transient decay simulation

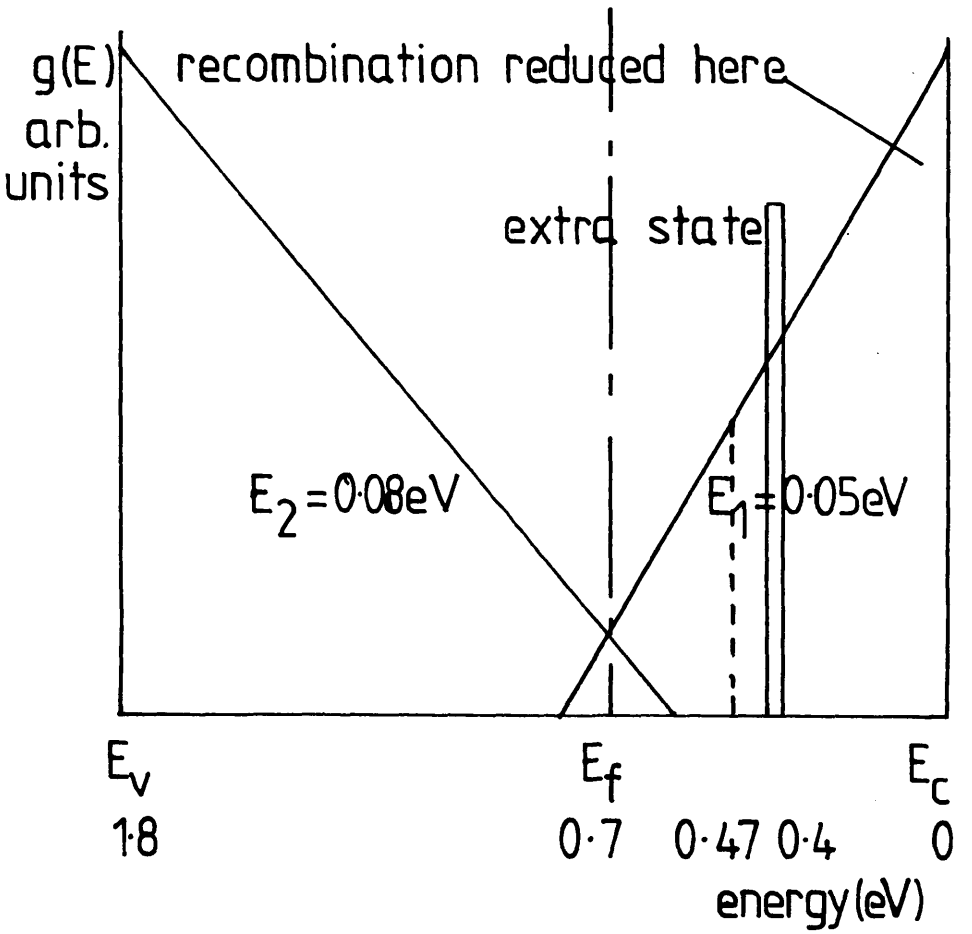

8.2.1 Characterisation

8.2.1.1 Determination of the Mobility Gap

As the sputtered samples were prepared by the author it was possible to prepare samples in the configuration required for each particular measurement by placing inside the deposition unit blank slides for optical absorption measurements in addition to the double gap cells used for the photoconductivity measurements. Fig8-33 shows a plot of $(\alpha h\omega)^{1/2}$ vs. $h\omega$ which has the straight line portion extrapolated to give a value of about 1.8eV for the mobility gap as explained in chapter 4. Due to sub-band gap absorption the graph is not linear over a substantial range but the portion of it which is linear gives a typical figure for E_c-E_v.

8.2.1.2 Dark Conductivity

Figure8-34 shows the dark conductivity of sputtered a-Si.H. The activation energy is 0.73eV, a typical figure for the undoped material. The value of σ_o is $390(\Omega cm)^{-1}$, which is compared to the same figure for the glow discharge material of $820(\Omega cm)^{-1}$. This value is not sufficiently lower than the glow discharge figure to suggest a change of conduction mechanism away from the extended states, but the lower figure may be one of the reasons for the apparently poorer performance of sputtered material in general.

8.2.2 Steady State Photoconductivity

8.2.2.1 Temperature Dependence

Fig8-35 shows the temperature dependence of the photoconductivity of the sputtered material for generation rates of $10^{18}cm^3s^{-1}$ and $10^{20}cm^3s^{-1}$, with $\alpha=10^4cm^{-1}$, using a red L.E.D. as the

Figure 8-33: Determination of the Mobility Gap

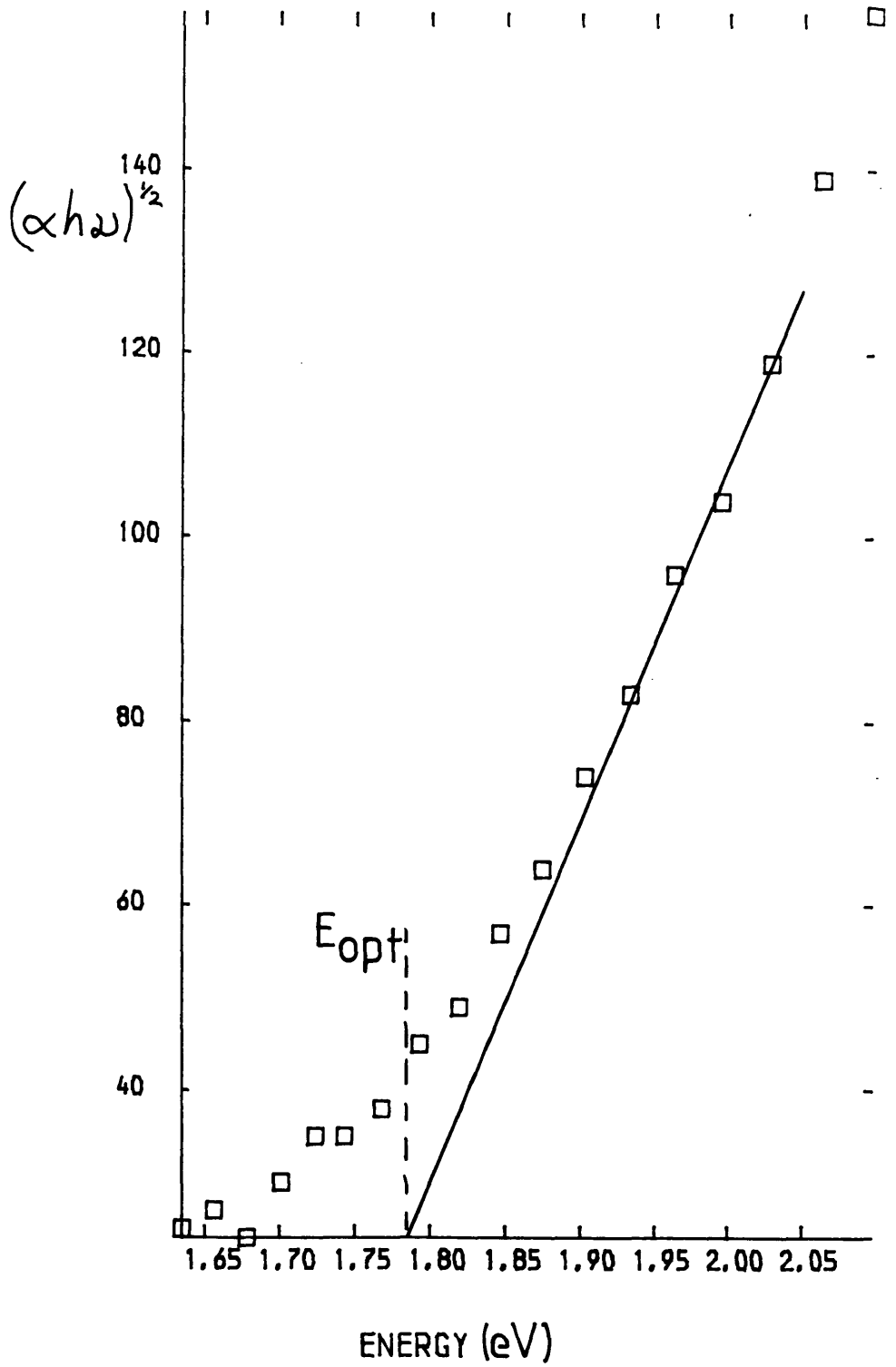

Figure 8-34: Dark Conductivity of a-Si:H

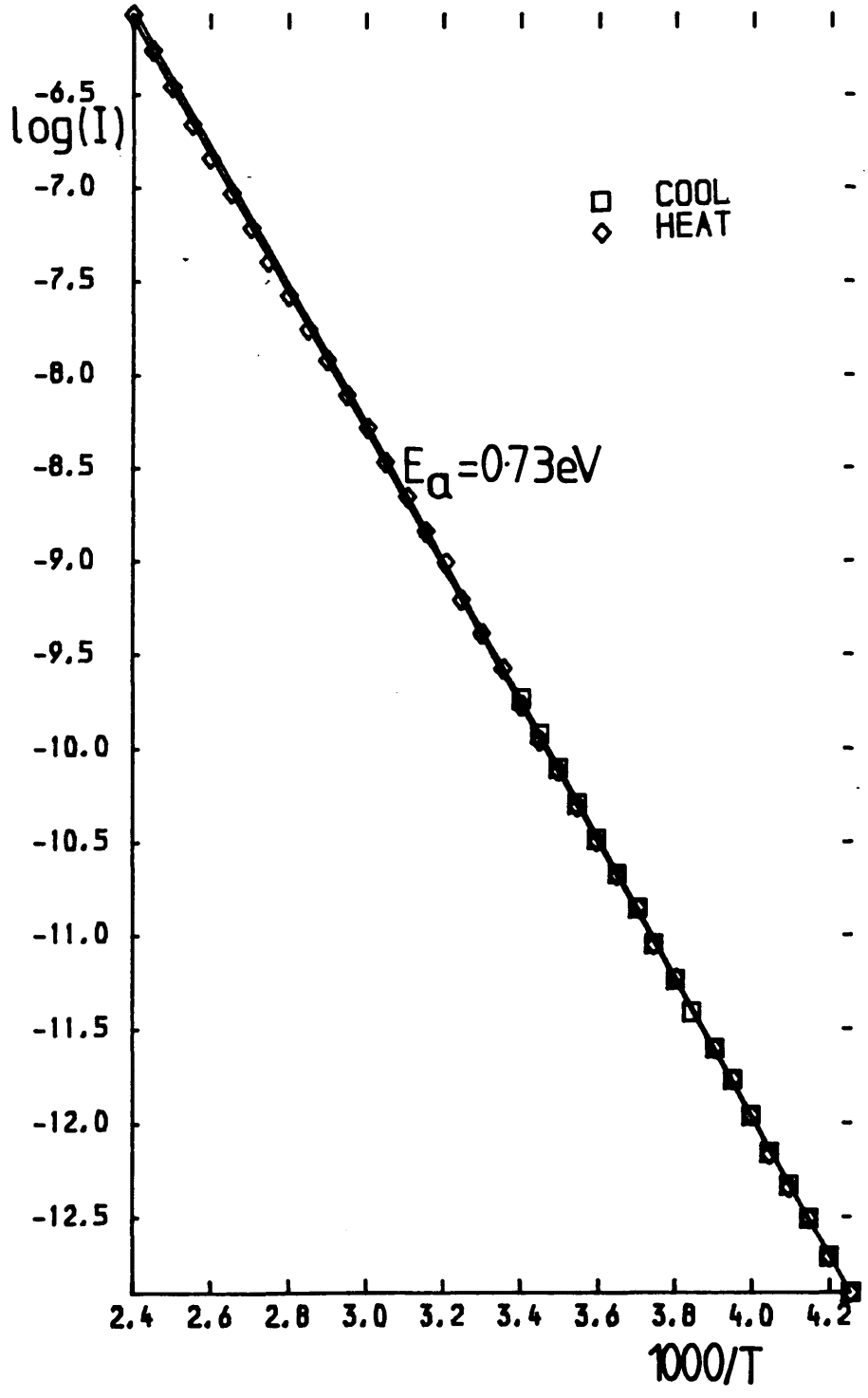

Figure 8-35: Temperature Dependence of the Sputtered Material

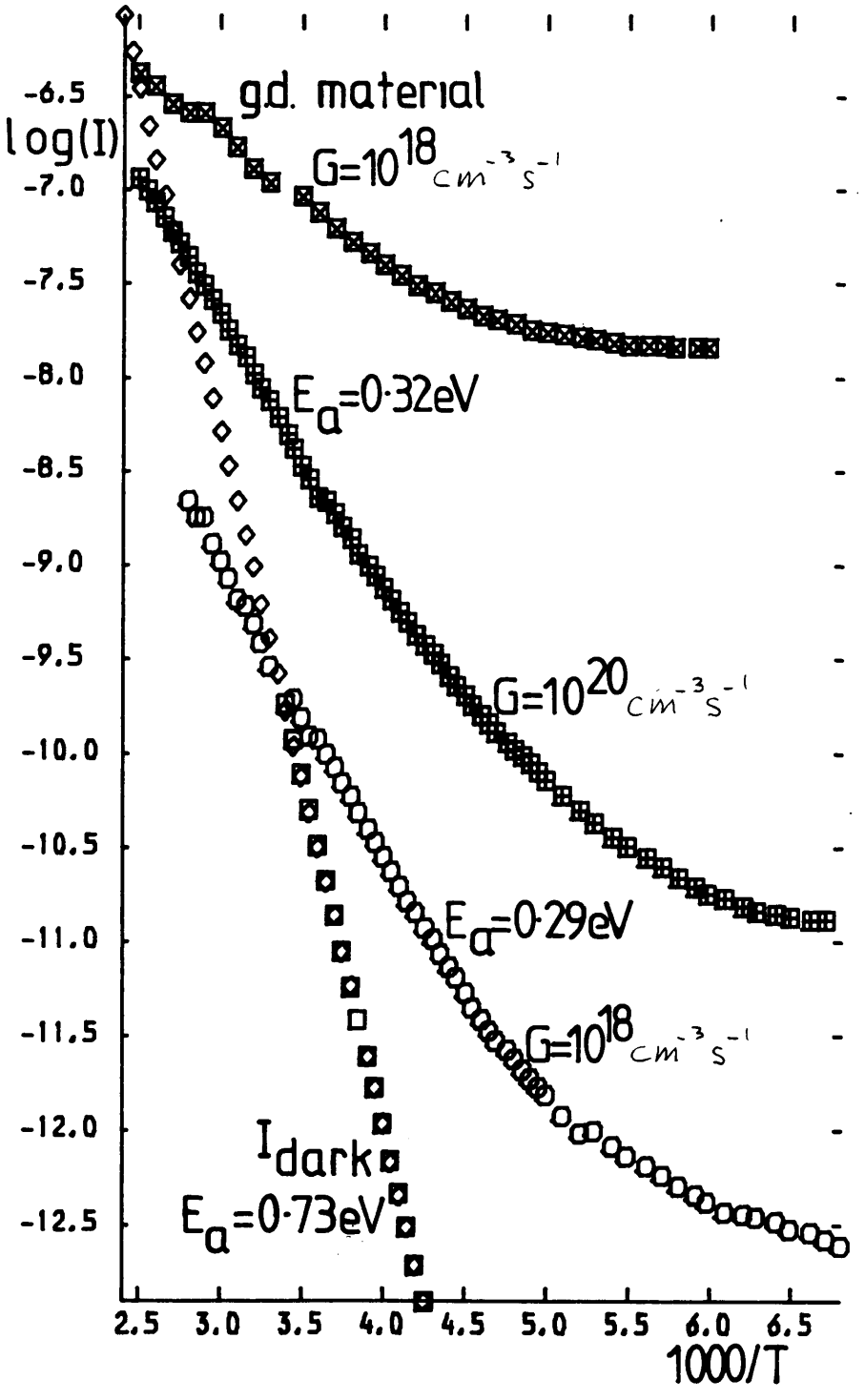

light source. Plotted on the same graph is the same information for the glow discharge material at the lower intensity Clearly the sputtered material is considerably less photosensitive than the glow discharge material.

The likely reasons for the low photosensitivity of the sputtered material are discussed next. The existence of a different conduction mechanism has been rejected above, which leaves recombination as the most likely cause. A second reason may be that the capture cross section of the recombination centres may be 100 times larger than in the glow discharge material, but the localised state density is the same. Calculation of the largest quasi-Fermi level shift, that for the highest intensity and lowest temperature, is 0.28eV. Under the same excitation the glow discharge material gives a 0.42eV shift. However, the critical energy for recombination in the glow discharge material is 0.24eV above E_{fo}, so the recombination centres in the sputtered material are at the same energy as the other, and one would expect them to have similar properties. It is therefore suggested that the insensitivity of the sputtered material is due to an increased localised state density. This is not a necessarily a fundamental property of the sputtered material since the work of the Harvard group would contradict this successfully, but the preparation conditions used by the author were possibly not good enough to produce electrically "good" material. This may be due to contamination by chalcogenide glasses previously deposited in the same chamber. Fortuna[69] has measured the impurity concentrations in a-Si:H films from the same deposition system as

used in this work, and found impurity concentrations of up to 3 atomic %, principally of As and Se.

Examination of the curve for the sputtered material shows that a well defined activation energy of about 0.3eV occurs over a large interval of temperature. The theories in chapter 2 would indicate that this implies discrete localised states 0.6eV below E_c if path 2 of the medium intensity regime is controlling the recombination. The value of 0.6eV agrees well with the results from the glow discharge material. Unfortunately this would not be consistent with the intensity dependence of the material which is shown in the next subsection to follow eq.(1.23), so no well defined activation energy should be found. Also as the dark current activation energy is 0.73eV, and the maximum Fermi energy shift is 0.28eV, this brings E_{fn} to 0.45eV below E_c, or 0.15eV above the discrete state inferred from the photoconductive activation energy described above. If a best straight line is drawn through the high temperature points on the glow discharge curve, a figure of 0.13 would be obtained for an activation energy, which is considerably different from the results from the sputtered material. As the temperature dependence of the sputtered material cannot be interpreted by the same methods as the glow discharge material, this is left for further work.

It can also be seen that the point at which the activation energy ceases to be well defined is not at the same temperature for both intensities. This suggests that as the activation energy

disappears the conductivity mechanism does not change, i.e. one still observes extended state conduction at low temperatures.

8.2.2.2 Intensity Dependence

Fig8-36 shows the intensity dependence of the sputtered material. The general form is the same as for the glow discharge material, i.e. the intensity dependence is as eq.(1.23) over several orders of magnitude in intensity. Also, the data do not fit the Rose analysis, i.e. $\gamma \neq T_c/T+T_c$ as illustrated in fig.8-37 which does not show γ tending to 1.0 as T falls to 0K. Because eq (1.23) holds, one can infer that sputtered material also contains a distributed density of localised states, but because the Fermi level shift is not sufficient to eventually produce monomolecular recombination, less information is available from the data.

8.2.2.3 Attempt to find the Effects of Diffusion

The temperature dependence of the photoconductivity of sputtered a-Si:H was measured at several wavelengths to examine the effect of diffusion. The middle wavelength used was from the red L.E.D. which with its wavelength centred at 655nm. had an absorption depth of approximately the depth of the sample(1.3μm). An I.R. L.E.D. of wavelength 940nm. was used to give a "flat" absorption of light due to its weak absorption, and also a yellow L.E.D. of wavelength 570nm. to produce a steep absorption profile. The intensities of the sources were adjusted to give the same photocurrent at room temperature, so the effects of the differing absorptions could be observed as the temperature changed.

Fig.8-38 shows the measurements obtained in this way. In the

Figure 8-36: Intensity Dependence of the Sputtered Material

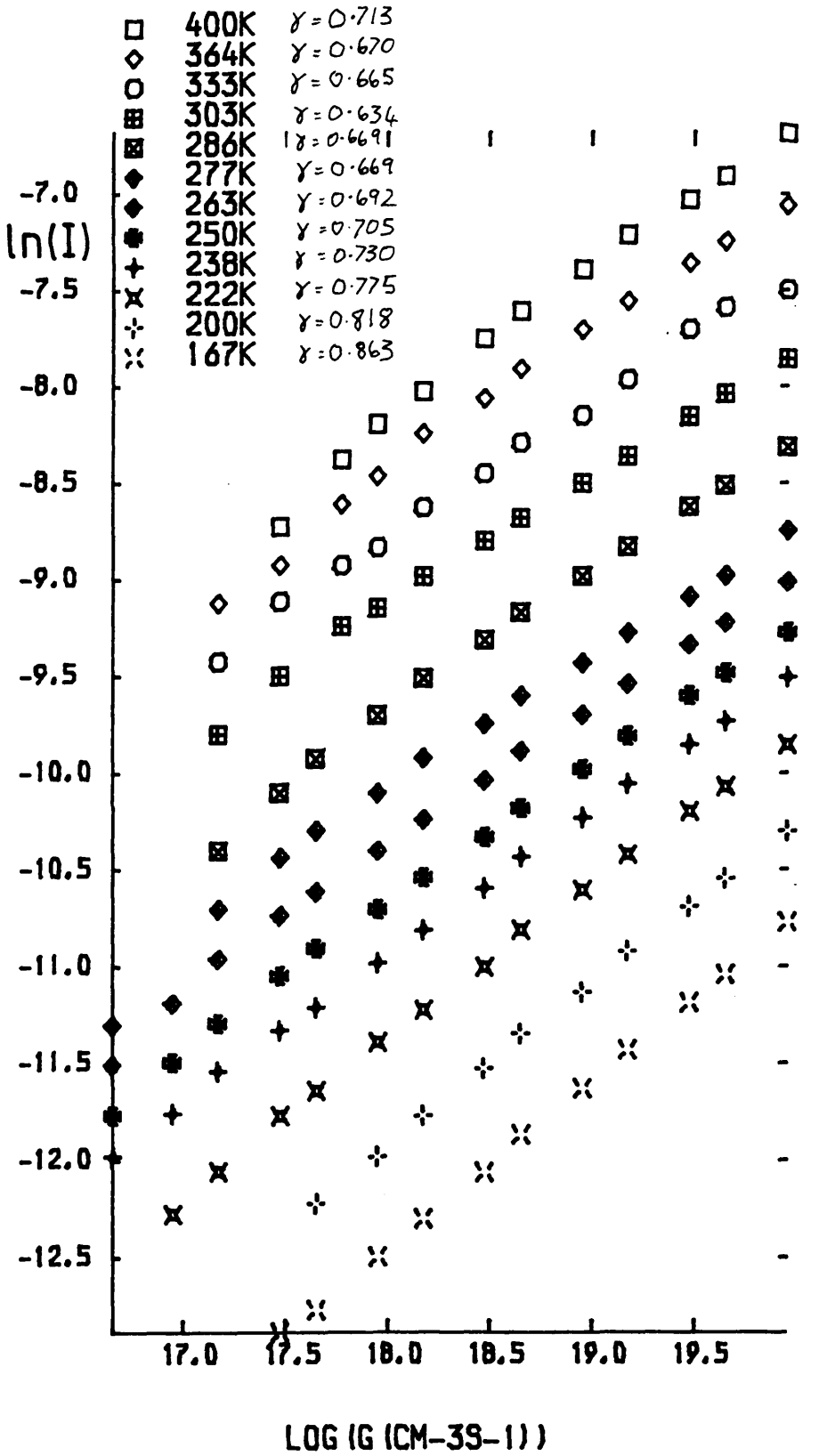

Figure 8-37: Temperature Dependence of γ in Sputtered a-Si:H

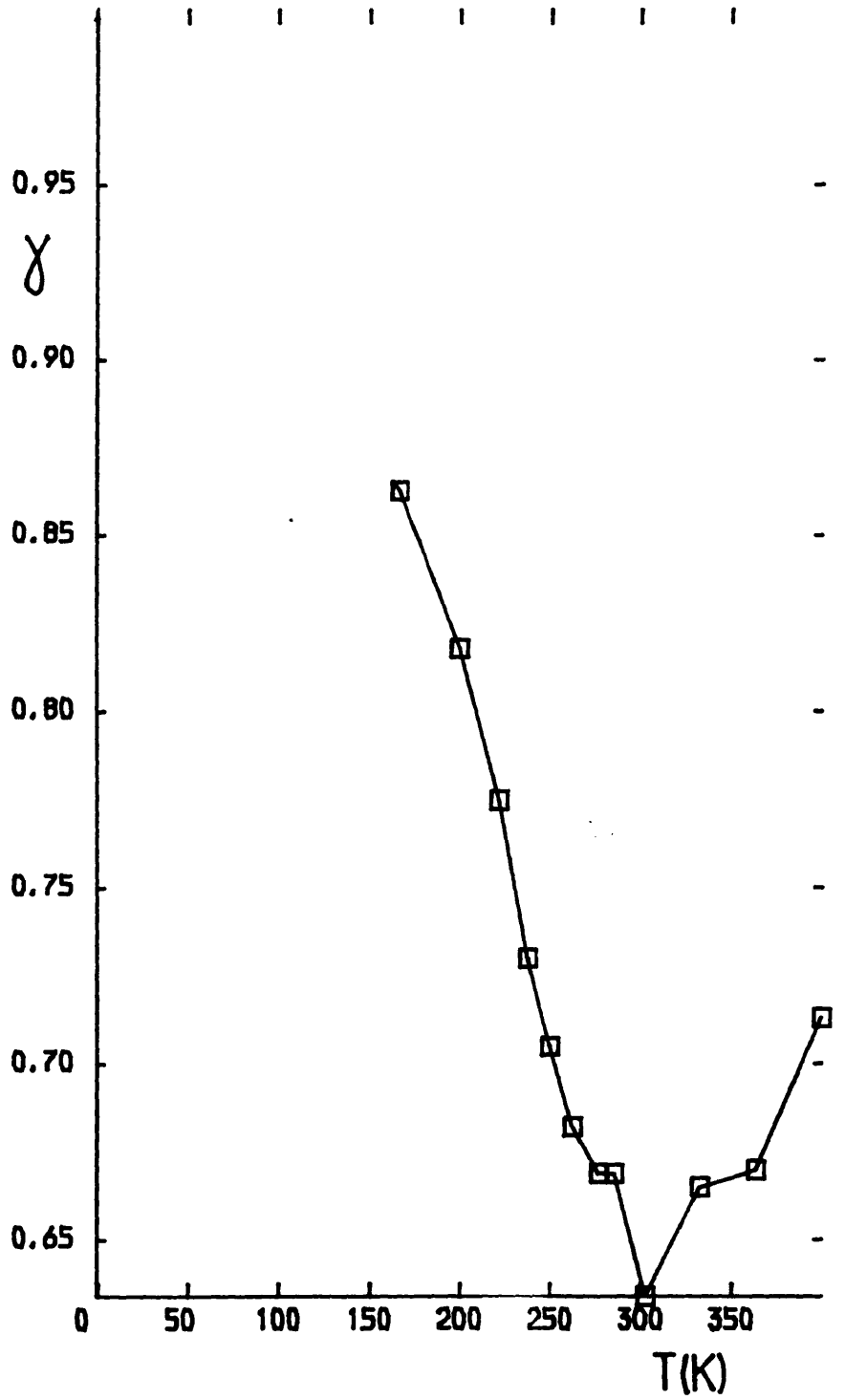

Figure 8-38: Temperature Dependence at Several Wavelengths

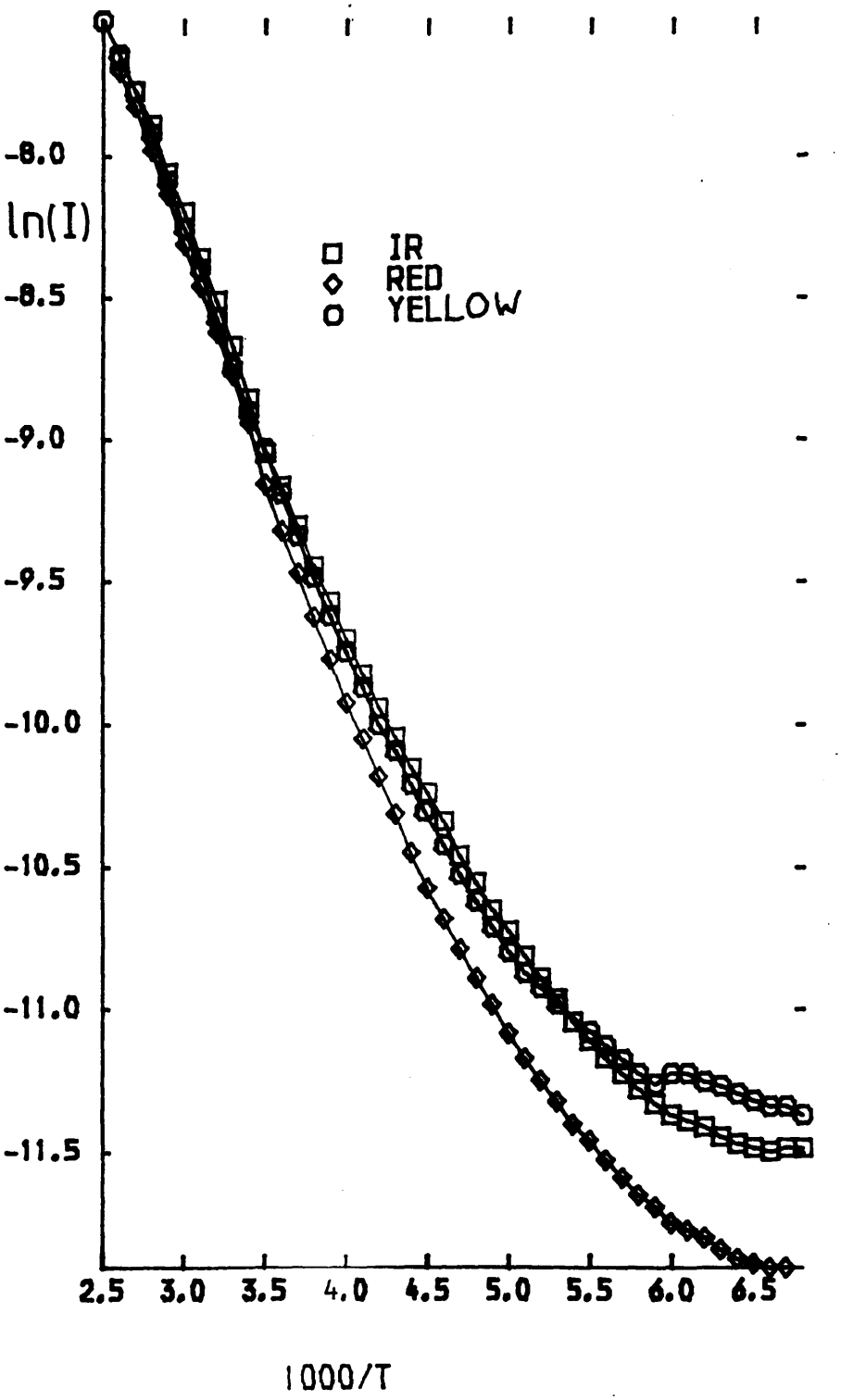

region of the well defined activation energy the photocurrents caused by all three diodes remain the same but at low temperatures the photocurrents from the red L E D. drop slightly below the others As this is the middle wavelength their is no clear trend. The overall difference was less than a factor of two however so perhaps diffusion acts such that an even distribution does indeed occur throughout the sample as assumed for the interpretation of the glow discharge material.

8 3 Measurements by Other Authors

In this section relevant measurements by other authors are compared to the results obtained in this work

8.3.1 Glow Discharge Material

8 3.1.1 Steady State Photoconductivity

The results obtained by Spear's Dundee group[9 10] have already been described in Chapter 4. Spear found the temperature dependence of the steady state photoconductivity to display a well defined activation energy and a transition to recombination regime III occurred at the same temperature for several light intensities in contrast to the results presented earlier in this chapter which indicate instead a transition to recombination regime III which is temperature dependent. This was interpreted as a change in conduction mechanism from extended state conduction to hopping in the localised states. Shockley Read processes were not used in Spear's model. This type of variation in the properties of a Si:H prepared in different laboratories is common, and will be seen again in this section.

McMahon [75] has measured the steady state photoconductivity in as grown and light soaked samples to examine the effect of the Staebler Wronski effect on the density of states. The experimental results for all the samples are different from those of this author. In particular some measurements show thermal quenching of the photoconductivity near room temperature i.e. the temperature dependence shows a "dip". Interestingly the model used by McMahon is similar in many ways to that used in this thesis. i.e. a dangling bond of density $10^{16} cm^{-3}$ in addition to exponential band tails. The D^o states were given a capture cross section of $10^{-16} cm^2$ and R=10. A Shockley Read mechanism was assumed.

Huang et. al.[76] have measured steady state and transient photoconductivity in undoped material. Intensity dependence measurements at various temperatures did not all follow eq (1.23). At low temperatures γ changed to about 0.6 rather than rising to 1.0 as in this thesis. In conjunction with flash decay measurements two values for T_c were obtained one of 300K for tail states down to about 0.35eV below E_c below which energy a value of 1000K for T_c was used. This model appeared reasonably similar to the Spear field effect density of states[6].

In the papers described above, either the measured results or the models used differ greatly from those presented in this work. The reason for this will be discussed at the end of this section.

8 3.1.2 Step Response

The only other measurement of step response seen by this author are by Street et. al [77] who found the step response to vary very weakly with temperature in contrast to the variation found in this work. These observations were made at very high excitation levels however and also were insufficiently detailed to allow a proper comparison.

8 3.1.3 Flash Decay

All the experiments described here have measured the transient photoconductivity in the low intensity monomolecular regime unlike the measurements presented in this thesis which were in the high intensity bimolecular regime.

Hvam and Brodsky[78] obtained transient decays similar in form to those presented in this thesis which were interpreted as due to multiple trapping and release between extended states and localised states in exponential tails. Some structure was observable in the data but in insufficient detail to allow comparison with the data presented in this work. Kagawa et. al [79] showed decays that differed strongly with pulse width but the duration of the pulses varied from 0.2μs to 10μs. The decay measurements were made over only one decade of time and show no structure so with these long excitation pulses there is thus little ground for comparison with the present results.

Pandya et. al. [80] and Schiff[81] have measured transient decays similar to those described earlier and have used a model

incorporating exponential band tails with superimposed Do states 0.4-0.5eV below E_c which is in reasonable agreement with the present work.

Oheda82 has obtained decays in undoped a Si H similar to those in this thesis fig.8 39. At 300K Oheda shows a curve very similar to those presented in this thesis e.g figs (8 24 & 8 25) but at low temperatures a non dispersive region at the early part of the response was observed and the beginning of the subsequent fall was used to define the onset of recombination.

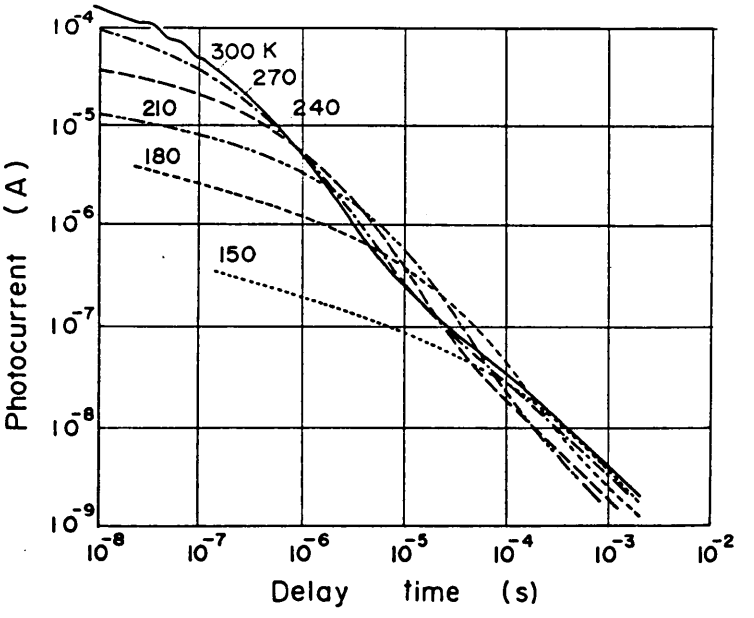

Transient photocurrent of undoped a-Si:H for a substrate temperature of 200°C, measured at several temperatures.

Figure 8 39 Transient Decays from Oheda82.

This time was related to a thermalisation energy by eq.(3.2) which

varied with temperature to give an activation energy of 0.2eV interpreted to be caused by a feature in the density of states at this energy. A possible alternative explanation is of a band tail whose density falls rapidly below about 0.2eV e.g a linear tail as proposed by Marshall[83] and others. The non dispersive region was not observed in the present work but this may be due to the bimolecular recombination conditions observed here which has the greatest effect at very short times.

8.3.2 Sputtered Material

8.3.2.1 Steady State Photoconductivity

Viktorovitch et. al [84] have measured steady state photoconductivity measurements on sputtered material. They obtained a well defined activation energy for the temperature dependence of about 0.14eV in contrast to the value of 0.3eV obtained here. This indicates the variation in properties of sputtered a Si H prepared in different laboratories.

Arene and Baixeras[85] measure diode and triode r.f. sputtered material. The results were very different for the two materials. Diode sputtering produced a normal temperature dependence and an intensity dependence which followed eq.(1.23). A well defined activation energy was not obtained unlike the behaviour of the sputtered material as described in this work The model which used the Simmons and Taylor approach to distributed states had very low capture cross sections of $10^{-18}cm^2$. The triode results showed thermal quenching of the photoconductivity i.e. there was a dip in

the temperature dependence of the photoconductivity between 260 and 400K This was explained by a model originated by Rosel[7] which incorporates two species of traps with different electron capture cross sections. As the quasi Fermi level is moved through these traps, different regimes of photoconductivity are observed and the electron lifetime varies considerably.

8.3.3 Conclusion

The papers by Arene and Baixeras[85] and Viktorovitch[84] demonstrates the large differences in properties of a-Si:H prepared under different conditions and different laboratories in particular for the sputtered material. This property of a-Si:H reduces the validity of any comparisons that can be made with work published by other groups. As not everybody uses the same model, the reason for this cannot necessarily be attributed to detailed variations in the density of states from sample to sample. However it is difficult to envisage any other reason as it does not appear reasonable to assume that material from one lab. should be fundamentally different from another. It would appear then that the steady state photoconductivity is a sensitive indication of the detailed density of states of a Si-H.

On the other hand the flash decay measurements described above have not been made in great detail by many groups. Where detail has been reported[82, 80], some similarities do reveal themselves, so this measurement would seem to be insensitive to the detailed density of states.

Chapter 9

Conclusions and Suggestions for Further Work

9.1 Conclusion

The conclusions of this thesis are that the major recombination centre in glow discharge a-Si:H is a distributed set of states with a capture cross-section of $10^{-15}cm^2$, which implies tnat the states are neutral. They have an energy range distributed downwards in energy from the critical energy for recombination at about 0.6eV below E_c to E_{fo}. The analyses of the two level Shockley-Read-Hall model and the single defect correlated state model both give similar results. This idea can be extended to the case of distributed states, so although the analysis of the steady state photoconductivity of the glow discharge material, which was presented in the last chapter, used a one electron model, the neutral recombination centres can be identified with D^o states, particularly as the dark Fermi level lies below these states. Recombination is by electron capture by D^o, and subsequent hole capture by the resultant D^-. Steady state photoconductivity and step response transient photoconductivity measurements indicate that the dangling bond is distributed in energy. The transient photodecay measurement indicates in addition, a relatively discrete state at 0.4eV below E_c. The existence of this level would not affect the experimental interpretation or modelling of the steady state photoconductivity as it lies above the critical energy for recombination, and would not contribute to the recombination process. This level should, however, have been observable at short

times in the step response measurement. As the flash decay measurements were performed with a yellow dye-laser, the short absorption depth at this wavelength would cause the photocarriers to be produced at the surface, so the extra state required to explain the flash decay data may be a property of the surface rather than the bulk.

Fig.9-1 shows a suggested density of states for undoped a-Si:H using the results in this work. The exact form of the tail states distribution remains to be found, as states close to the mobility edges are outside the scope of this work. Marshall[75] has reported capture cross sections of 10^{-17}-10^{-16}cm^2 for the tail states from drift mobility measurements, which is consistent with the reduced recombination rate outside the critical energies reported here.

9.2 Suggestions for Further Work

This thesis has measured the steady state photoconductivity, the step response and the transient photoconductivity of undoped a-Si:H. As for further work, there is so much of this to be done that selection would need to be considered by any future worker. In particular, only material from one laboratory has been measured, and a-Si is so notoriously variable from different sources, the same measurements need to be made on material from other sources. In particular, the measurements could be carried out using other frequencies of light to attempt to find the effect of diffusion.

For the transient measurements, faster apparatus would allow

Figure 9-1: Suggested Density of States for undoped a-Si

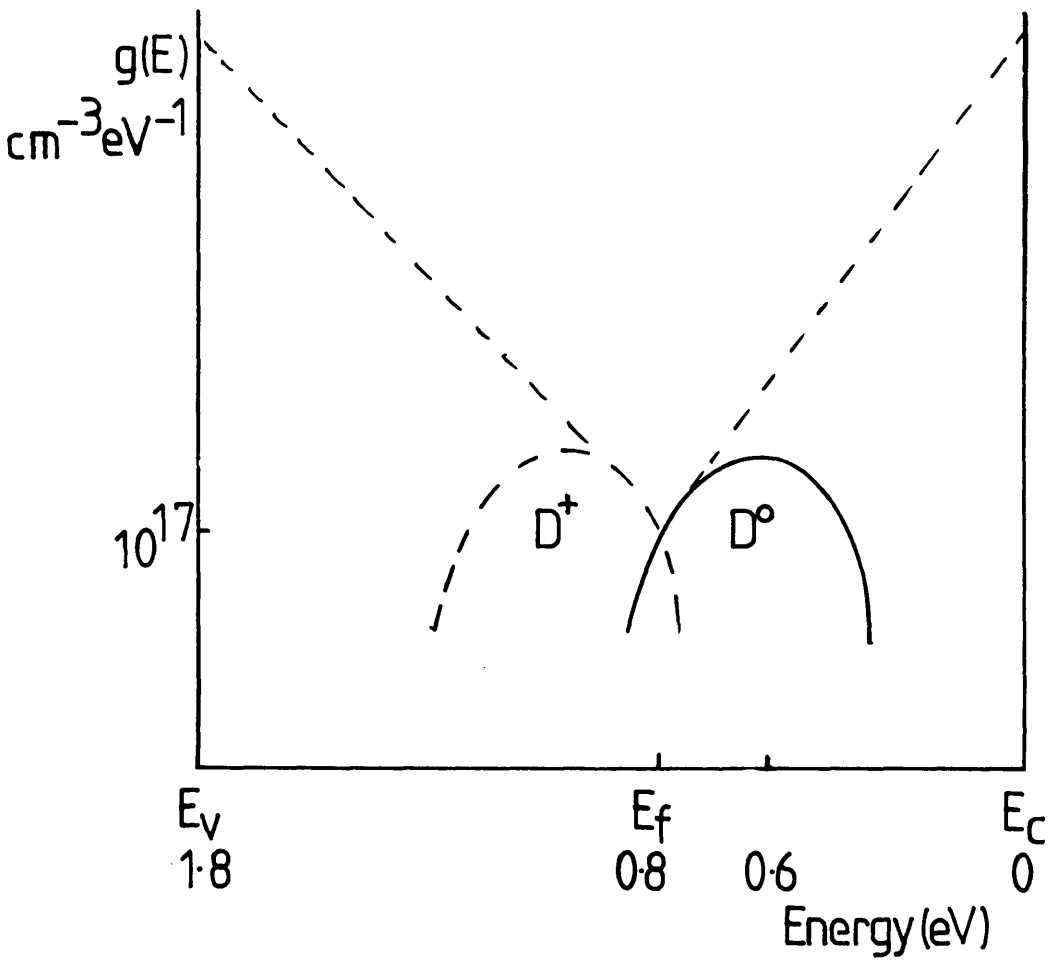

measurement at shorter times, which promises important information on g(E) closer to E_c. Computer averaged multiple measurements would considerably reduce noise.

Measurements on n and p-doped a-Si:H and biased thin film transistors would examine a situation where E_{fo} has been moved in the mobility gap. This would alter the D^+, D^o and D^- densities. As this would cause the charge state of the recombination centres to change, recombination would be greatly altered.

The computer simulation has provided important information on the photoconductive processes, but a discrepancy appears in the interpretation, i.e. an extra discrete state is needed to interpret the results on the flash decay measurements. As this could be due to the existance of surface states, it is suggested that a 2-) model including the effects of surface band bending and diffusion should be developed. A computer model including the effects of correlation is already under development.

Appendix I

In chapter 2, in the section dealing with the recombination in the case with correlated states, it was mentioned that the full expressions for the occupancy fractions F^+, F^o and F^- were necessary to calculate the recombination rate. An outline of the derivation is included here.

Fig.5-1 shows all the possible transitions in the energy level diagram including correlation. The transition probabilities are repeated here.

$a=nC_n^+$, electron capture by $D^+ \rightarrow D^o$
$b=n_1^+C_n^+$, hole capture by $D^o \rightarrow D^+$

$c=p_o^oC_p^o$, hole release by $D^+ \rightarrow D^o$
$d=p_oC_p^o$, hole capture by $D^o \rightarrow D^+$

$e=nC_n^o$, electron capture by $D^o \rightarrow D^-$
$g=n_1C_n^o$, electron release by $D^- \rightarrow D^o$

$h=p_1^-C_p^-$, hole release by $D^o \rightarrow D^-$
$j=p_oC_p^-$, hole capture by $D^- \rightarrow D^o$

As the occupancy fractions reach steady values in the steady state, one can treat independently the steady state transfer between D^+ and D^o states using transitions a-d, and the steady state between D^o and D^- states using transitions e-j.

For the $D^+ \rightarrow D^o$ transitions,

$$F^+/F^o=(b+d)/(a+c)$$
$$=\frac{\text{total probability of } D^o \rightarrow D^+ \text{ transfer}}{\text{total probability of } D^+ \rightarrow D^o \text{ transfer}} \qquad (A-1)$$

and for the $D^o \rightarrow D^-$ transitions,

$$F^o/F^-=(g+j)/(e+h) \qquad (A-2)$$

Since

$$F^+ + F^0 + F^- = 1 \tag{A.3}$$

equations (A.1) and (A.2) can be solved for the F functions. This gives

$$F^0 = \left\{ 1 + \frac{n_1^+ C_n^+ + p C_p^0}{n C_n^+ + p_1^0 C_p^0} + \frac{n C_n^0 + p_1^- C_p^-}{n_1^0 C_n^0 + p C_p^-} \right\}^{-1} \tag{A.4}$$

and

$$F^+ = \left\{ 1 + \frac{n C_n^+ + p_1^0 C_p^0}{p C_p^0 + n_1^+ C_n^+} + \frac{(n C_n^0 + p_1^- C_p^-)(n C_n^+ + p_1^0 C_p^0)}{(p C_p^0 + n_1^+ C_n^+)(p C_p^- + n_1^0 C_n^0)} \right\}^{-1} \tag{A.5}$$

and

$$F^- = \left\{ 1 + \frac{p C_p^- + n_1^0 C_n^0}{n C_n^0 + p_1^- C_p^-} + \frac{(p C_p^0 + n_1^+ C_n^+)(p C_p^- + n_1^0 C_n^0)}{(n C_n^0 + p_1^- C_p^-)(n C_n^+ + p_1^0 C_p^0)} \right\}^{-1} \tag{A.6}$$

Appendix II

This is the computer program STEADY mentioned in the main text. It is in FORTRAN.

```
C       STEADY STATE PHOTOCONDUCTIVITY PROGRAM
C       WITH GAP CENTRE RECOMBINATION ONLY
        INTEGER NL,H,TM,GM,H1,HS
        DOUBLE PRECISION EC,EA,ED,G,K,T,KT,DE,E1,E2,E3
        DOUBLE PRECISION Q,Q1,Q2,Q3,E,EF,NO,NC,NV
        DOUBLE PRESISION PO,RA,RD,CNA,CND
        DOUBLE PRECISION NE,NN,NN1,PE,PE1
        DOUBLE PRECISION PE2,PE3,EP,N
        DOUBLE PRECISION EX1,EX2,EX3,EX4,G1
        DOUBLE PRECISION QA(1000),QD(1000),GA(1000)
        DOUBLE PRECISION FA(1000),PD(1000),FO(1000)
        DOUBLE PRECISION NI(1000),PI(1000),NTH(50),PTH(50)
        DOUBLE PRECISION RA1(1000),RA2(1000),RD1(1000)
        DOUBLE PRECISION RD2(1000),GD(1000),PO(1000)
        DOUBLE PRECISION RECA(500),RECD(500),REC,RR,XM,XO
        DOUBLE PRECISION YM,YO
        DOUBLE PRECISION RAI(500,10),RDI(500,10)
        DOUBLE PRECISION PHOT(50,50),GEN(50,50),X(50,50)
        DOUBLE PRECISION Y(50,50)
        DOUBLE PRECISION GAMMA(50,50), X1(50,50)
        DOUBLE PRECISION FTA(500,10),PTD(500,10),Y1(500)
        REAL EG,EA1,ED2,XOO,XMM,EA3,ED4
        COMMON /C1/N,KT,NO,PO,NC,NV,EC,DE,FO,PO,NTH,PTH
        COMMON /C2/NE,RA,RD,FA,PD,NI,PI,RA1,RA2,RD1,RD2
        COMMON /C3/NL,Q,QA,QD,GA,GD
        DATA EC,K,G/1.8,8.6142D-5,7.74D+20/
        DATA EA,ED/0.055,0.075/
        DATA TM,GM/6,36/
        DT=50.0
        EG=1.8
        XO=+1.0D+30
        XOO=XO
        XOR=XO
        XM=-1.0D+38
        XMM=XM
        XMR=XM
        YO=+1.0D+35
        YM=-1.0D+35
        WRITE(5,10)
10      FORMAT(' START TEMPERATURE? T')
        READ(5,20)T
20      FORMAT(F5.1)
        T1=T
C       NO. OF LEVELS NL
        NL=200
        WRITE(5,800)
800     FORMAT(1H ,' INPUT NET DOPANT CHARGE DENSITY,N')
```

```
      READ(5,820)N
820   FORMAT(F)
C     SELECT TURNOVER LEVELS
      WRITE(5,29)
29    FORMAT(1H ,' INPUT BREAK LEVELS EA1,EA3,ED2,ED4,')
      READ(5,31)EA1,EA3,ED2,ED4
31    FORMAT(4F)
C     FLAT REGION DENSITY,G1
      G1=1.0D17
C     LEVEL NUMBERS
      IE1=IFIX(FLOAT(NL)*EA1/EG)
      IE3=IFIX(FLOAT(NL)*EA3/EG)
      IE2=IFIX(FLOAT(NL)*ED2/EG)
      IE4=IFIX(FLOAT(NL)*ED4/EG)
      IF(IE1.GT.NL-1)IE1=NL-1
      IF(IE2.LT.1)IE2=1
      EX1=0.05
      EX2=0.05
      EX3=(EC-EA3)/DLOG(G/G1)
      EX4=(ED4)/DLOG(G/G1)
C     KT PRODUCT
      DO 550 J=1,TM
      KT=K*T
C     BAND EDGE DENSITY OF STATES,NC,NV
      NC=G*KT
      NV=NC
C     DISCRETIZATION WIDTH,DE
      DE=EC/DFLOAT(NL)
C     SET UP DENSITY OF STATES GA AND GD
C     EXPONENTIAL TAILS
      DO 30 I=1,NL-1
      IF(I.LT.IE4)GD(I)=G*DE*DEXP(-DE*DFLOAT(I)/EX4)
      IF(I.GE.IE4.AND.I.LT.IE2)GD(I)=G1*DE
      IF(I.GE.IE2)GD(I)=G1*DE*DEXP(-DE*
     1DFLOAT(I-IE2)/EX2)
      IF(I.LT.IE1)GA(I)=DE*G1*DEXP(-DE*
     1DFLOAT(IE1-I)/EX1)
      IF(I.GE.IE1.AND.I.LT.IE3)GA(I)=G1*DE
      IF(I.GE.IE3)GA(I)=DE*G*DEXP(-DE*DFLOAT(NL-I)/EX3)
      WRITE(5,*)GD(I),GA(I)
30    CONTINUE
C     THERMAL EQUILIBRIUM ITERATION FOR EF
C     USING CHARGE NEUTRALITY
      E1=EC-0.1
      CALL TECHS(E1)
      Q1=Q
      E2=0.1
      CALL TECHS(E2)
      Q2=Q
C     NEWTON-RAPHSON SECANT METHOD
40    IF(DABS(Q2-Q1)-1.0)60,60,42
42    IF(DABS(E2-E1)-1.0D-14)60,60,45
45    E3=E2-Q2*(E2-E1)/(Q2-Q1)
C     WRITE(5,47)E3
C47   FORMAT(' E3=',F20.14)
```

```
50      CALL TECHS(E3)
        Q3=Q
        Q1=Q2
        E1=E2
        Q2=Q3
        E2=E3
        GOTO 40
60      EF=E3
        WRITE(5,70)EF
70      FORMAT(' EF=',F20.16)
        WRITE(5,65)P0
65      FORMAT(' P0=',D24.16)
        NTH(J)=N0
        PTH(J)=P0
C       STEADY STATE STATISTICS PROGRAM
C       SET UP EMISSION TERMS NI(I),P(I)
        DO 140 I=1,NL-1
C       IF((EC-)E*FLOAT(I))/KT-80.)150,150,160
150     NI(I)=)EXP()E*)FLOAT(I)-EC)/KT+)LOG(NC))
C       GOTO 190
C160    NI(I)=0.0
C190    IF()E*FLOAT(I))/KT-80.)170,170,180
C180    PI(I)=0.0
C       GOTO 140
170     PI(I)=)EXP(-)E*)FLOAT(I)/KT+)LOG(NV))
140      CONTINUE
C       NEW TOTAL ELECTRON DENSITY,NE
C       STEP UP IN EQUAL RATIOS
        NN1=0.0001*NTH(1)/NTH(J)
        HS=1
        H1=1
        DO 570 H=1,GM
        NN=10.0**(0.25*)FLOAT(H-1))
        NE=NTH(J)*(1.0+NN1*NN)
C       SHOCKLEY-READ TERMS
        RA=0.01
        RD=100.0
        DO 240 I=1,NL-1
        RA1(I)=RA*NE+PI(I)
        RA2(I)=RA*(NE+NI(I))+PI(I)
        RD1(I)=RD*NI(I)
        RD2(I)=RD*(NE+NI(I))+PI(I)
240     CONTINUE
C       EXCESS HOLE DENSITY GUESS ITERATION PE1,PE2
        PE1=0.0
        CALL SR(PE1)
        Q1=Q
        PE2=0.001*NE
        CALL SR(PE2)
        Q2=Q
C       TYPE *,Q1,Q2
C       NEWTON-RAPHSON METHOD
250     IF(DABS((Q2-Q1)/Q2)-1.0D-14)260,260,270
270     IF(DABS((PE2-PE1)/PE2)-1.0D-14)260,260,280
280     PE3=PE2-Q2*(PE2-PE1)/(Q2-Q1)
```

```
C       WRITE(5,320)PE3
C320    FORMAT(' PE3=',D24.16)
        CALL SR(PE3)
        Q3=Q
        Q1=Q2
        PE1=PE2
        Q2=Q3
        PE2=PE3
        GOTO 250
260     PE=PE3
C       WRITE(5,290)PE
C290    FORMAT(' PE=',D24.16)
C       WRITE(5,300)P0
C300    FORMAT(' P0=',D24.16)
C       COMPUTE RECOMBINATION RATE
C       RECOMBINATION ONLY BETWEEN LEVELS IE1&IE2
        CNA=1.0D-10
        CND=1.0D-8
        RR=0.0
        DO 745 I=1,NL-1
        RECA(I)=0.0
        RECD(I)=0.0
745     CONTINUE
        DO 750 I=1,NL-1
        RECA(I)=CNA*GA(I)/RA2(I)
        RECD(I)=CND*GD(I)/RD2(I)
        RR=RR+RECA(I)+RECD(I)
750     CONTINUE
        REC=(NE*PE-N0*P0)*RR
        TYPE *,REC,NE,NN
C       OUTPUT ARRAY-EXCESS DENSITY VS RECOMB RATE
        PHOT(H,J)=NE-N0
        Y(H,J)=DLOG10(PHOT(H,J))
        IF(Y(H,J).GT.YM)YM=Y(H,J)
        IF(Y(H,J).LT.YO)YO=Y(H,J)
        GEN(H,J)=REC
        X(H,J)=DLOG10(GEN(H,J))
        IF(X(H,J).GT.XM)XM=X(H,J)
        IF(X(H,J).LT.XO)XO=X(H,J)
        TYPE *,PHOT(H,J),GEN(H,J),T
        IF(F.EQ.1)GOTO 570
        GAMMA(H-1,J)=(Y(H,J)-Y(H-1,J))/(X(H,J)-X(H-1,J))
        X1(H-1,J)=0.5*(X(H-1,J)+X(H,J))
C       TAIL STATE OCCUPANCY
C       ELECTRONS IN C-BAND TAIL
C       HOLES IN V-BAND TAIL
        IF(H.LT.H1)GOTO 765
        DO 760 I=1,NL-1
        FTA(I,HS)=(FA(I)*GA(I))
        PTD(I,HS)=(PD(I)*GD(I))
        IF(FTA(I,HS).GT.XMM)XMM=FTA(I,HS)
        IF(PTD(I,HS).GT.XMM)XMM=PTD(I,HS)
        IF(FTA(I,HS).LT.XOO)XOO=FTA(I,HS)
        IF(PTD(I,HS).LT.XOO)XOO=PTD(I,HS)
        Y1(I)=DE*)FLOAT(I)
```

```
      RAI(I,HS)=(NE*PE-NO*PO)*RECA(I)
      IF(RAI(I,HS).GT.XMR)XMR=RAI(I,HS)
      IF(RAI(I,HS).LT.XOR)XOR=RAI(I,HS)
      RDI(I,HS)=(NE*PE-NO*PO)*RECD(I)
      IF(RDI(I,HS).GT.XMR)XMR=RDI(I,HS)
      IF(RDI(I,HS).LT.XOR)XOR=RDI(I,HS)
760   CONTINUE
      HS=HS+1
      H1=HS*5
765   CONTINUE
570   CONTINUE
      T=T-DT
550   CONTINUE
      CALL PAPER(1)
      PSX=0.2
      PSY=0.2
      CALL PSPACE(PSX,0.95,PSY,0.95)
      CALL MAP(X0-0.1,XM+0.1,Y0-0.1,YM+0.1)
      CALL AXES
      CALL SCALES
C     CALL GRATIC
      DO 650 J=1,TM
      DO 650 H=1,GM
      CALL POSITN(X(H,J),Y(H,J))
      IF(H-GM)660,650,650
660   CALL JOIN(X(H+1,J),Y(H+1,J))
650   CONTINUE
      IPSX=IFIX(PSX*58.0-5.0)
      IPSY=IFIX(35.0*(1.0-PSY)+3.0)
      CALL PLACE(IPSX+10,IPSY)
      CALL TYPECS('LOG GENERATION RATE',19)
      CALL PLACE(IPSX,IPSY-5)
      CALL CTRORI(1.0)
      CALL TYPECS('LOG FREE ELECTRON DENSITY',25)
      CALL CTRORI(0.0)
      CALL PLACE(IPSX+2,IPSY+2)
      CALL TYPECS('EA=',3)
      CALL TYPENF(EA 3)
      CALL TYPECS('    ED=',7)
      CALL TYPENF(ED,3)
      CALL TYPECS('    T1=',7)
      CALL TYPENF(T1,1)
      CALL TYPECS('    DT=',7)
      CALL TYPENF(DT,1)
      CALL PLACE(IPSX+2,IPSY+3)
      CALL TYPECS('EG=',3)
      CALL TYPENF(EG,3)
      CALL TYPECS('    RA=',7)
      CALL TYPENF(RA 4)
      CALL TYPECS('    RD=',7)
      CALL TYPENF(RD,4)
      CALL PLACE(IPSX+2,IPSY+4)
      CALL TYPECS('CNA=',4)
      CALL TYPENE(CNA,2)
      CALL TYPECS('    CND=',8)
```

```
      CALL TYPENE(CND,2)
      CALL FRAME
      CALL PSPACE(PSX,0.95,PSY,0.95)
      CALL MAP(XO-0.1,XM+0.1,0.0,1.01)
      CALL AXES
      CALL SCALES
C     CALL GRATIC
      DO 700 J=1,TM
      DO 700 H=1,GM-1
      CALL POSITN(X1(H,J),GAMMA(H,J))
      IF(H.EQ.GM-1)GOTO 700
      CALL JOIN(X1(H+1,J),GAMMA(H+1,J))
700   CONTINUE
      GOTO 840
840   CONTINUE
      CALL GREND
      STOP
      END
C     SUBROUTINE TECHS-THERMAL EQUILIBRIUM CHARGE SUM
      SUBROUTINE TECHS(E)
      INTEGER NL
      DOUBLE PRECISION N,EC,KT,DE,NC,NV,E,Q,NO,PO
      DOUBLE PRECISION QA(1000),QD(1000),GA(1000)
      DOUBLE PRECISION GD(1000)
      DOUBLE PRECISION FO(1000),PO(1000),NTH(50),PTH(50)
      COMMON /C1/N,KT,NO,PO,NC,NV,EC,DE,FO,PO,NTH,PTH
      COMMON /C3/NL,Q,QA,QD,GA,GD
      Q=0.0
      DO 80 I=1,NL-1
      IF((DE*DFLOAT(I)-E)/KT-80.0)90,90,100
100   FO(I)=0.0
      PO(I)=1.0
      GOTO 120
90    IF((E-DE*DFLOAT(I))/KT-80.0)110,110,115
115   FO(I)=1.0
      PO(I)=0.0
      GOTO 120
110   FO(I)=1.0/(1.0+DEXP((DE*DFLOAT(I)-E)/KT))
      PO(I)=1.0/(1.0+DEXP((E-DE*DFLOAT(I))/KT))
120   QA(I)=GA(I)*FO(I)
      QD(I)=GD(I)*PO(I)
      Q=Q-QA(I)+QD(I)
80    CONTINUE
C     WRITE(5,400)
C400  FORMAT(' OK SO FAR')

      NO=DEXP((E-EC)/KT+DLOG(NC))
      PO=DEXP(-E/KT+DLOG(NV))
      Q=Q-NO+PO+N
      RETURN
      END
      SUBROUTINE SR(EP)
C     SHOCKLEY-READ CHARGE SUM
      INTEGER NL
      DOUBLE PRECISION NE,RA,RD,Q,EP
```

```
      DOUBLE PRECISION FA(1000),PD(1000),NI(1000)
      DOUBLE PRECISION PI(1000),GD(1000),RD2(1000)
      DOUBLE PRECISION QA(1000),QD(1000),GA(1000)
      DOUBLE PRECISION RA1(1000),RA2(1000),RD1(1000)
      COMMON /C2/NE,RA,RD,FA,PD,NI,PI,RA1,RA2,RD1,RD2
      COMMON /C3/NL,Q,QA,QD,GA,GD
      Q=0.0
      DO 350 I=1,NL-1
      FA(I)=RA1(I)/(RA2(I)+EP)
      PD(I)=(RD1(I)+EP)/(RD2(I)+EP)
      QA(I)=GA(I)*FA(I)
      QD(I)=GD(I)*PD(I)
      Q=Q-QA(I)+QD(I)
350   CONTINUE
C     TYPE *,Q
      Q=Q+EP-NE
      RETURN
      END
```

Appendix III

This is the computer program MATR3 mentioned in the main text. It is in FORTRAN.

```
C       TRANSIENT PHOTOCONDUCTIVITY SIMULATION
C       TRANSITION MATRIX METHOD
        DOUBLE PRECISION A(100,100),B(100,100),C(100,100)
        DOUBLE PRECISION G(100),N1(100),N(100,60,5)
        DOUBLE PRECISION DT,DE,CN,S,T,RD1,RD2,KT,T1
        REAL ET1,X(100),Y(100,10),ET2
D650
        INTEGER TS,NL,H,IET1,IET2,JT
        WRITE(5,10)
10      FORMAT(1H ,' INPUT TS,NL,TC,DT,T1')
        READ(5,20)TS,NL,TC,DT,T1
20      FORMAT(2I,3F)
C       SINGLE LEVEL DEPTH SELECTION
        WRITE(5,22)
22      FORMAT(1H ' INPUT DISCRETE LEVEL DEPTHS, ET1,ET2
        (EV)')
        READ(5,24)ET1,ET2
24      FORMAT(2F)
C       RELATIVE DENSITY OF STATES
        WRITE(5,26)
26      FORMAT(1H ,' INPUT RELATIVE DENSITIES OF DISCRETE
        LEVELS,RD1,RD2')
        READ(5,28),RD1,RD2
28      FORMAT(2F)
C       TEMPERATURE STEPS
        DO 250 JT=1,4
        T=T1+(JT-1)*25
C       COMPUTE REDUCED ENERGY STEP,DE
        KT=8.625D-5*T
        DE=1.0/DFLOAT(NL)*KT)
C       THIS TRUNCATES TAIL AT 1.0EV
C       LOCATE LEVEL NEAREST ET1,ET2
        IET1=IFIX(ET1*FLOAT(NL)+0.5)
        IET2=IFIX(ET2*FLOAT(NL)+0.5)
C       IET=DISCRETE LEVEL NUMBER
C       SET UP DENSITY OF STATES
C       AND 'RELEASE DENSITY',N1(I)
        S=0.0
        DO 30 I=1,NL
        G(I)=DE*DEXP(-DFLOAT(I)*DE*T/TC)
C       IS THIS CORRECT?
        S=S+G(I)
        N1(I)=DEXP(-DFLOAT(I)*DE)
30      CONTINUE
        S=S-G(IET1)-G(IET2)
        G(IET1)=G(IET1)*RD1
        G(IET2)=G(IET2)*RD2
```

```
          S=S+G(IET1)+G(IET2)
C         NORMALIZE CAPTURE COEFFICIENT,CN
          CN=1.0/S
C         SET UP TRANSITION MATRIX,A(I,J)
          A(1,1)=1.0-)T
          DO 40 I=2,NL+1
          A(1,I)=N1(I-1)*CN*)T
          A(I,1)=G(I-1)*CN*)T
          A(I,I)=1.0-N1(I-1)*CN*)T
40        CONTINUE
C         SET UP DUMMY MATRIX,B(I,J)
          DO 50 I=1,NL+1
          DO 50 J=1,NL+1
          B(I,J)=A(I,J)
50        CONTINUE
C         COLLECT PARAMETER VALUES IN ARRAY N( )
C         INITIAL STEP
          DO 60 I=1,NL+1
          N(I,1,JT)=B(I,1)
60        CONTINUE
C         MATRIX MULTIPLICATION
          DO 70 L=2,TS
          DO 80 I=1,NL+1
          DO 80 J=1,NL+1
          DO 80 K=1,NL+1
          C(I,J)=C(I,J)+B(I,K)*B(K,J)
80        CONTINUE
C         COLLECT PARAMETERS IN ARRAY N( )
          DO 90 I=1,NL+1
          N(I,L,JT)=C(I,1)
90        CONTINUE
C         UPDATE MATRIX B;ZEROIZE C
          DO 85 M=1,NL+1
          DO 85 H=1,NL+1
          B(M,H)=C(M,H)
          C(M,H)=0.0
85        CONTINUE
70        CONTINUE
          DO 110 I=1,TS
          WRITE(5,100)N(1,I,JT),I
100       FORMAT(F,I)
110       CONTINUE
C         SET UP X AND Y AXES
          DO 200 I=1,TS
          X(I)=LOG10()T)+FLOAT(I-1)*LOG10(2.0)
          Y(I,JT)=LOG10(N(1,I,JT))+10.0
200       CONTINUE
250       CONTINUE
          CALL PAPER(1)
          CALL MAP(X(1),X(TS),Y(TS,1)-0.1,10.01)
          CALL AXES
          CALL SCALES
          CALL GRATIC
          DO 270 JT=1,4
          DO 220 I=1,TS
```

```
        CALL POSITN(X(I),Y(I,JT))
        IF(I.EQ.TS)GOTO 221
        CALL JOIN(X(I+1),Y(I+1,JT))
221     CONTINUE
220     CONTINUE
270     CONTINUE
        CALL GREND
        STOP
        END
```

Appendix IV

This is the computer program, TRANS, mentioned in the main text. It is in FORTRAN.

```
      IMPLICIT DOUBLE PRECISION (A-Z)
      INTEGER IK, TS,NS,JM,KM,IMM,JMM,KMM,I,IY,NT,TV,
      INTEGER NR,N3,N4
      PARAMETER (NS=60,TS=80,IMM=82,JMM=1,KMM=6)
      PARAMETER (KB=8.625)-5)
      DIMENSION G(TS),N1(TS),P1(TS),CN(TS),CP(TS)
     1,J(TS,TS),K(TS,TS),YM(TS),YS(TS),ZM(TS),ZS(TS)
     2,DY(TS),F(TS),X(IMM,JMM),Y(IMM,KMM),IC(10,3)
        DIMENSION XT(IMM),YL(IMM,KMM)
        WRITE(5,11)
11      FORMAT(' TIME STEPS, AN INTEGER')
        READ(5,*)IM
      JM=JMM
      KM=KMM
      WRITE(5,10)
10    FORMAT(' TEMPERATURE,T')
      READ(5,*)T
C      WRITE(5,20)
C 20    FORMAT(' INPUT REL. DOPING RQ=')
C      READ(5,*)RQ
        RQ=0
      RC=100.0
      RA=1.0/RC
      RD=RC
      KT=KB*T
      EG=1.8
        E3=0.4
        E4=0.5
        N3=IDINT(E3/EG*)BLE(NS+1)+0.5)
        N4=IDINT(E4/EG*)BLE(NS+1)+0.5)
        DR3=7.0
        DR4=1.0
        WRITE(5,5001)
5001    FORMAT(' INPUT THE RECOMBINATION EDGES')
        READ(5,*)ER1,ER2
      DE=EG/(NS+1)
      DK=DE/KT
      GOTO 997
897   DO 30 I=2,NT+1
        CC=1.0
        IF(DBLE(I-1)*DK*KT.GT.ER1)CC=10.0
      CN(I)=CC/S1
      CP(I)=CN(I)/RA
30    CONTINUE
      DO 40 I=NT+2,TV-1
        CC=1.0
        IF(DBLE(I-TV+NS+1)*DK*KT.LT.ER2)CC=10.0
```

```
      CP(I)=CC/S1
      CN(I)=RD*CP(I)
40    CONTINUE
      M=S2
      SM=S2*(1.+RQ)
      TQ=S2*RQ
      DO 50 I=TV-1,2,-1
      IF (SM.GE.G(I)) YS(I)=G(I)
      IF (SM.LT.G(I)) YS(I)=SM
      SM=SM-YS(I)
50    CONTINUE
      YO=0
      DO 60 I=2,TV-1
      ZS(I)=G(I)-YS(I)
60    CONTINUE
C      WRITE(5,65)S2,SM
C 65    FORMAT(2G14.6)
      YS(1)=YO
      YS(TV)=YS(1)
      DO 70 I=1,TV
      YM(I)=YS(I)
      ZM(I)=G(I)-YM(I)
70    CONTINUE
      YT=0.0
      IY=0
      I=1
      KM=0
      WRITE(5,80)
80    FORMAT(' GR=GEN. RATE')
      WRITE(5,90)
90    FORMAT(' JP=0 FOR STEADY STATE, 1 FOR TRANSIENT')
      WRITE(5,100)
100   FORMAT(' IY=RESULT INDEX')
      WRITE(5,110)
110   FORMAT(' QE=FLASH INITIAL REL. HEIGHT')
      WRITE(5,120)
120   FORMAT(' INPUT GR=999 TO END PROCESS')
125   WRITE(5,130)I
130   FORMAT(' I.C. NO.',I6)
      WRITE(5,140)
140   FORMAT(' INPUT GR JP QE')
      READ(5,*)IC(I,1),IC(I,2),IC(I,3)
      IF (IC(I,1).EQ.999) GOTO 150
      IF (IC(I,2).GT.0) KM=KM+1
      NR=I
      I=I+1
      GOTO 125
150   DO 240 H=1,NR
      GR=IC(H,1)
      JP=IC(H,2)
      QE=IC(H,3)
      IF (JP.GT.0.0) IY=IY+1
      IF (JP.EQ.1.0) YO=YS(1)
      IF (JP.EQ.1.0) YS(1)=YS(1)+QE*YT
      IF (JP.EQ.1.0) YS(TV)=YS(TV)+QE*YT
```

```
        IF(GR.EQ.0.0.AND.JP.EQ.1.)YO=YT
      TT=0.0
      SN=0.0
      TL=1.D-3
      QR=1.D-5
      QC=QR
      CR=1.0
      DT=0.01
      IF (JP.EQ.0.0) THEN
      MV=11
      ELSE
      MV=IM
      ENDIF
      DO 160 L=1,MV
165   GOTO 994
894   GOTO 995
895   GOTO 996
C 896   WRITE(5,170))Y(1)
C 170   FORMAT(' )Y(1)= ',G14.6)
C      WRITE(5,180)YM(1)
C 180   FORMAT(' YM(1)= ',G14.6)
896     IF (ABS()Y(1)/YM(1)).LT.TL) GOTO 190
      GOTO 165
190   TT=TT+)T
      DO 195 I=1,NT+1
      YS(I)=YM(I)
      ZS(I)=G(I)-YM(I)
195   CONTINUE
      DO 200 I=NT+2,TV-1
      ZS(I)=ZM(I)
      YS(I)=G(I)-ZM(I)
200   CONTINUE
      YS(TV)=YM(TV)
      IF (JP.EQ.0.0) GOTO 210
      Y(L,IY)=(YS(1)-YO)
      X(L,1)=TT
210   RD=(YS(1)-YO)
C      WRITE(5,220)RD,TT
220   FORMAT(' REL. DY(1)= ',2G14.6)
C      WRITE(5,230)L,IY
230   FORMAT(' TIME STEP NO. ',G14.6,' DATA NO. ',I5)
      DT=TT
      SN=SN+1.0
      IF (JP.EQ.0.0) )T=99999.*TT
      IF (TT.GT.1.D20) )T=1.0)18
160   CONTINUE
      IF (GR.EQ.0.0.AND.JP.EQ.0.0) YT=YS(1)
240   CONTINUE
C      WRITE(5,*)YS(TV)
       GOTO 4440
994   S3=0.0
      S4=0.0
      S5=0.0
      S7=0.0
      S8=0.0
```

```
      IF (TT.GT.0.01) CR=YS(TV)/YS(1)
      IF (DABS(YS(1)).GT.DABS(YS(TV))) THEN
      QC=QR*CR
      ELSE
      QR=QC/CR
      END IF
      DO 1010 I=2,TV-1
      U1=CN(I)*(YM(1)+N1(I))
      U2=CP(I)*(YM(TV)+P1(I))
      J(I,I)=-U1-U2
      J(1,I)=U1+QR
      J(I,1)=CN(I)*ZM(I)
      J(TV,I)=-U2-QC
      S3=S3+J(I,1)
      S4=S4+YM(I)*CN(I)*N1(I)
      IF (I.LT.NT+2) THEN
      S5=S5+YM(I)
      ELSE
      S5=S5-ZM(I)
      END IF
      J(I,TV)=-YM(I)*CP(I)
      S7=S7+J(I,TV)
      S8=S8+CP(I)*P1(I)*ZM(I)
1010  CONTINUE
      J(1,1)=-S3+QR
      J(1,TV)=-QR
      J(TV,1)=-QC
      J(TV,TV)=S7+QC
      DO 1020 I=2,TV-1
      K(I,I)=1.-DT*J(I,I)
      K(1,I)=-DT*J(1,I)
      K(TV,I)=-DT*J(TV,I)
      K(I,1)=-DT*J(I,1)
      K(I,TV)=-DT*J(I,TV)
1020  CONTINUE
      K(1,1)=1.-DT*J(1,1)
      K(TV,TV)=1.-DT*J(TV,TV)
      K(1,TV)=-DT*J(1,TV)
      K(TV,1)=-DT*J(TV,1)
      GOTO 894
995   DO 2010 I=2,TV-1
      F(I)=ZM(I)*(YM(1)*CN(I)+CP(I)*P1(I))-YM(I)*(CN(I
     1)*N1(I)+YM(TV)*CP(I))
2010  CONTINUE
      S9=QR*(S5+YM(1)-YM(TV)-TQ)
      F(1)=-YM(1)*S3+S4+S9+GR
      F(TV)=YM(TV)*S7+S8-CR*S9+GR
      GOTO 895
996   DO 3010 I=1,TV-1
      IF (I.LT.NT+2) THEN
      DY(I)=DT*F(I)-YM(I)+YS(I)
      ELSE
      DY(I)=DT*F(I)+ZM(I)-ZS(I)
      END IF
3010  CONTINUE
```

```
      DY(TV)=DT*F(TV)-YM(TV)+YS(TV)
      DO 3020 I=2,TV-1
      E1=K(1,I)/K(I,I)
      E2=K(TV,I)/K(I,I)
      DY(1)=DY(1)-E1*DY(I)
      K(1,1)=K(1,1)-E1*K(I,1)
      K(1,TV)=K(1,TV)-E1*K(I,TV)
      DY(TV)=DY(TV)-E2*DY(I)
      K(TV,1)=K(TV,1)-E2*K(I,1)
      K(TV,TV)=K(TV,TV)-E2*K(I,TV)
3020  CONTINUE
      E1=K(TV,1)/K(1,1)
      DY(TV)=DY(TV)-E1*DY(1)
      K(TV,TV)=K(TV,TV)-E1*K(1,TV)
      DY(1)=DY(1)-DY(TV)*K(1,TV)/K(TV,TV)
      DO 3030 I=2,TV-1
      E1=K(I,1)/K(1,1)
      E2=K(I,TV)/K(TV,TV)
      DY(I)=DY(I)-E1*DY(1)-E2*DY(TV)
3030  CONTINUE
      DO 3040 I=1,TV
      DY(I)=DY(I)/K(I,I)
3040  CONTINUE
      DO 3050 I=1,TV-1
      IF (I.LT.NT+2) THEN
      YM(I)=YM(I)+DY(I)
      ELSE
      ZM(I)=ZM(I)-DY(I)
      END IF
      IF (I.LT.NT+2) THEN
      ZM(I)=G(I)-YM(I)
      ELSE
      YM(I)=G(I)-ZM(I)
      END IF
3050  CONTINUE
      YM(TV)=YM(TV)+DY(TV)
      GOTO 896
997   E1=0.05
      E2=0.08
      G1=1.
      G2=1.
      NT=INT((NS+1)*(1-(1/(1+E1/E2)))+1)
      TV=((NS+1)+3)
      S1=0.0
      DO 4610 I=2,NT+1
      G(I)=DK*G1*DEXP(-1.0*DBLE(I-1)*DE/E1)
                IF(I.EQ.N3)G(I)=DR3*G(I)
        IF(I.EQ.N4)G(I)=DR4*G(I)
      S1=S1+G(I)
      N1(I)=DEXP(-1.0*DBLE(I-1)*DK)
      P1(I)=DEXP(-1.0*DBLE(NS+2-I)*DK)
4610  CONTINUE
C       S2 IS THE TOTAL VALENCE BAND STATES
      S2=0.0
      DO 4020 I=NT+2,TV-1
```

```
      G(I)=)K*G2*)EXP(-1.0*)BLE(TV-I)*)E/E2)
      S2=S2+G(I)
      N1(I)=)EXP(-1.0*)BLE(I-TV+NS+1)*)K)
      P1(I)=)EXP(-1.0*)BLE(TV-I)*)K)

4020  CONTINUE
      DO 4030 I=2,TV-1
C      WRITE(5,*)I,G(I)
4030  CONTINUE
C      WRITE(5,*)S1,S2
C       WRITE(5,*)NS,NT,TV,N3
      GOTO 897

C       GRAPHICS BIT
C       TIME AXIS
4440    DO 4450 I=1,IM
        XT(I)=ALOG10(X(I,1))
4450    CONTINUE
        XL=ALOG10(X(1,1))
        XH=ALOG10(X(IM,1))
C       FREE CARRIER - Y-AXIS
        YTL=1.0E30
        YTH=-1.0E30
        DO 4500 IK=1,KM
        DO 4500 I=1,IM
        IF(Y(I,IK).EQ.0.0)Y(I,IK)=Y(I-1,IK)
        YL(I,IK)=ALOG10()ABS(Y(I,IK)))
        IF (YL(I,IK).GT.YTH)YTH=YL(I,IK)
        IF(YL(I,IK).LT.YTL)YTL=YL(I,IK)
4500    CONTINUE
C       MAP & SCALES
        PSX=0.2
        PSY=0.2
        IPSX=IDINT(PSX*58.-0.5)
        IPSY=IDINT(35.*(1.-PSY)+3.)
        CALL PAPER(1)
        CALL PSPACE(PSX,0.95,PSY,0.95)
        CALL MAP(XL,XH,YTL-0.01,YTH+0.01)
        CALL SCALES
        CALL BORDER
        DO 4550 IK=1,KM
        DO 4550 I=1,IM
        CALL POSITN(XT(I),YL(I,IK))
        IF(I.EQ.IM)GOTO 4550
        CALL JOIN(XT(I+1),YL(I+1,IK))
4550    CONTINUE
        CALL GREND
        STOP
        END
```

REFERENCES

1. Mott N.F.& Davis E.A Electronic Properties in Non crystalline Materials. Clarendon Press, 1979.
2. Anderson,D.A Phys Rev. Vol. 109 1492 1958.
3. Chittick R.C et.al J.Electrochem Soc. Vol 116 77 1969
4. Mott,N.F Adv.Phys Vol 16 46, 1967.
5. Cohen,M.H. Fritzsche,H. & Ovshinsky S.R Phys Rev.Lett. Vol. 22 1065 1969.
6. Madan,A Le Comber,P.G. & Spear,W.E. J. Non-Cryst. Solids Vol. 20, 239 1976.
7. Spear,W.E. & Le Comber P.G. J Non Cryst. Solids Vol 8 10, 727 1972.
8. Le Comber,P.G & Spear,W.E. Phys. Rev. Lett. Vol 25 509 1970.
9. Spear,W.E. Loveland,R.J. & Al Sharbaty A J. Non Cryst. Solids Vol. 15 410, 1974.
10. Loveland,R.J. Spear,W.E. & Al-Sharbaty A J. Non-Cryst. Solids Vol. 13, 55 1973/74.
11. Goodman,A.M & Fritzche,H. Phil. Mag. B Vol. 42 149, 1980.
12. Spear W.E. & Le Comber,P.G. Solid State Comms Vol 17, 1193, 1975.
13 Lewis A.J. "Tetrahedrally Bonded Amorphous Semiconductors", Street R.A. & Biegleson,R.K eds A.I.P. 1974 pp 27.
14. Anderson, D.A & Spear, W.E., Phil. Mag. Vol. 36 695. 1977.
15. Orenstein,J. & Kastner,M Phys. Rev. Lett. Vol. 46, 1421, 1981.
16. Tiedje,T. Semiconductors and Semimetals Vol 21 C 207. 1984.
17. Rose,A Concepts in Photoconductivity and Allied Problems Krieger, 1978.
18. Kastner,M.A. & Monroe,D. Solar Energy Materials Vol. 8, 41, 1982.
19. Hack M. Guha,S. & Shur,M Phys. Rev. B Vol. 30, 6991. 1984.
20. Anderson,P.W. Phys. Rev. Lett., Vol. 34, 953 1975.
21. Mott,N.F. Davis,E.A. & Street,R.A Phil. Mag. Vol. 32, 961, 1975.
22. Street,R.A. & Mott N.F Phys Rev. Lett. Vol. 35 1293, 1975.
23. Adler,D. & Yoffe,E.J. Phys Rev. Lett. Vol. 36, 1197. 1976.
24. Kastner,M Adler,D. & Fritzsche,H. Phys. Rev Lett Vol. 37, 1504 1976.
25. Kastner,M. & Fritzsche,H. Phil Mag. B Vol. 37, 199. 1978.
26. Davis,E.A. Amorphous Semiconductors. Springer Verlag. 1979.
27. Mott,N.F. Phil. Mag. B Vol. 34, 1101, 1976.
28. Connell,G. A. N. in Brodsky M. H. Amorphous Semiconductors, Springer Verlag,80, 1979
29 Ryvkin, S.M Photoelectric Effects in Semiconductors. Consultants Bureau,New York, 1969.
30. Shockley W. & Read, W.T. Phys. Rev. Vol. 87. 835, 1952.
31. Simmons, J.G. & Taylor, G.W. Phys. Rev. B Vol. 4, 502, 1971.
32. Main,C. Photoconductivity and Noise in Amorphous

Chalcogenides, PhD dissertation, Edinburgh University 1974.
33. Taylor, G.W & Simmons, J.G. J. Non Cryst. Solids. Vol. 8 10, 940, 1972.
34. Simmons, J.G. & Taylor, G.W J. Phys. C Vol. 6. 3706 1973.
35 Scher.H. & Montroll E.W Phys Rev.B Vol. 12. 2455, 1975.
36. Tiedje,T. & Rose,A. Solid State Comms. Vol. 37, 49, 1980.
37. Orenstein,J.. Kastner,M.A & Vaninov V. Phil.Mag.B Vol 46, 23, 1982.
38. Halpern,V.. Phil.Mag.B Vol. 51, L49, 1985.
39. Marshall,J.M. & Main.C Phil.Mag.B, Vol. 47, 471, 1983.
40. Marshall,J.M. et.al Phil.Mag.B Vol. 47, 211, 1983.
41. Michiel,H. et.al. Phil.Mag.B. Vol. 48. 187, 1983.
42. Marshall,J.M et.al. Phil.Mag.B Vol. 52. 997. 1985.
43. Arkhipov,V.I. & Rudenko A I., Phil.Mag.B Vol 45. 189. 1982.
44. Rudenko,A I. & Arkhipov,V.I. Phil.Mag.B Vol. 45, 209 1982.
45. Street,R.A. Phys.Rev.B Vol 32. 3910, 1985.
46. Arkhipov,V.I..Popova,J.A & Rudenko.A I.. Phil.Mag.B Vol. 48, 401, 1983.
47. Hoheisel, M. et.al. J. Non Cryst. Solids, Vol 59 & 60. 457, 1983.
48. Card H.C. et. al., Solar Energy Materials, Vol. 6, 175. 1982.
49. Evangelisti, F. et.al. J. Non Cryst. Solids Vol. 55. 191, 1983.
50. Evangelisti, F. et.al. Solid State Comms Vol. 47, 107, 1983.
51. Staebler, D.L. & Wronski, C.R App. Phys. Lett. Vol. 31, 292, 1977.
52. Bhattacharya, E. & Narasimhan, K.L.. Phys. Rev. B Vol. 28, 2287, 1983.
53. Bhattacharya, E. & Narasimhan, K.L.. Phil. Mag. B Vol. 49. 271, 1984.
54. Hack.M. ,Guha,S. &Shur,M.. Phys. Rev. B Vol. 30, 271, 1984.
55 Hack M. ,Guha,S &Shur,M "Optical Effects in Amorphous Semiconductors", Taylor,P.C & Bishop S.G. eds. A I.P. 1984, pp. 40.
56. Kagawa,T. Matsumoto,N. & Kumabe,K. Phys. Rev. B Vol. 28, 4570, 1983.
57. Okamoto.H. & Hamakawa,Y., Solid State Comms Vol 24 23, 1977.
58. Okamoto,H. & Hamakawa,Y. J. Non-Cryst. Solids Vol. 33, 225, 1979.
59. Okamoto.H.et.al. Phil.Mag.B, Vol. 49, 231, 1984.
60. Lewis,A J., Phys. Rev. B Vol. 14, 658, 1976.
61. Connel,G.A N. & Pawlik,J.R Phys Rev. B Vol. 13, 787, 1976.
62. Paul,W. et.al., Solid State Comms. Vol. 20. 969, 1976.
63. Moustakas,T.D., Anderson,D.A & Paul,W Solid State Comms. Vol. 23, 155. 1977.
64. Moustakas,T.D. Journal of Electronic Materials, Vol. 8, 391, 1979.
65. Moustakas,T.D., Semiconductors and Semimetals, Vol. 21A 55. 1984.

66. Paul W. & Anderson D.A. Solar Energy Materials, Vol. 5 229 1981.
67. Le Comber P.G. & Spear W.E. Phil. Mag Lett. Vol. 53, L1 1986.
68. Barclay R.P The Electronic Transport Properties of Undoped and Doped Arsenic Triselenide PhD dissertation. Dundee College of Technology 1985.
69. Fortuna, H.S. Electronic Transport Properties of Thin Films of Amorphous Silicon. PhD dissertation. Dundee College of Technology 1984.
70. Easton,B.C. et. al. Vacuum Vol. 34, 371, 1984.
71. Wronski,C.R. Semiconductors and Semimetals, Vol. 21C 347, 1984.
72. Spear,W.E. et. al., Phil. Mag. B Vol. 41, 419 1980.
73. Hepburn,A.R Personal Communication 1986.
74. Street,R.A., Phil.Mag.B Vol. 49 L15, 1984.
75. McMahon,T.J. & Xi,J.P. Phys.Rev.B Vol. 34, 2475, 1986.
76. Huang C.-Y. et.al. Phys.Rev.B Vol. 27, 7460, 1981.
77. Street,R.A. et.al. Phys.Rev.B Vol. 30, 5861, 1984.
78. Hvam,J.M. & Brodsky,M.H., Phys Rev.Lett. Vol. 46 371 1981.
79. Kagawa,T. et.al. Phys.Rev.B Vol. 26, 4714, 1982.
80. Pandya,R. et.al. J.Non Cryst.Solids Vol. 66, 193, 1984.
81. Schiff E.A. "Tetrahedrally Bonded Amorphous Semiconductors", Adler,D. & Fritzsche,H. eds., Plenum Press, 1985, pp. 357.
82. Oheda,H., Phil.Mag.B Vol. 52 857, 1985.
83. Marshall J.M. et.al. Phil.Mag.B Vol. 54, 997, 1986.
84. Viktorovitch P. et.al "Tetrahedrally Bonded Amorphous Semiconductors", Street.R.A. et.al. eds., A.I.P. 1981, pp. 186.
85. Arene,E. & Baixeras,J. Phys.Rev.B Vol. 30 2016, 1984.
86. Marshall J.M. et. al. Phil.Mag.B Vol. 54, 51 1986.